A final drive device for torque vectoring in small racing cars

Sven Kalkan

Thesis for the degree of Master of Science in Engineering
Division of Combustion engines
Department of Energy Sciences
Faculty of Engineering | Lund University

A final drive device for torque vectoring in small racing cars

Sven Kalkan

June 2019, Lund

This degree project for the degree of Master of Science in Engineering has been conducted at the Division of Combustion engines, Department of Energy Sciences, Faculty of Engineering, Lund University, and at BorgWarner PowerDrive Systems (PDS) in Landskrona, Sweden

Supervisor at the Division of Combustion engines was Professor Martin Tunér
Supervisor at BorgWarner was Isak Andersson
Examiner at Lund University was Professor Sebastian Verhelst

Thesis for the Degree of Master of Science in Engineering

ISRN LUTMDN/TMHP-19/5442-SE

ISSN 0282-1990

Division of Combustion engines
Department of Energy Sciences
Faculty of Engineering, Lund University
Box 118, 221 00 Lund
Sweden

www.energy.lth.se

Abstract

The agility of the car can be improved by distributing the longitudinal tire forces unevenly between the wheels. The resulting yaw moment helps the car to steer in transient driving scenarios, like on a slalom course. The available grip in steady state cornering can also be increased along with stability. The goal in this project is to develop a final drive device for torque vectoring in a small racing car in order to make it faster around the race track.

It is shown that torque vectoring can improve the usable tire grip. Different differential concepts, both passive and active, are presented and discussed. The torque vectoring concepts are rated according to suitability in a Formula Student car, and two alternatives of a dual clutch concept are chosen for further analysis. A lap-simulation program is used to evaluate if the concepts are feasible to use in a race car, and to quantify requirements for torque capacity, and cooling.

A system requirements specification is created and a design is developed in a 3D-CAD program. The performed analysis for clutch dimensioning, cooling capacity and structural finite element analysis is presented. The remaining work is presented and discussed in the end.

Acknowledgements

This report is the result of a master's thesis carried out at the Department of Energy Sciences, Faculty of Engineering (LTH), at Lund University in collaboration with BorgWarner PowerDrive Systems (PDS) in Landskrona, Sweden and Lund Formula Student.

I would like to express my gratitude to BorgWarner PDS for letting me do this slightly special thesis, it would not have been possible to do without your support. I would especially like to thank Isak Andersson and Hans Jacobsson, for all support, technical discussions and answers to my endless questions.

I would also like to thank Martin Tunér and Sebastian Verhelst at the Department of Energy Sciences for all support and academic administration of this thesis.

Lund, June 2019

Sven Kalkan

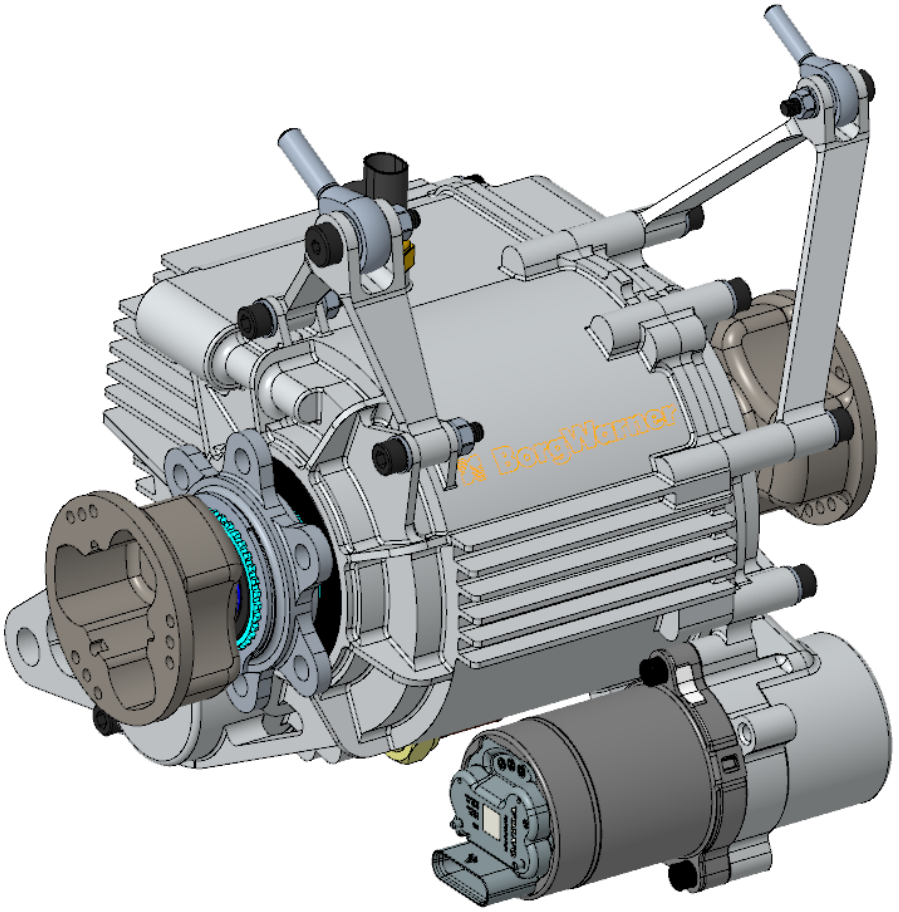
BorgWarner

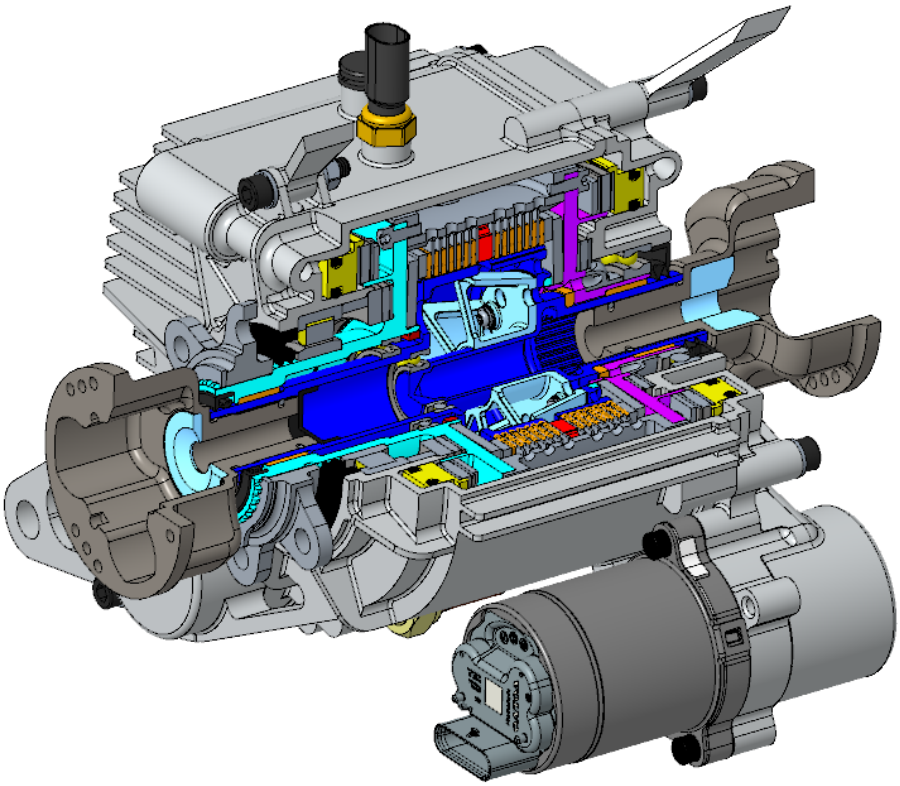

Contents

Acronyms and abbreviations

RWD - "Rear Wheel Drive"
FWD - "Front Wheel Drive"
AWD - "All Wheel Drive"
ESC - "Electronic Stability Control"
LSD - "Limited Slip Differential"
ELSD - "Electronic Limited Slip Differential"
LFS - "Lund Formula Student"
FS - "Formula Student"
TV - "Torque Vectoring"
NVH - "Noise, Vibration and Harshness"
SRS - "System Requirements Specification"
FEA - "Finite Element Analysis"
NC - "Normally Closed"
NO - "Normally Open"

Nomenclature

R_{out} - Radius of friction circle, outer wheel
R_{in} - Radius of friction circle, inner wheel
$F_{z,out}$ - Tire normal force, outer wheel
$F_{z,in}$ - Tire normal force, inner wheel
m - Car mass
g - Gravitational acceleration (9,82 m/s^2)
L_a - Center of gravity to front axle distance
L_{wb} - Wheelbase
L_t - Trackwidth
h_{cg} - Center of gravity height
a_x - Longitudinal acceleration
a_y - Lateral acceleration
F_x - Total longitudinal force
$F'_{y,out}$ - Tire lateral force, outer wheel, with torque vectoring
$F'_{y,in}$ - Tire lateral force, inner wheel, with torque vectoring
$F_{y,out}$ - Tire lateral force, outer wheel, without torque vectoring
F_T - Tractive force per wheel, without torque vectoring
F_{TV} - Increase/decrease of tractive force due to torque vectoring

F_c - Axial clutch force
R_i - Friction disc inner radius
R_o - Friction disc outer radius
p - Friction disc pressure
μ - Coefficient of friction
n - Number of friction surfaces
M_c - Clutch torque
F_p - Piston force
A_p - Piston area
p_h - Hydraulic pressure
F_s - Spring force

$M_{w,out}$ - Wheel torque, outer wheel
$M_{w,in}$ - Wheel torque, inner wheel
$M_{w,tot}$ - Wheel torque, total
r_w - Wheel radius
$\omega_{w,out}$ - Wheel rotational speed, outer wheel
$\omega_{w,in}$ - Wheel rotational speed, inner wheel
$P_{loss,slip}$ - Clutch slip power loss
$P_{loss,actuators}$ - Actuator power loss
$P_{el,actuators}$ - Actuator electrical power input
$F_{thrust,housing}$ - Axial force on clutch housing bearing
$F_{thrust,out}$ - Axial force on outer piston bearing
$F_{thrust,in}$ - Axial force on inner piston bearing
$M_{loss,thrust}$ - Needle thrust bearings total loss torque
f_l - Thrust bearing loss coefficient
$d_{m,pistonbearing}$ - Mean diameter of piston thrust bearing
$d_{m,housingbearing}$ - Mean diameter of clutch housing thrust bearing
$P_{loss,thrust}$ - Needle thrust bearings total loss power

F_{chain} - Chain tension force
$r_{sprocket}$ - Chain sprocket radius
$M_{cv,bending}$ - Bending moment on CV-joint due to driveshaft angle
α_{cv} - Driveshaft angle in CV-joint compared to straight

$F_{r,b1}$ - Radial force bearing 1 (roller bearing)
$F_{r,b2}$ - Radial force bearing 2 (ball bearing)

$M_{b,h1}$ - Bending moment tripod housing 1
$M_{b,h2}$ - Bending moment tripod housing 2

T_a - Ambient temperature
T_a - Ambient temperature
$T_{oil,max}$ - Max allowed oil temperature
Q - Cooling power
$h_{c,air-aluminium}$ - Heat convection coefficient air to aluminium
$h_{c,oil-aluminium}$ - Heat convection coefficient oil to aluminium
$k_{aluminium}$ - Heat conduction coefficient aluminium
$A_{housing,out}$ - Housing outside area
$A_{housing,in}$ - Housing inside area
$t_{housing}$ - Housing thickness

1 Introduction

1.1 Background

1.1.1 Formula Student

Formula Student is one of the most established engineering competitions for students. Student teams design and build racing cars and compete against each other on international competitions in both dynamic and static events. The dynamic events are:

- Acceleration - a 75 m long straight where power, longitudinal grip, mass and aerodynamic drag are the most influencing car parameters.
- Skidpad - driving in a circle with a diameter of 18,25 m in both directions. Mass, aerodynamic downforce, lateral grip and driveability is crucial to succeed in this event.
- Autocross - an approximately one km long track with straights, slaloms, long sweeping corners, hairpins and chicanes. All car parameters mentioned above are important for this event, but also responsiveness because the track is very transient.
- Endurance - 22 km on the same track as autocross, with a driver change in the middle. It has the same demands on the car as the autocross event, but reliability plays a larger role here.
- Efficiency - based on the consumed energy in relation to speed at the endurance event.

The static events are events where the car is not driven, but instead they are intended to test the knowledge of the students. The static events are:

- Engineering design - A discussion where the quality of the reasoning and analysis that is behind all design choices is judged. Good, innovative and well motivated designs are rewarded.
- Cost and manufacturing - Tests the team's understanding of cost and manufacturing processes, make or buy decisions and differences between prototype and mass production.
- Business plan presentation - Evaluates the team's ability to develop and present a business model of the product, a prototype race car.

For a deeper explanation of the different events, and other rules, see [3].

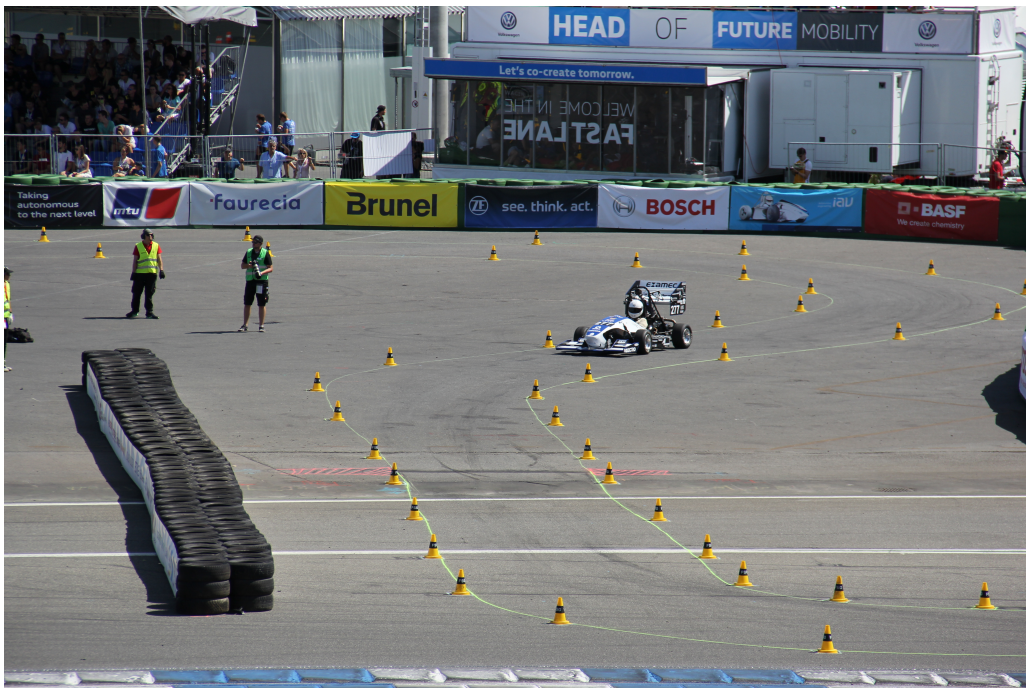

Figure 1: *LFS-18 car on Formula Student Germany endurance event*

The events are testing many different aspects of both the car and the team so it is not enough to optimize the car in just one aspect to win the competition. It is favorable to have a car that is designed with all events in mind, for example by having built-in adjustability in suspension, aerodynamics and powertrain. Well implemented active systems, like torque vectoring, are beneficial in almost all events because it can increase the grip, driveability and responsiveness of the car.

The relatively open ruleset encourages teams to think outside the box which leads to a wide variety in the cars produced. Combustion powertrain cars typically have engines of 1 to 4 cylinders, with or without turbo/supercharging. The power is limited by an intake air restrictor of 20 mm in diameter for gasoline engines (19 mm for E85). The engine power is varying from 25 to 65 kW. Almost all combustion cars have RWD, but there are exceptions with AWD. Electric cars are power limited at 80 kW and both RWD and AWD is common. The weight (without driver) is ranging from 135 kg to 300 kg. A wheelbase of around 1,55 m and trackwidth of around 1,2 m is most commonly used [2].

1.1.2 Lund Formula Student

The Lund Formula Student team has been designing and building cars since 2006 and is currently in the spring of 2019 building its 11th car, the LFS-19. There has typically been 30-45 team members every year. The year starts in September with the concept and design phase, continued with the manufacturing and assembly phase in the spring next year. Car testing is started in May to have a race ready car for the competitions in July and August.

Lots of different concepts have been tried out through the years; Steel spaceframes and carbon fiber monocoques, double wishbone suspension and de-dion axle suspension, wings, 1- and 4-cylinder engines and even one hybrid powertrain. The four latest cars, LFS-16 to LFS-19 have all been iterations of a concept that uses a steel spaceframe, 4-cylinder 600 cc Honda motorcycle engine, RWD, direct actuated springs and dampers and 10-inch wheels. Continuous improvements have been made through the years, where every subsystem is getting more and more refined.

Almost all cars have used a Drexler limited slip differential, which is a common choice among the Formula Student teams. It is a torque sensing LSD, which means that the locking torque is depending on the input torque. The next step would be to use an active differential to increase the result potential in the dynamic events by improving grip, driveability and responsiveness. It would also increase the level of innovation and use of modern technology, which is of course positive in the design event.

Figure 2: *LFS-18 car on Formula Student Germany autocross event*

1.1.3 Torque vectoring

The torque sensing limited slip differential is a quite good choice in Formula Student because it combines the good maneuverability of an open differential with the high traction potential of a locked axle through "semi-locking" the axle and thus allowing a difference in driving torque between the driving wheels. The major benefit of the LSD compared to an open differential is the increased traction at corner exit, where the inner wheel typically loses traction with an open differential. However, the handling performance can be increased even further with a torque vectoring system.

Torque vectoring is a technology used in automotive differentials. It provides with the possibility to actively control the torque that is sent to the driving wheels. It can be implemented in various ways. One way is to use an open differential and automatically apply the brake on the wheel where less torque is wanted. An other way is to use an open differential and with the use of clutches or planetary gears and an electric motor take torque from one wheel and give it to the other. A third way is to not use a differential at all, only one clutch to each driving wheel. All these concepts have slightly different characteristics with their own pros and cons, but the idea is the same: To affect the vehicle's handling by introducing a yawing moment.

The use of torque vectoring has its origin in racing, which is maybe not so surprising. It makes the car faster in several ways. In transient maneuvers, for example when driving on a slalom course, it is beneficial to apply a yaw moment on the car in order to reach a higher yaw acceleration in the wanted direction. Torque vectoring can also be used to stabilize the car, especially when the driver is driving close to the grip limit. Sudden oversteer (also known as snap oversteer) can be damped efficiently by applying more torque to the inner wheel, just to give an example. Transient maneuvers and stabilization is probably where torque vectoring shows its greatest benefits, but it can also increase cornering speed, as will be shown later.

The benefits of TV are probably best used in racing and sports cars, but there could also be a market potential for it in the road vehicle industry as a safety device. ESC systems work by applying a stabilizing yaw moment by braking wheels independently. With TV it would be possible to also drive the wheels independently and thus also stabilize the vehicle without braking.

1.1.4 BorgWarner

BorgWarner has long experience in automotive propulsion systems. It is a global company that makes a wide variety of parts and systems for vehicles. The BorgWarner facility that is located in Landskrona, Sweden belongs to the division PowerDrive Systems (PDS). They focus on torque distribution systems for combustion, hybrid and electric vehicle drivelines. Some of the products are automatically controlled couplings for on-demand AWD, in drivelines that are normally FWD or RWD. They also have an electronic limited slip differential for FWD cars called FXD in their product portfolio. Their experience within torque distribution systems and the geographical location makes them a perfect partner for this project.

BorgWarner has been sponsoring the Lund Formula Student team for multiple years and this project is one step to even closer collaboration.

1.2 Project goals

The objective of the thesis is to deliver a manufactured and assembled mechanical prototype of a torque vectoring device that can be used on a formula student car in the future. The thesis is aimed at answering the following question:

Is it possible to make a transmission that allows independent driving wheel torque control on a combustion engine driven formula student car, without vastly exceeding mass and size of an LSD?

This is broken down into subgoals:

- Motivate the need of the device.
- Make a system requirements specification.
- Motivate the chosen concept and explain about other existing similar concepts.
- Deliver a 3D-model of the device.
- Deliver 2D manufacturing drawings.
- Order the prototype components.
- Assemble the unit.

Some bonus goals were also set in order to have something to chase if time allows.

- Make a test plan.
- Perform basic functional testing of the device in a test rig at BorgWarner.

The main area of use for the product would be on a combustion car. Electric cars with torque vectoring usually have two or four motors that can drive the wheels indepentently, and in those cases a torque vectoring device is not needed. But there are also electric cars with only one motor per driven axle and in that case a torque vectoring device could be used. The LFS-team might start building electric cars in the close future, starting with a single motor for the first cars. The device was therefor dimensioned so that it can be used on both combustion and electric cars.

Although outside of the thesis scope, it is worth mentioning that it is in the interest of the LFS-team to use the device. The goal is to use the device on competitions with the LFS-20 car.

1.3 Limitations

Due to time and resource constraints some related activities have to be excluded from the scope of this thesis.

- Design of the control software.

- Implementation of control software.
- Assembly of dual clutch into vehicle.
- Evaluation of the dual clutch's effect on laptime and car performance.

The challenge of designing and implementing the control software could be as big as the rest of this thesis and therefor it deserves to be a thesis on its own. Therefore, in this thesis, only the mechanical design of the device is considered.

After discussions within the Lund formula student team it was concluded that the most suitable timeslot for assembly of device into vehicle would be after the competitions in August 2019 in the car that is being designed and built during 2018/2019, the LFS-19. It would be a very large and stretched out thesis if the assembly of the device into the car was included.

It would be highly interesting to evaluate different differential concepts and control strategies and their impact on car performance and laptime through lap-simulation before making a concept choice. Unfortunately, at the moment, the Lund Formula Student team doesn't have a suitable vehicle simulation program that can evaluate yaw moment generating devices. Therefor this analysis had to be excluded from the scope.

The focus in this thesis is on the mechanical design of the device and not control or software. The device is intended for a RWD car, and therefor all discussions are based on RWD cars, unless otherwise is mentioned. Torque vectoring concepts that use the wheel brakes are not discussed because they are not a "final drive torque vectoring device".

2 Approach and methods

2.1 Project phases

In the initial plan, the project was divided in the following phases:

- Literature study
- Concept evaluation
- Feasibility analysis
- Concept choice
- Creation of system requirements specification
- 3D-CAD design
- Structural FE-analysis
- Creation of 2D-drawings and choice of manufacturing tolerances
- Parts ordering
- Assembly
- Testing

It started with a literature study where existing concepts were studied. A concept evaluation was made in order to decide which concepts to continue working with. An analysis was made on the remaining concepts to decide whether they were feasible to use in an FS car or not. A system requirements specification was made, partly based on the analysis. A conceptual design was then made in 3D-CAD. It was successively refined to a more and more detailed design, while iteratively confirming design choices (shaft dimensioning, bearing choices, material choices and so on) by hand calculations. When the design was detailed and mature enough, FE-analysis was performed on heavily loaded parts and the design was refined iteratively. Unfortunately, the time ran out at that point, ending up with a design that was 90% ready for the next step. The timeplan was obviously too optimistic to start with. Nevertheless, lots of progress has been made, and it is definitely possible to continue with the work and make the first prototype.

There is a quote that says: "Shoot for the moon. Even if you miss, you'll land among the stars". I think this is one of those situations.

2.2 Evaluation methods

One way to make choices is to generate lots of concepts or alternatives, rate them in some way and then pick the best alternative to continue with. A good thing with that methodology is the relatively low risk that a good alternative have been missed in the consideration. The problem is that it could be time consuming, and that a certain degree of knowledge about the different alternatives is required in order to make a rating that actually represents the expected performance. This approach was used in the comparison and choice of differential concept because that choice was very crucial to the outcome of the thesis.

However, when it comes to design choices, an iterative method was used instead in order to save time. There were many small decisions that had to be taken all the time. Should it be a roller bearing or a ball bearing? Screwed joint or welded joint? And similar questions. The iterative approach meant that for this type of questions, the alternative that seemed to be the best was chosen and the work was continued. If it later showed up to be bad, then it had to be changed and re-iterated. If the same method would have been used for these design choices as for the concept, then almost all time would be spent on making choices instead of designing.

In some cases experience from BorgWarner and Lund Formula Student was the only base for a choice and no time was spent on trying to justify it. Instead time was spent on solving other issues that there was less available information about.

2.3 Tools

Lap-time simulations were made in a Matlab based program from Lund Formula Student. Creo 2.0 was used for CAD. Structural FE-analysis was made in Ansys Workbench and spline dimensioning was performed in KISSsoft. Along with that, excel based in-house developed calculation tools from BorgWarner were used.

3 Theory

3.1 Why differentials are used

Consider a four wheeled RWD car with a standard combustion powertrain driving along a curved path, it is in a so called cornering situation. The outside wheels will have to travel a longer distance than the inside wheels at the same time, which means that the outside wheels have to rotate faster than the inside wheels. The front wheels are not interconnected with each other and therefor it is not a problem to have differing rotational speeds on them. The rear wheels on the other hand, are interconnected with each other because both of them have to be connected to the engine. Somewhere between the engine and the wheels, some device is needed to allow the two wheels to rotate with different velocity, but still be able to propel the car. The main function of a differential is to allow the driving wheels to rotate at different speeds while being able to apply driving torque [9]. The function of different types of differentials is further explained in the concepts section. Figure 7 shows the position of the differential in a RWD car.

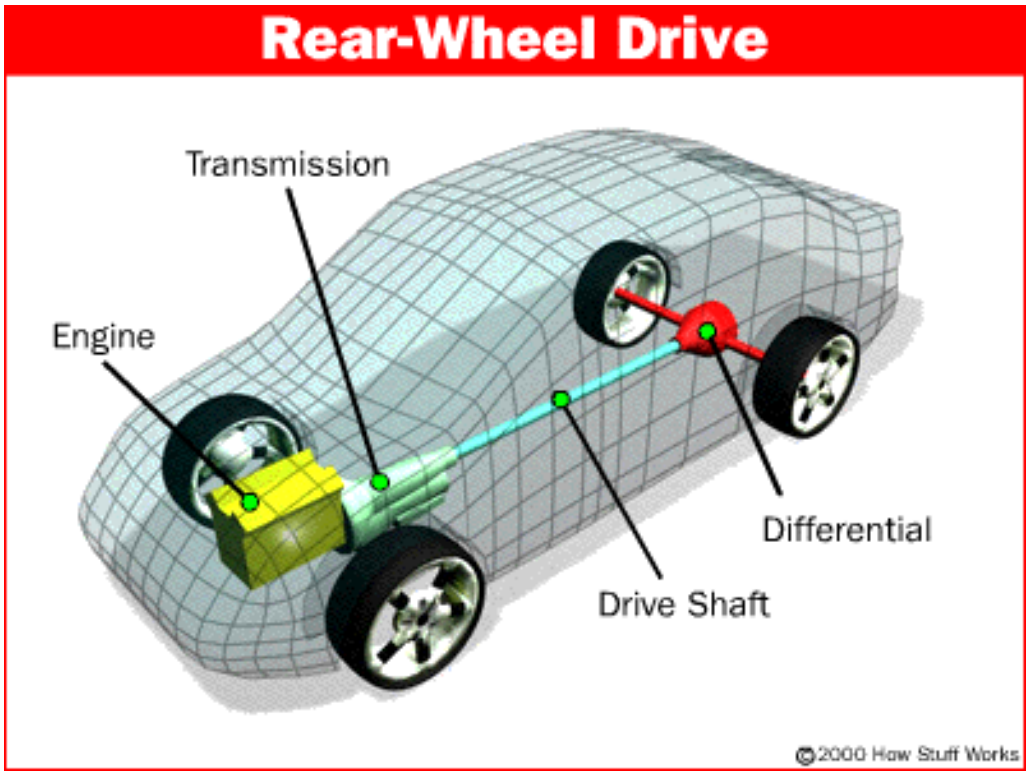

Figure 3: *Differential position on RWD car*

3.2 Torque vectoring

As discussed in the background above, transient maneuvers and stabilization is probably where torque vectoring shows its greatest benefits. A relatively advanced vehicle simulation tool would be needed to quantify the advantages in those aspects though. It was therefor decided that an analysis of that would be out of the scope for this thesis.

A third situation where torque vectoring improves the performance is in acceleration out of a corner. The available lateral tire grip will increase if more of the driving torque is sent to the outer wheel than the inner wheel. The result is a higher possible lateral acceleration, or in other words, higher cornering velocity. The idea is to distribute more torque to the outer wheel because it has more grip due to the higher normal load acting on it because of lateral load transfer.

An analysis was made based on the analysis in [10] using the vehicle data in table 2. It is a quite simple analysis with some rough approximations. The intention was only to prove the point

that TV is beneficial in cornering, and not to perform an exact analysis. A friction circle was used as a tire model, which means that the tires are just represented with a single friction coefficient. A coefficient of 1,7 was used because it seems to be good average, based on the result of the tire analysis seen in figure 27. A RWD car was assumed and the front tires are not included in the equations. No aerodynamic forces are taken into account. In the non-TV case, the same driving torque is assumed for both wheels, which is the case for an open differential. It is assumed that the inner wheel only takes longitudinal force and no lateral force in the non-TV case, which is of course a rough approximation. Further, it is assumed that the lateral load transfer distribution is in the same proportion as the front/rear weight distribution.

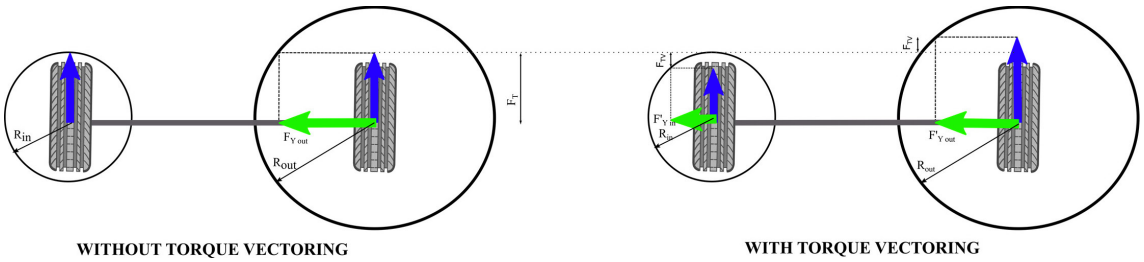

Figure 4: *Increase in net axle lateral force by torque vectoring*

The radius of the friction circle expresses the available grip in Newton. Static weight distribution, longitudinal load transfer and lateral load transfer were taken into account to find the normal load of the inner and outer rear tires. Pre determined values of a_y were used as input to equations 1 and 2. Equations 1-3 were solved iteratively to get the a_x that corresponds to the a_y used as input when the car driven on the tire grip limit.

$$R_{out} = \mu F_{z,out} = \mu(\frac{1}{2}(\frac{mgL_a}{L_{wb}} + \frac{ma_x h_{cg}}{L_{wb}}) + abs(a_y)\frac{mh_{cg}L_a}{L_t L_{wb}}) \tag{1}$$

$$R_{in} = \mu F_{z,in} = \mu(\frac{1}{2}(\frac{mgL_a}{L_{wb}} + \frac{ma_x h_{cg}}{L_{wb}}) - abs(a_y)\frac{mh_{cg}L_a}{L_t L_{wb}}) \tag{2}$$

$$a_x = \frac{F_x}{m} = \frac{2R_{in}}{m} \tag{3}$$

$$\Delta F_y = F'_{y,out} + F'_{y,in} - F_{y,out} = \sqrt{R_{out}^2 - (F_T + F_{TV})^2} + \sqrt{R_{in}^2 - (F_T - F_{TV})^2} - \sqrt{R_{out}^2 - F_T^2} \tag{4}$$

The potential increase in lateral force is shown in figure 5, where $0 <= F_{TV} <= F_T$.

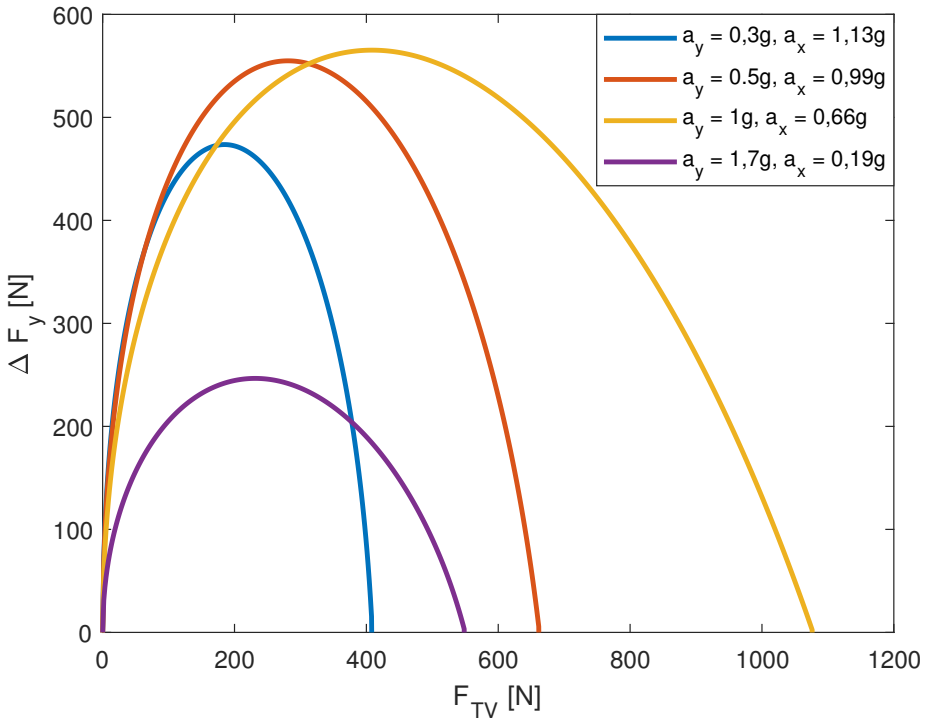

Figure 5: *Increase in net axle lateral force as a function of torque vectoring force*

The potential increase in lateral acceleration is given by:

$$\Delta a_y = \frac{\Delta F_y}{m} \tag{5}$$

$$\Delta a_{y,rel} = \frac{\Delta a_y}{a_y} \tag{6}$$

Figure 6 shows the relative potential increase in lateral acceleration.

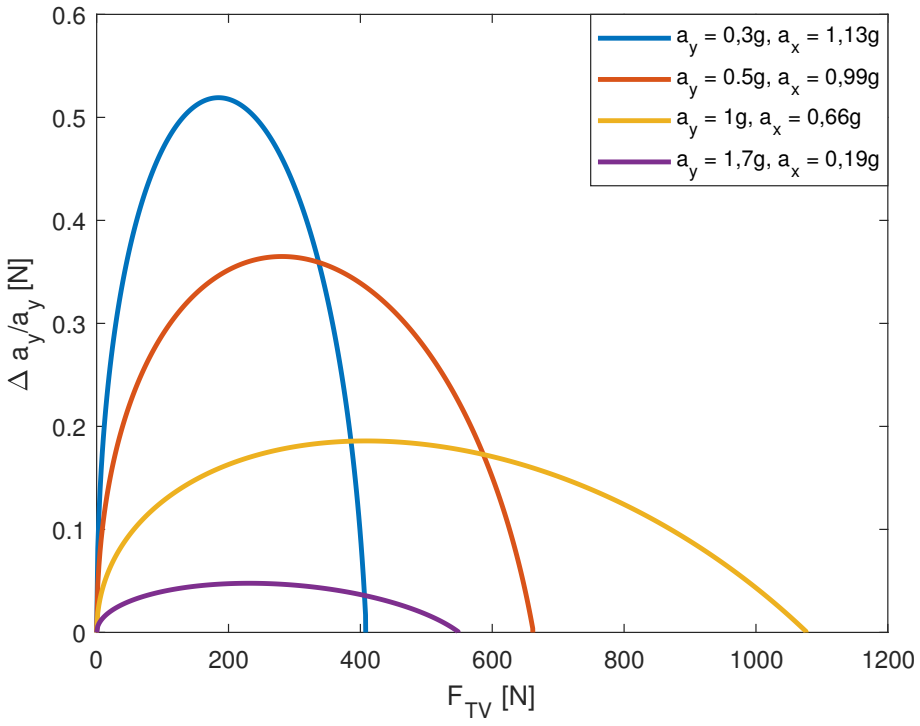

Figure 6: *Relative increase in lateral acceleration as a function of torque vectoring force*

It can be seen that there exists an optimal F_{TV} to maximize the possible lateral acceleration. It was derived analytically in [12] and it is shown in equation 7.

$$\Delta F_{TV,max} = \frac{F_T(R_{out} - F_T)}{F_T + R_{out}} \tag{7}$$

The conclusion of the simplified analysis is that torque vectoring makes the car quicker by allowing a higher lateral acceleration at a given longitudinal acceleration. In other words, the car can accelerate quicker out of corners.

3.3 Clutch model

A clutch model was needed for dimensioning of multi plate clutches. It was based on reference [18]. The axial clutch force in a multi plate clutch can be described by equation 8

$$F_c = \int_{R_i}^{R_o} 2\pi r p(r) dr = \int_{R_i}^{R_o} 2\pi r \frac{\text{constant}}{r} dr = 2\pi(R_o - R_i) * \text{constant} \tag{8}$$

By using $p(r) = \frac{\text{constant}}{r}$ together with equation 8, the pressure distribution over the friction discs can be described in equation 9.

$$p(r) = \frac{F_c}{2\pi r(R_o - R_i)} \tag{9}$$

Thus, the maximum friction disc pressure is:

$$p_{max} = p(R_i) = \frac{F_{c,max}}{2\pi R_i(R_o - R_i)} \tag{10}$$

The torque transferred by the clutch is described by:

$$M_c = \mu n \int_{R_i}^{R_o} 2\pi r^2 p(r) dr = \mu n F_c \frac{R_o + R_i}{2} \tag{11}$$

It shows that the effective friction force $\mu n F_c$ is acting on the mean radius $\frac{R_o+R_i}{2}$. Equations 10 and 11 together give the maximum transferrable torque, or torque capacity.

$$M_{c,max} = \mu n(2\pi p_{max} R_i(R_o - R_i))\frac{R_i + R_o}{2} = \pi n \mu p_{max}(R_i R_o^2 - R_i^3) \tag{12}$$

With two friction surfaces per disc, the following equation shows the torque capacity per disc.

$$\frac{M_{c,max}}{n_{discs}} = 2\pi \mu p_{max}(R_i R_o^2 - R_i^3) \tag{13}$$

4 Differential concepts

There are different types of differentials. The main difference between the concepts is how the torque is distributed between the driving wheels. The torque distribution has a large effect on the handling of the vehicle because it affects the yaw moment. In this section, some of the most common concepts are presented and discussed briefly. First the classic concepts presented so the reader can easier understand the benefits with the more advanced concepts. The active differential concepts that are presented are the most simple ones. There are other more complex concepts with planetary gearsets and electric motors for example, but they are not discussed because they are too complex for the scope of this thesis anyway.

4.1 Open differential

The open differential is maybe the most common type of differential used on cars, due to simplicity, reliability, safety and low cost compared to other alternatives. Its main characteristics is that it always gives the same torque to both wheels (if losses are neglected) and that the input velocity is the average of the two wheel velocities.

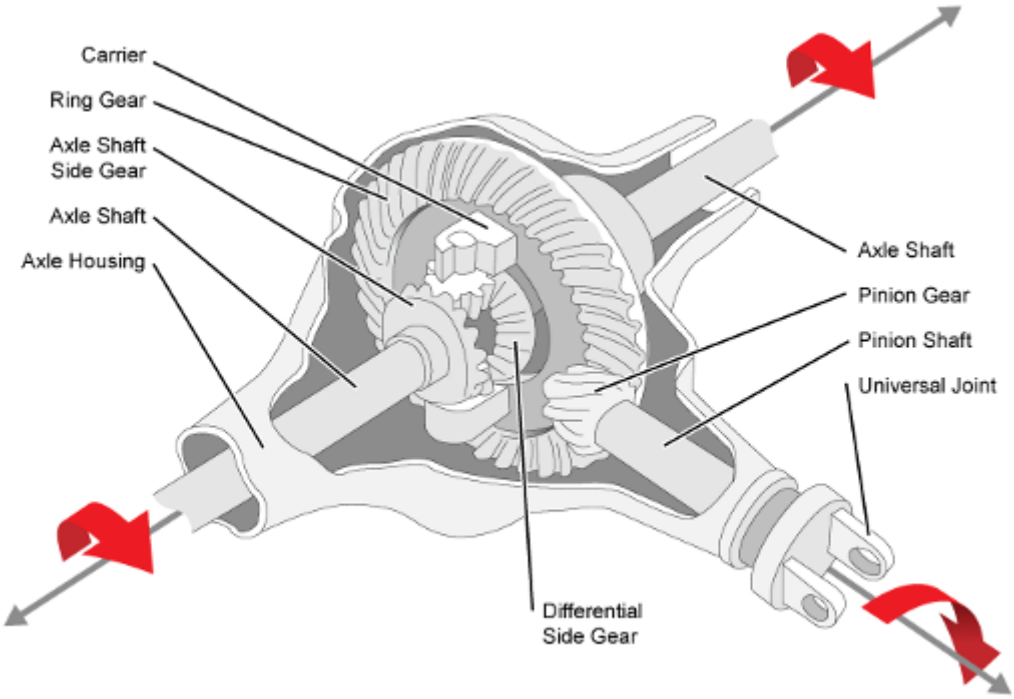

Figure 7: *Open differential*

The open differential will not induce any yaw moment on a car with driven wheels of the same radius. This leads to a car that is predictable and easy to drive. There will be no sudden changes in vehicle behaviour when hitting the throttle or letting go of it. The open differential is less suitable for racing purposes though. The most problematic situation is at corner exit, when the driver wants to accelerate out of the corner. The inner driving wheel will have less grip than the outer driving wheel due to load transfer. Therefor the inner wheel will lose traction and start spinning. The outer wheel will get the same driving torque as the inner wheel due to the principle of how the differential works. This means that the outer wheel will have grip that is unused and the car will not accelerate as quick as it could if the tire grip was used more efficiently.

Another problem with the open differential is when driving on uneven ground or icy surfaces where the available grip is different for the wheels. If one driven wheel is on ice, it will literally have no grip at all, which means that the car will get stuck. Some kind of differential locking is therefor usually used on terrain vehicles.

4.2 Spool and locking differential

The opposite of a differential is to not have a differential and instead just lock the driving wheels together. That results in equal velocity for left and right wheels, and unequal torque distribution. The difference in driving torque could theoretically be infinite, but there are of course practical limits to this.

Not permitting the driving wheels to rotate at different speeds will lead to increased tire wear due to scuffing. It can also lead to high forces on the drivetrain when turning sharp with the car on high grip surfaces.

The wheels can either be connected with a spool (figure 8), or with a locking differential (figure 9). A spool is just a solid axle that connects the wheels. A locking differential is a normal open differential that has the possibility to lock the wheels together when needed, usually with manual operation. This is common on terrain vehicles.

Figure 8: *Spool*

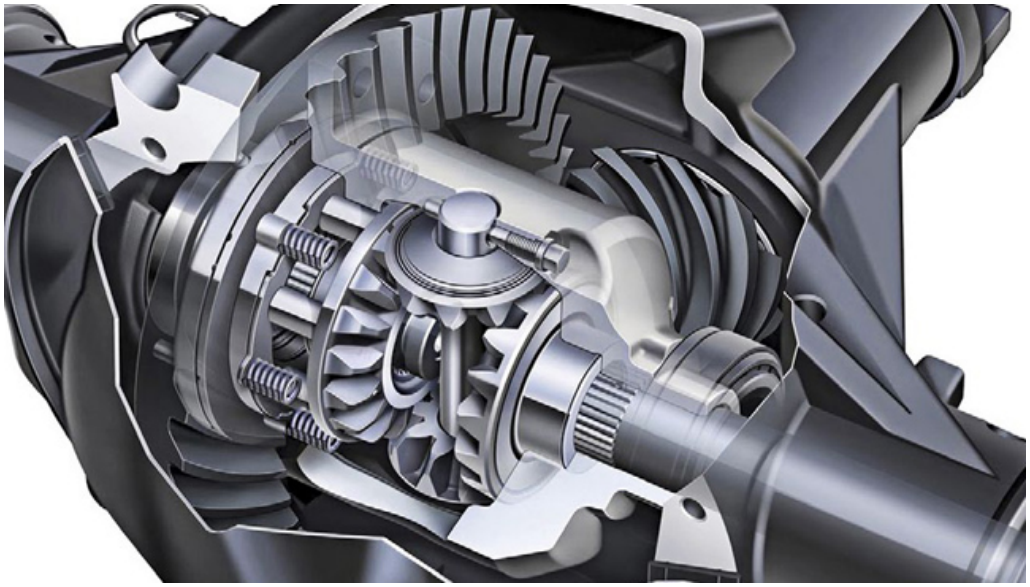

Figure 9: *Locking differential*

Using a locked axle is common in drag racing. Those cars are just going straight and therefor no differential is needed. With an open differential there would still be a risk that one of the wheels start to spin because it has slightly less grip than the other wheel. This would lead to a loss in acceleration because all available longitudinal grip would not be used.

The effect of a locked axle on the vehicle behaviour is a bit more complicated than the open differential. It has a stabilizing effect on the car in the linear and transitional region of the tire, the car will tend to understeer. On a RWD car, this can quickly become the opposite when the driver applies throttle at corner exit [19].

The understeering tendency can be explained with a simplified example. Consider a car driving in a corner. The outside wheel has a longer path to roll than the inside wheel at the same time, but the wheels are rolling with the same velocity because they are locked together. The road force acting on the wheels will therefor try to slow down the outside wheel and speed up the inside wheel. Those forces create a yaw moment that is opposite to the corner direction, and thus tends to understeer the car.

If the driver hits the throttle hard at corner exit, the wheel torques will start to increase. The rear wheels will then start to spin and lose traction, both in longitudinal and lateral direction. This can lead to snap oversteer due to the sudden change in direction of the yaw moment acting on the car. It is needless to say that a really good driver is required to be able to drive a locked axle car at full potential on a racetrack.

What would happen with an open differential car in the same situation? The inside wheel would start to spin and lose traction. The outside wheel would still have grip though and thus be able to take up lateral force, especially since there is not much longitudinal force on it. It would be a far less surprising situation, without any snap oversteer. But on the other hand, the longitudinal grip potential would also be lower already from the start.

It is worth mentioning that some chassis parameters can be altered to reduce the initial understeering tendency of a locked axle. The normal load on the rear inside wheel can be reduced (or eliminated by lifting it off the ground in the most extreme case) when cornering. Most of the lateral and longitudinal force (or all of it) will then be handled by the outside wheel. The car will suffer less from the initial understeer mentioned above, because the yaw moment contribution from longitudinal force will tend to oversteer the car already from the start. This should also reduce the snap oversteer effect because it is already oversteered from the start. This is probably a good recipe for a spooled car, but on the other side, total tire grip is decreased when one tire is in the air, due to the increased load on the other tires and load sensitivity.

The inside rear wheel will receive less normal load with increased front castor angle, or by biasing the lateral load transfer distribution further to the rear. This can for example be achieved through increased rear anti-roll bar or spring stiffness or through decreased front anti-roll bar or spring stiffness. Going into detail with this is far beyond the scope of this thesis.

4.3 Limited slip differentials

A limited slip differential is a blend of the open differential and the spool. The axle shafts are connected to the carrier with a torque transferring device. If the device is fully open and do not transfer any torque, the LSD will behave as an open differential and T_c equals zero in equation 14. On the contrary, if the device is locked, it will behave like a spool and T_c can be seen as infinite. If the device can transfer a limited amount of torque, it will allow a certain limited difference in torque between the wheels. The amount of locking action can be constant, proportional to input torque (torque sensing LSD) or proportional to wheel velocity difference (speed sensing LSD). Only torque sensing LSDs will be further discussed because they are much more common in racing vehicles.

Equation 14 describes the maximum torque difference for a torque sensing differential

$$T_l - T_r \leq sgn(\omega_l - \omega_r) * T_c \tag{14}$$

$$T_c = C * T_{in} + B \tag{15}$$

where sgn gives the sign of the expression. T_c is the torque transferred by the differential clutch and is described in equation 15. There is a proportional term C and a constant B, where B is the maximum torque difference with $T_{in} = 0$, also called torque preload. Torque sensing differentials can be divided into three categories, 1-way, 1,5-way and 2-way. In a 1-way LSD C will be zero if $T_{in} < 0$. In a 2-way LSD C will be the same regardless of input torque direction. A 1,5-way LSD has different C depending on input torque direction. T_{in} is positive for driving torque and negative for braking torque applied to the differential. Normally the braking torque only comes from engine braking. In rare cases a single inboard brake is used then that will also contribute to the differential braking torque.

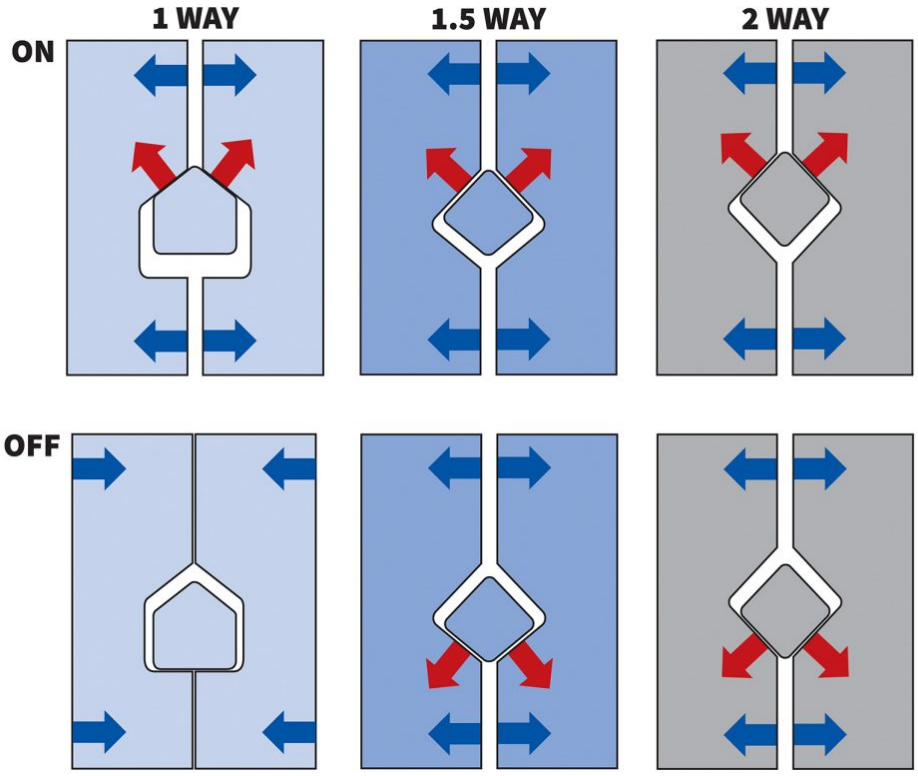

Figure 10: *1-way, 1.5-way and 2-way LSD principle*

4.3.1 Salisbury differential

The salisbury differential uses two clutch packs to achieve a locking action. The clutch packs are preloaded with a spring, and also compressed proportionally to the input torque through the ramps. The Drexler LSD is a 1,5-way salisbury differential commonly used in Formula student vehicles and is shown in figure 11. The proportional constant can be changed by changing the ramp angle.

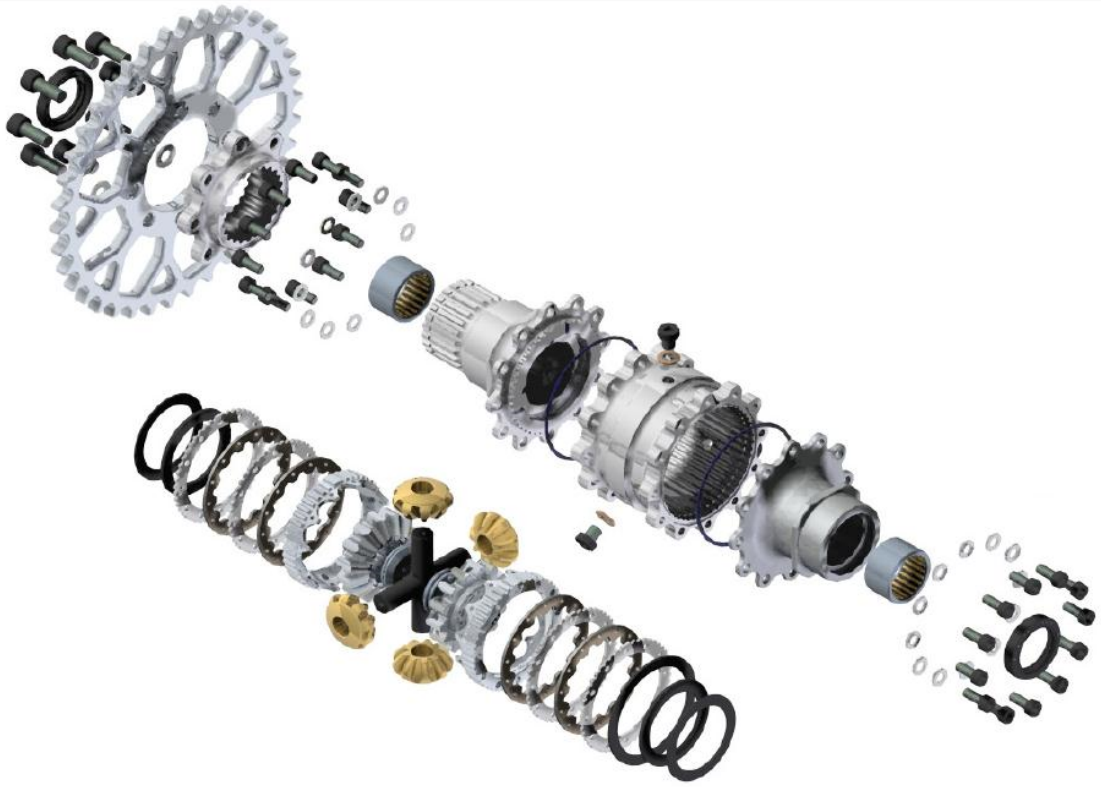

Figure 11: *Drexler limited slip differential for Formula student*

The differential will behave like a spool when the torque difference between the wheels is less than the torque that the clutch can transfer when not slipping. In this case, the torque distribution between the wheels will be determined by the normal load, slip ratio, camber and slip angle. When the torque difference increases and reaches the maximum torque that can be transferred by the clutch, the clutch will instead determine the torque difference. It is always the slower wheel that will have the higher torque.

The behaviour is reminding of the locked axle described above. In the same way there will be an understeering tendency with the LSD as well. When the wheel with the least amount of grip starts to loose traction and spin, torque will still be transferred to the other wheel. Torque can only be transferred from the faster wheel to the slower wheel. This means that the inner wheel will still spin, like with the open differential, but more torque can be transferred to the wheel with more grip.

4.3.2 Torsen

The Torsen differential is another type of LSD. It uses helical gears with high helix angle to produce the friction that locks the differential. One difference in the behaviour between the Torsen and the Salisbury is that the Torsen has little or no torque preload. If one wheel is in the air, the Torsen will work as an open differential so it will not be able to transmit any torque to the other wheel. For more details see [19]

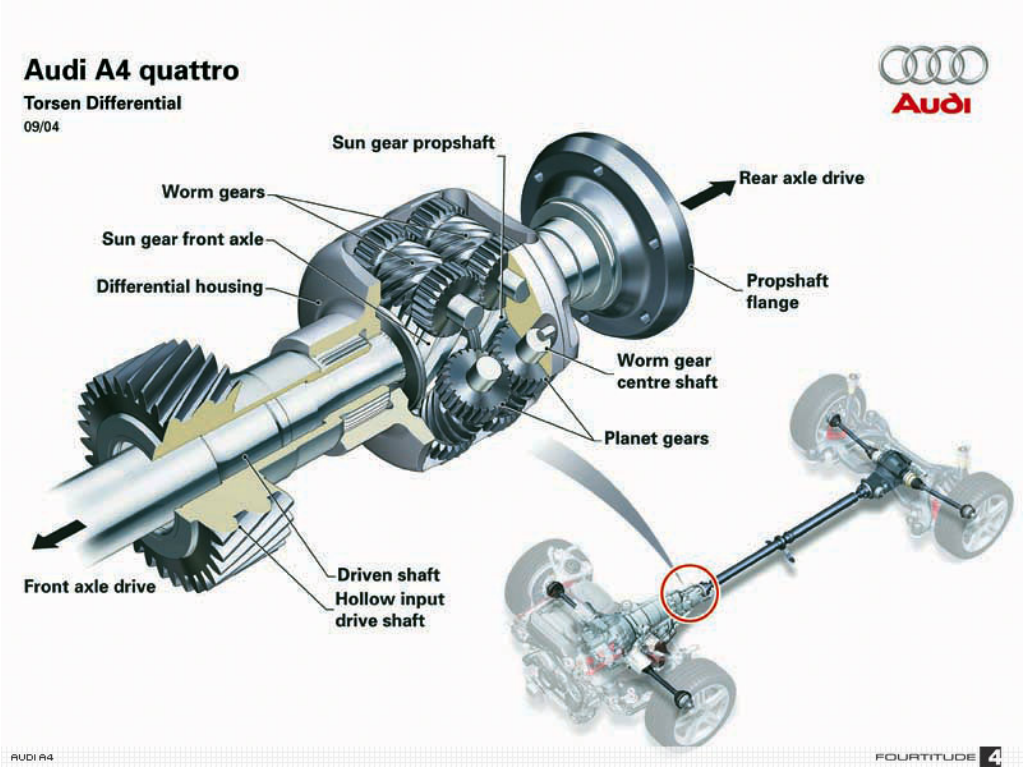

Figure 12: *Torsen T-1*

4.3.3 Electronic LSD

The eLSD works as a normal passive LSD but with controllable locking torque. This means that it can work both as an open differential and as a locked axle, and everything in-between. A computer runs a control algorithm that first determines the desired locking torque at the instant, and then sends a signal to some kind of actuator to actually apply the desired torque. Various sensors are used to determine the desirable locking torque, typically input speed, wheel speeds and yaw velocity is used for the calculation [11]. Throttle position, longitudinal and lateral acceleration, steering angle and brake pressure are other signals that could be used to refine the control algorithm.

The active control of the differential makes it possible to adjust the locking torque to suit the current driving condition which improves the grip in general. Vehicle stability is also improved, which is maybe the most important aspect. One example on this is to again consider the case of snap oversteer with a spool axle. At the instant when the rear end starts to lose traction, the eLSD could decrease the locking torque. That would lead to spinning of the inside wheel, but the outside wheel would still maintain traction and by that, decrease the sudden grip loss. It would result in a more stable car and give the driver more confidence when driving close to the performance limit.

The BorgWarner FXD is a front axle differential clutch used in FWD cars, for example VW Golf GTI and Ford Focus ST. The clutch connects one of the axle shafts to the carrier and is shown in figure 13. The grey shaft is the axle shaft and the purple shaft is connected to the carrier. The clutch is connecting the two shafts. The hydraulically actuated yellow piston compresses the clutch pack to increase the locking torque. The hydraulic pressure is created by an electronic actuator (not visible in figure) which in turn is controlled by a computer.

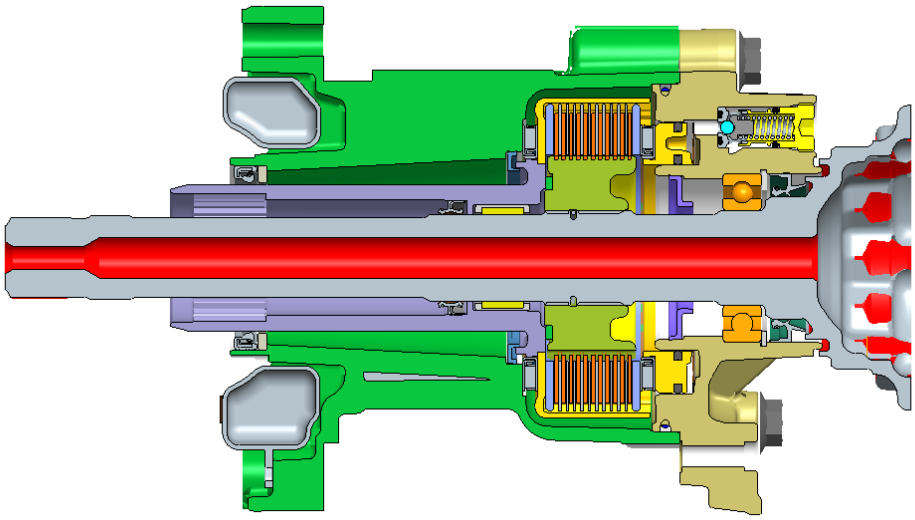

Figure 13: *BorgWarner FXD, electric LSD clutch*

4.4 Open differential with two clutches

One way to get torque vectoring possibility is to use an open differential and use a device to add torque to one of the axle shafts. An example is shown in figure 14. A layshaft is added to an open differential. The layshaft is driven by the differential carrier, but with a gear ratio that makes the layshaft rotate faster. The layshaft is connected to each of the axle shafts via a normally open clutch and a gearset. By partially engaging one of the clutches, torque can be transferred from the layshaft to the axle shaft on the same side as the clutch, provided that the layshaft rotates faster than the axle shaft. The clutches have to be actuated by some kind of device, electro-hydraulical or electro-mechanical for example.

It is a relatively simple and intuitive concept, but requires many gears and clutches which leads to high weight, space requirements and cost.

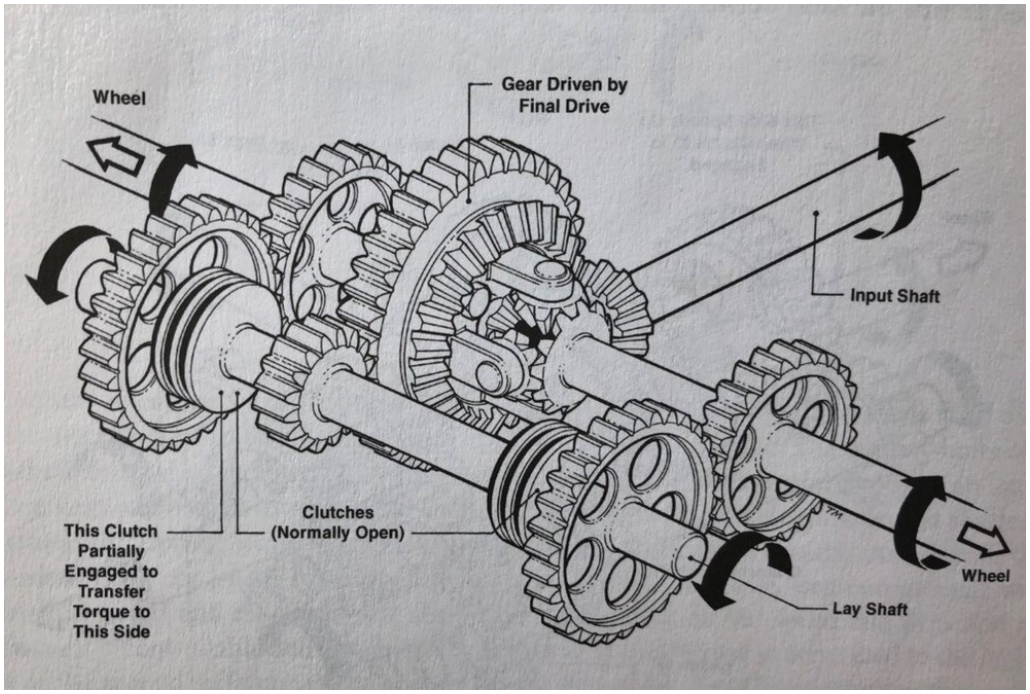

Figure 14: *Open differential with torque vectoring [20]*

The Mitsubishi Active Yaw Control uses a similar concept. The difference is that both clutches are connected to the same axle shaft. The layshaft is used to speed up one clutch and slow down the other clutch. Depending on which clutch is actuated, it either "gives" torque to the shaft or "takes" torque from the shaft. The system is shown in figure 15. The torque flow is shown in figure 16. The latter is the newer version with a planetary gear differential, but it works with the same principle.

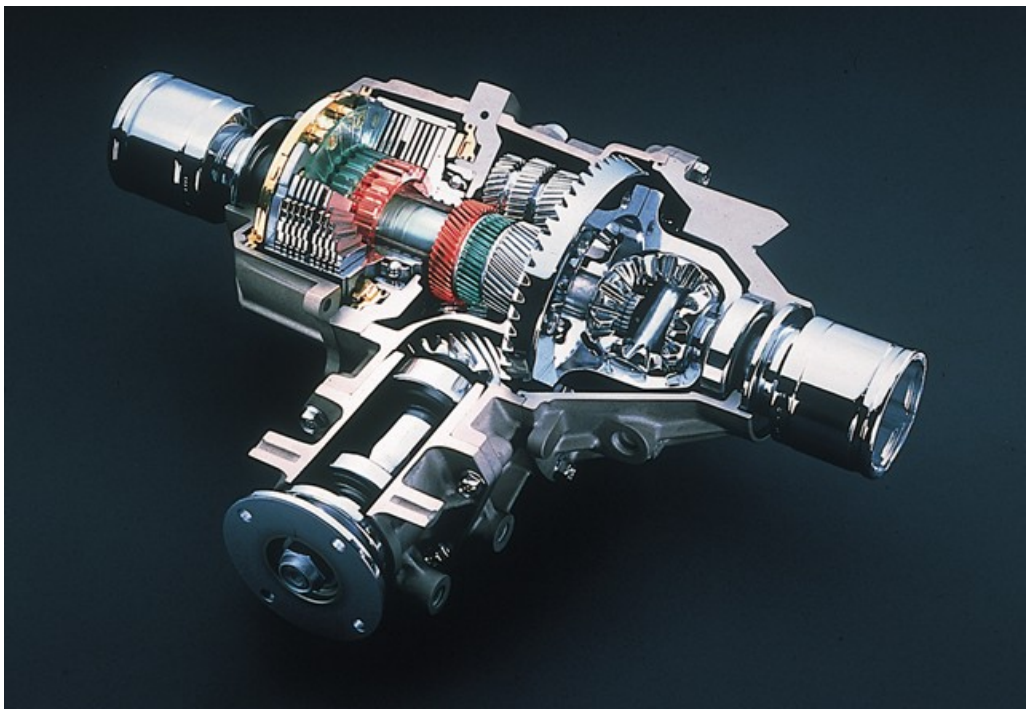

Figure 15: *Mitsubishi AYC with bevel gear differential*

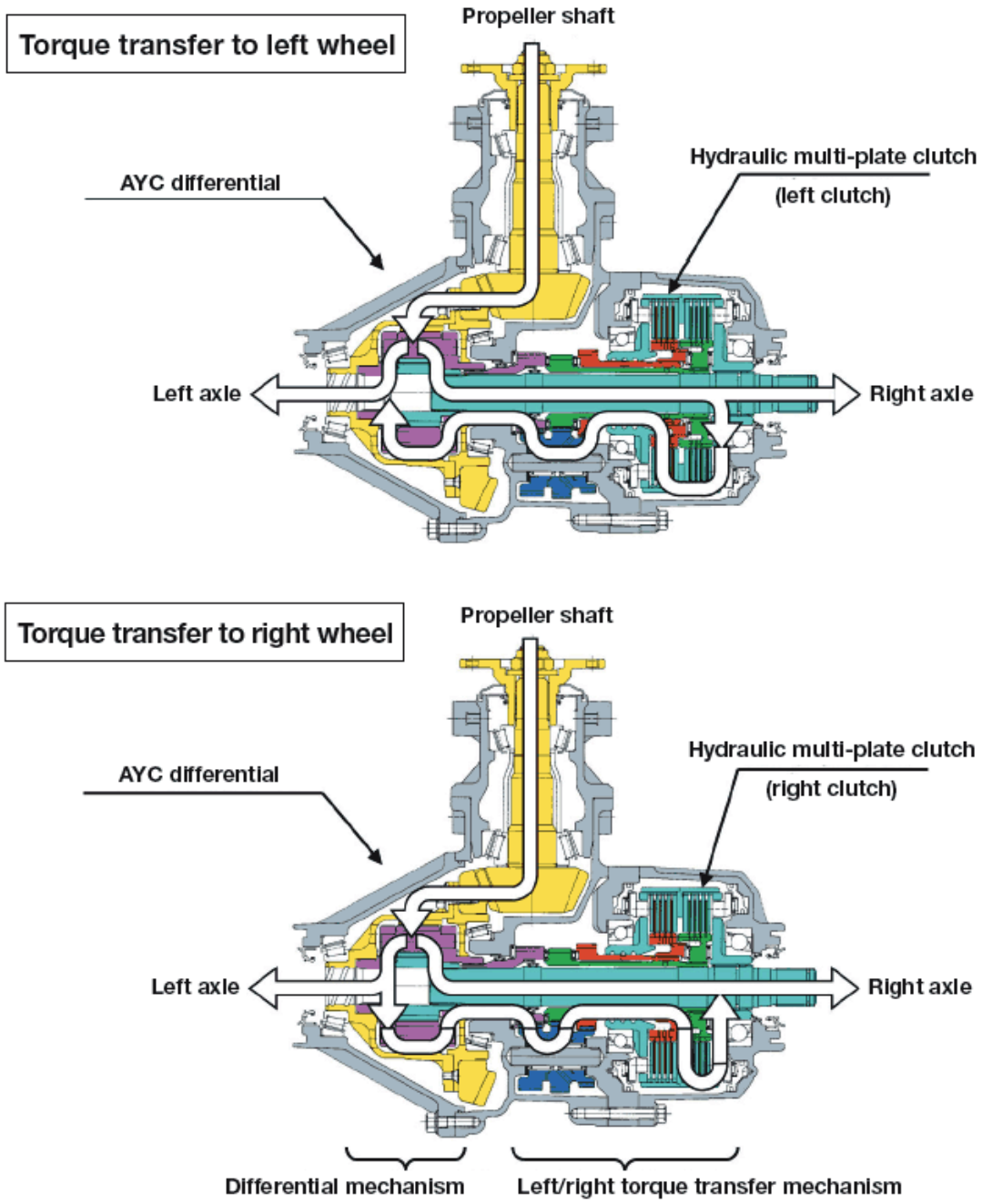

Figure 16: *Mitsubishi AYC with planetary gear differential*

4.5 Dual clutch

The dual clutch concept uses two independently controlled clutch packs that are connected to their respective wheel. It allows the wheels to rotate with different speeds if controlled properly and allows torque to be distributed independently between the wheels. In contrast to the eLSD, it is possible to apply more torque on the faster wheel than on the slower wheel. This concept does not use any differential, it only uses two clutches.

When driving in a corner, the outside wheel can have a fully closed clutch (no clutch slip) while the inside wheel clutch is partially open and slipping, transferring a controlled amount of torque. The outside wheel torque can be calculated, if the input torque is known. The yaw moment contribution can be calculated from the wheel torques and that can be used in a control algorithm to control the yaw rate. Both clutches can be disconnected simultaneously so there is also a possibility to use it for launch control when doing a fast start from standstill.

The clutches have to be actuated by some kind of device, electro-hydraulical or electro-mechanical for example. The concept can be implemented both with normally open (NO) and normally closed (NC) clutches. NO is suitable if it is used on the rear axle for an on demand AWD application with possibility for torque vectoring. Then it can easily be disconnected by not actuating the clutches, and the vehicle becomes FWD. If it is used as a permanent drive, for example permanent RWD, then an NC clutch could be suitable in order to possibly decrease the amount of actuation needed on the clutches.

GKN Twinster is a product that is already on the market. It is used in cars with on-demand AWD on the rear axle. It is shown in figure 17.

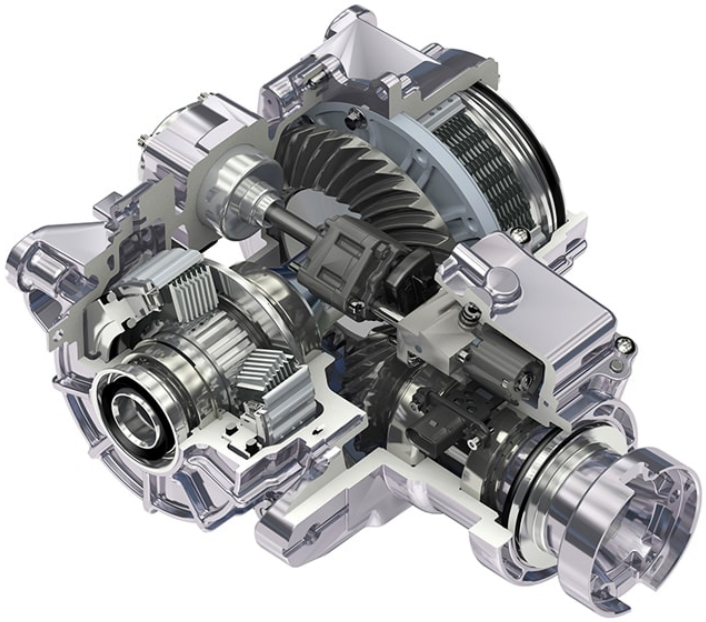

Figure 17: *GKN Twinster*

5 Concept evaluation

Three of the presented concepts above allow active control of the cross axle torque; eLSD, open differential with two clutches and dual clutch. The dual clutch was split into two different concepts, one NO and one NC dual clutch. A comparison was made in order to evaluate which of them is the most suitable for a Formula Student car.

The concepts were rated from 1 to 5 by the author, where 5 is the best, according to four different criterions that were considered to be of high importance. Torque distribution freedom is the ability to distribute torque independently between the wheels. The more freedom, the better the possibility to produce the desired yaw moment at any instant. Mass and size speaks for itself. Robustness is graded by the consequence if something fails. Design complexity is graded by an estimation of how much time, competence and money it takes to make a device that is working. The scoring is shown in table 1.

	eLSD	**Open differential with two clutches**	**Dual clutch NO**	**Dual clutch NC**
Torque distribution freedom	2	5	4	4
Mass and size	4	1	4	3
Robustness	5	5	3	5
Design complexity	3	1	4	3
Sum	**14**	**12**	**15**	**15**

Table 1: *Concept comparison*

The eLSD got a lower grade in torque distribution freedom than the other concepts. An LSD can only give more torque to the slower wheel than the faster wheel and not vice versa. The open differential with two clutches can do both. The dual clutch will primarily give more torque to the faster wheel, if it is assumed that the faster clutch is controlled so that it is not slipping. It is possible to give more torque to the slower wheel as well, but only if both clutches are slipping. The most common case with torque vectoring is to have more torque on the faster outer wheel.

When it comes to mass and size, the open differential with two clutches is the worst because it contains a differential, two clutches that need electronic actuation and six gears (excluding the differential). The eLSD has one electronically actuated clutch and one open differential, which could be fitted in a relatively neat package. The dual clutch can also be made compact. The NC-clutch is a bit worse due to the need for springs and therefor also more complicated actuation.

The NO dual clutch was deemed to have lower robustness than the other alternatives. If the control signal has to be turned off, perhaps due to a broken sensor, bad power supply or overheating of the differential unit, the car will not have any propulsion at all. The NC dual clutch will become a locked axle if electricity is turned off and the other two concepts will behave as normal open differentials, which means that they will still be able to propel the car. In Formula Student, testing time is usually critical. It is therefor definitely positive if a system that is not working well can be turned off so that the car testing can still be continued until the problem is fixed.

The design complexity grading almost follows the mass and size grading. The argument is the same, the more different subsystems, the more there is to design.

The open differential with two clutches recieved the worst total score. It is probably a very good concept for a larger car, but for an FS car it is too large and heavy. Also it is very optimistic to believe that a complex concept like that can be realized within the scope of a master thesis. This concept was therefor excluded.

The rest of the concepts recieved a very similar score. The eLSD has similar or worse design complexity than the other two concepts, but it has less torque distribution freedom, which means less performance gain for the same design effort and cost. It was therefor also excluded.

It was decided that both of the remaining concepts should be further analyzed in order to learn more about their characteristics and through that be able to make a good choice. It was also a bit worrying that no other application of the dual clutch concept as a permanent drive could be found. Would the continuous clutch slippage lead to excessive heat generation and insufficient efficiency in a permanent drive application?

6 The chosen concept

In this subsection the chosen concept of the normally closed dual clutch is presented and an alternative choice is briefly discussed.

It started with a hand drawn concept that was inspired by a BorgWarner product for an AWD-application that never made it to mass production. The sketch was refined iteratively and the final version is shown in figure 18. No other concepts were generated due to lack of time. It was instead prioritized to continue with the design of the chosen concept which seemed promising.

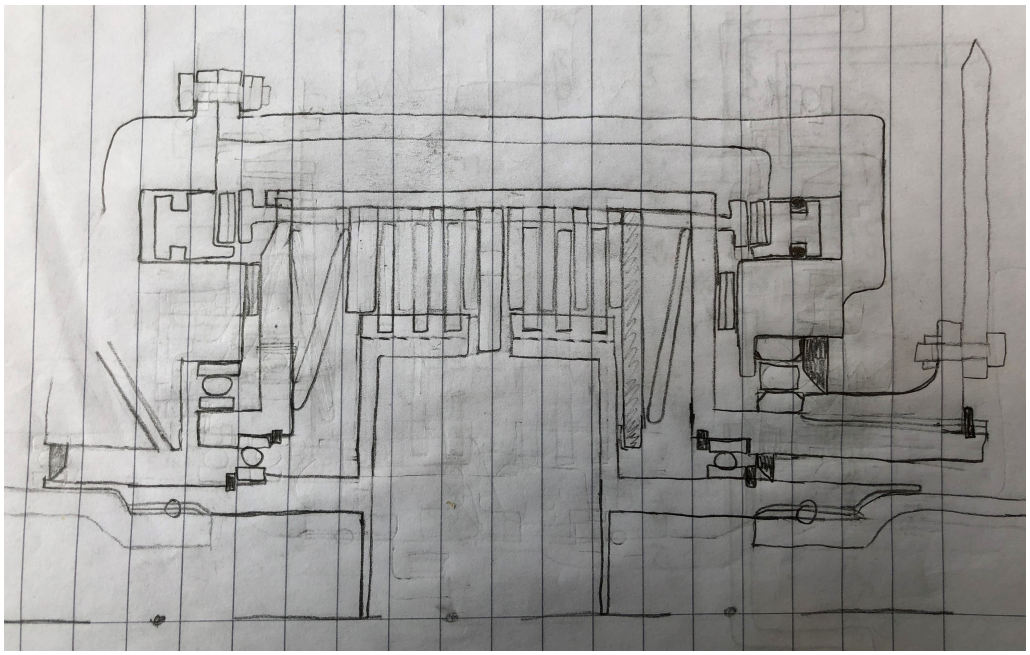

Figure 18: Dual clutch concept sketch

Some initial hand calculations were made for the sizing of the clutches, springs, pistons and shafts and a CAD-model of the concept was created. It is presented in figures 19 - 21. Some parts are missing on the pictures, but the general idea can be seen anyway.

The location of the unit is behind the engine, centered between the rear wheels of the car. The output shaft of the engine and gearbox is located on the left side. The driving torque is transferred to the input sprocket on the dual clutch via a chain. The sprocket transfers the torque to the sprocket carrier (grey) that is connected to the clutch drum shaft (turquoise) via splines. The clutch drum shaft transfers the torque to the outer friction discs (grey) through splines in the clutch drum. Friction transfers the torque from outer to the inner friction discs (brown) and the torque is further transferred to the hubs (blue) through splines. Each hub is connected to its tripod housing via splines and the torque is transferred from the hub to the driveshaft via a tripod joint. For a better understanding see appendix B.

The axial force in the clutch pack comes from the preloaded disc springs that are located on the outside of the thick outer friction disc of each of the two clutch packs. The red mid disc acts as a wall between the clutch packs and takes up the axial force from each clutch pack. It is located in a machined slot in the clutch drum and axially fixed by resting against the side face of the splines in the clutch drum, see figures 47 and 48. Some kind of rotational fixing is also needed for the mid disc, but missing in the pictures. Two hydraulic actuators, one for each piston, produce a hydraulic pressure in the pocket behind the pistons (yellow). The pocket can be seen in figure 20 where one housing half is included. The hydraulic pressure gives rise to an axial piston force that is transferred to the thick outer friction disc through the push cage (green). This force acts against the disc spring. An increase in piston force leads to a decrease in clutch compression force, and thus also a decrease in clutch torque capacity.

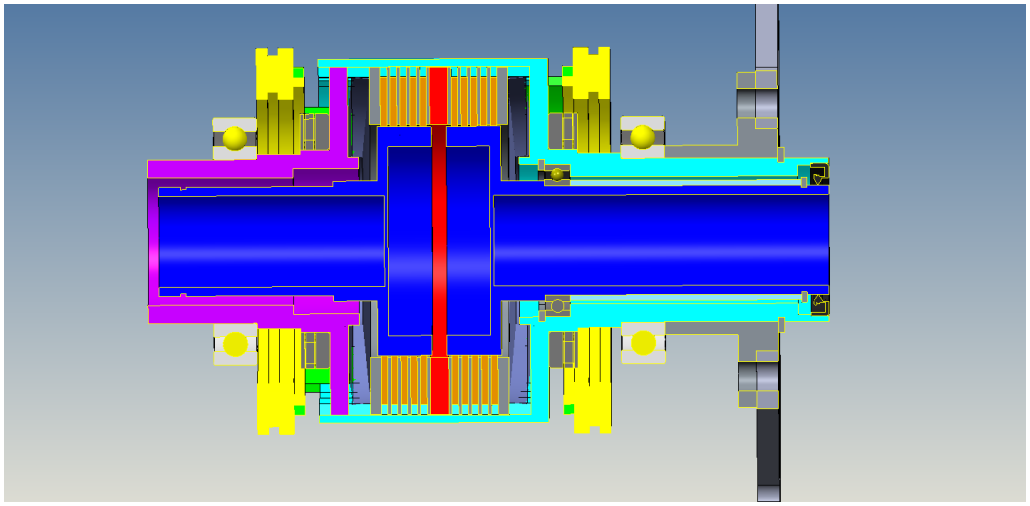

Figure 19: Normally closed concept

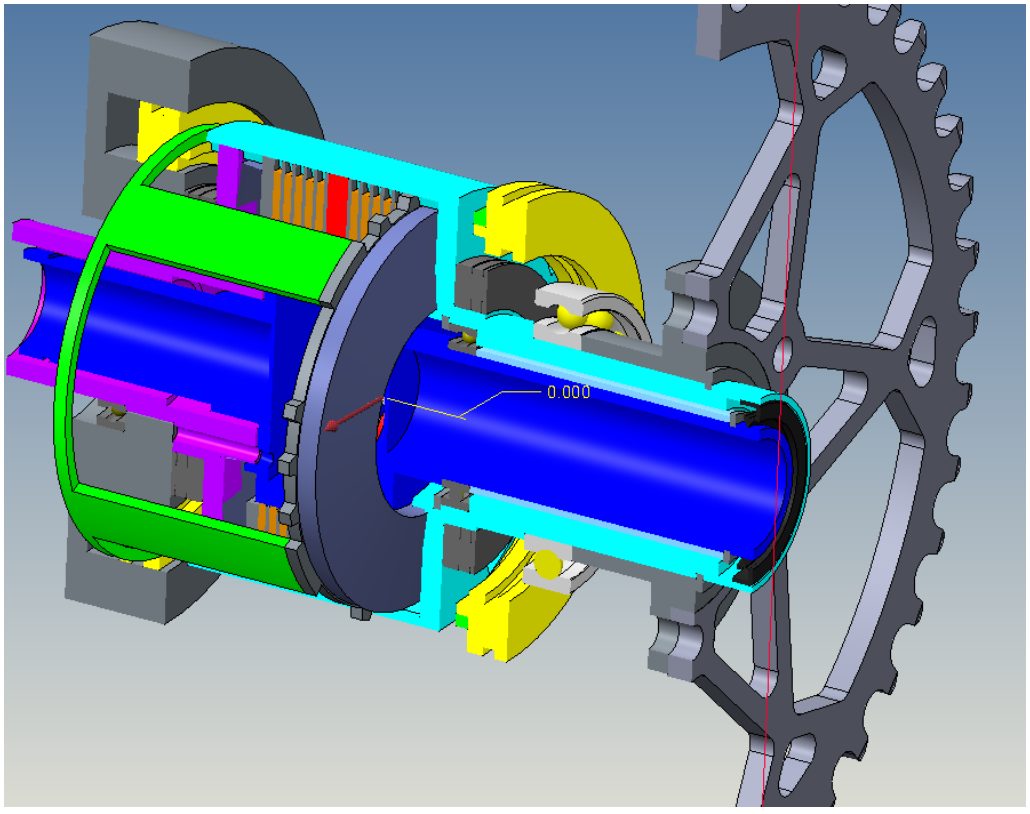

Figure 20: Normally closed concept with part of housing included

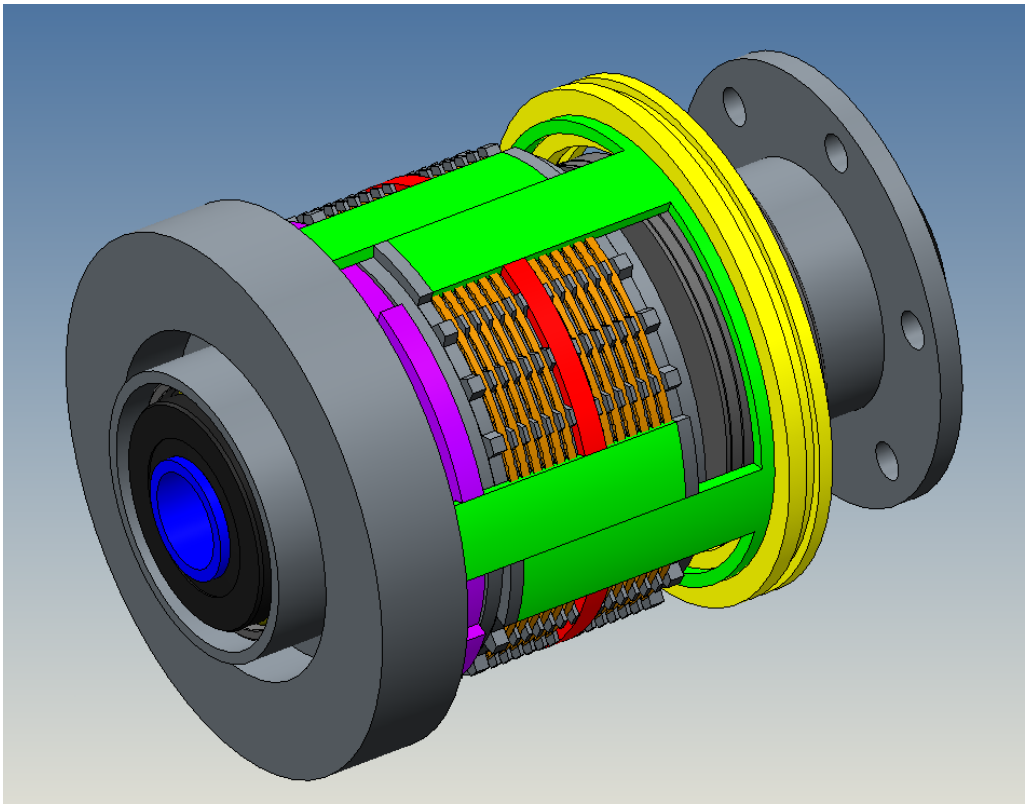

Figure 21: Normally closed concept with part of housing included

Two different locations of the input sprocket were considered. One alternative was to put it axially centered and directly connected to the clutch drum (outside the red mid disc in figure 19) and one was to have it on the left side of both clutches, asymmetrically (as in figure 19). A centered location would lead to a shorter load path from chain force to outer clutch discs and would also result in a shorter unit overall which could result in lower weight. The downside is that the housing would have to be split in two halves at the sprocket interface which gives rise to some challenges. One would be to seal the interfaces between housing, sprocket and clutch drum. The other would be to handle the axial load created by the pistons since the housing halves can not be in straight contact due to the rotating sprocket that is in the way. It would either require a bracket that goes around the sprocket to connect the housing halves and take the axial force or the force have been sent through the shafts somehow. In either way it would be a heavy and/or complex design. The asymmetric solution was chosen because of its lower complexity.

The chosen concept has now been presented. A deeper look will be taken into the analysis and design of the different subsystems of the dual clutch in the following subsections.

7 Dual clutch concept analysis

An analysis of the dual clutch concept was made to confirm the feasibility in a race vehicle application since no information about a similar study could be found. The difference between the NO and NC concepts was also further explored. Focus was put on calculation of transmission efficiency and energy consumption to identify eventual heat and power supply problems. Further, the required torque capacity of the clutches was derived. The complexity and detail of the analysis had to be kept down so that it would not take up too much of the already short design time. A lap-time simulation software was used as a base, developed in Matlab in-house by Lund Formula Student. It was therefor possible to adapt the software to include a model of the dual clutch. Unfortunately, it was not possible to evaluate the effect of TV on vehicle performance in the software. Making a simulation model in a more complex software to evaluate the effect of TV was considered to be out of scope for this thesis.

7.1 The lap-time simulation software

7.1.1 In general about the software

The feasibility of the dual clutch concept was evaluated with the use of a lapsim software. It is based on a simplified four-wheel model, which is a point mass model that takes normal load distribution between the wheels into account to include the effect of tire load sensitivity. The tire data input is two functions, lateral friction coefficient vs normal force and longitudinal friction coefficient vs normal force. The suspension is modeled as completely rigid and the ground is completely flat. The lateral load transfer distribution is the same as the static longitudinal weight distribution. No yaw inertia/moment is included in the model, which means that the effect on vehicle performance from driving torque distribution between the wheels can not be evaluated.

The simulation is based on a GGV-diagram that is generated from the vehicle data parameters. The surface shows the acceleration limit in lateral and longitudinal directions combined, as a function of velocity. The vehicle acceleration is always on this surface, which means that it assumes a perfect driver that is always on either the power limit or the grip limit. A GGV-diagram based on the data in tables 2 and 3 and figure 27 is shown in figure 22.

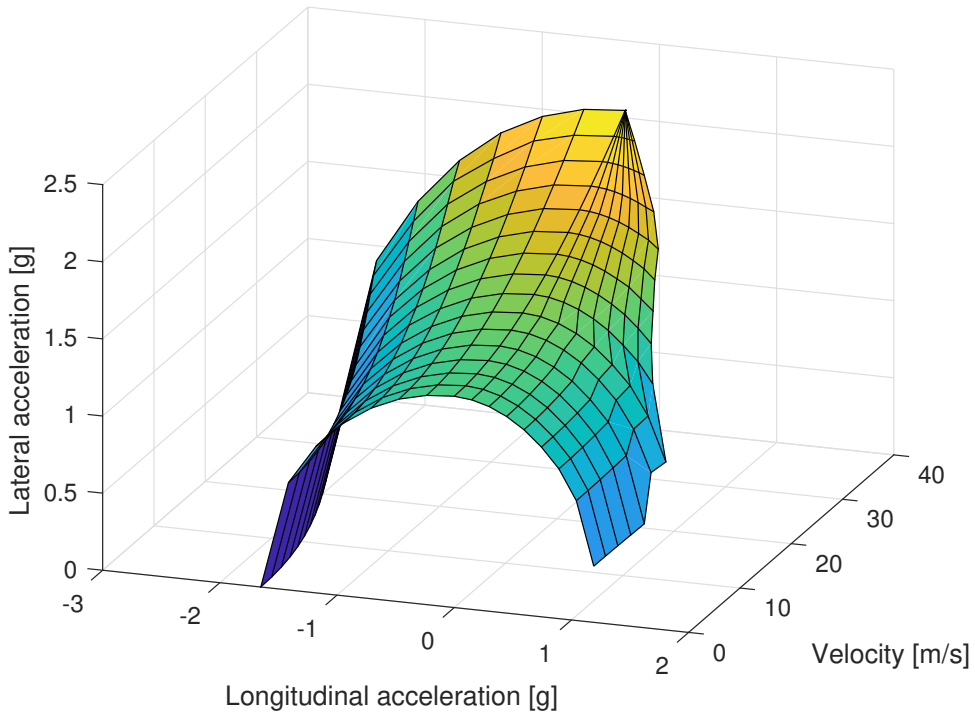

Figure 22: *GGV-diagram*

The track data is entered as sections with length and a constant radius, where the typical section length for the available data is around 1 meter. All apexes are identified to begin with and then the maximum possible velocity in each apex is calculated with the assumption that the longitudinal acceleration is zero. An apex is defined as a section where both the previous and the next section have a larger radius, i.e the tightest part of a corner. The maximum possible velocity in each point before and after each apex is then calculated using the GGV-diagram. This calculation is extends beyond the previous/next apex because not all apexes will limit the maximum possible velocity. The actual velocity in a certain point on the track will be the minimum of the maximum possible velocities determined from apexes nearby the point. When the velocity and acceleration in all points is known, the laptime can be calculated, along with wheel torques, power etc.

7.1.2 Clutch model

The design was early limited to using a multiple friction disc clutch because of the large available in-house knowledge and experience of this type of clutch at BorgWarner. The normal pressure acting on the friction discs can be derived using Archards wear model.

$$p(r) = \frac{\text{constant}}{r} \tag{16}$$

For a clutch with a pressure distribution according to equation (16) the torque capacity is described according to equation (17)

$$M_c = \mu n F_c \frac{R_i + R_o}{2} \tag{17}$$

The axial clutch force F_c is the same as the piston force F_p which is a function of the piston area A_p and the hydraulic pressure p_h. For a normally open clutch:

$$F_c = F_p = p_h A_p \tag{18}$$

The parameters μ, n, R_i, R_o and A_p are depending on the design of the clutch. In this concept analysis it is not of interest to look into the details of the design. Therefore these parameters are lumped together to a coefficient.

$$C_{design} = \mu n A_p \frac{R_i + R_o}{2} \tag{19}$$

Adding together equations 17, 18 and 19 results in

$$M_c = p_h C_{design} \tag{20}$$

There is a maximum pressure $p_{h,max}$ that can be allowed in the hydraulic system, and therefore there is also a maximum torque $M_{c,max}$ that can be transmitted for a given C_{design}. $M_{c,max}$ is also limited by maximum allowable friction disc pressure, and possibly even other factors. That is neglected in this analysis, but instead looked into more in detail in section 9.2.

$$C_{design} = \frac{M_{c,max}}{p_{h,max}} \tag{21}$$

What equation 21 shows is that C_{design} can be seen as a sizing factor. The relation between M and p_h for a normally open clutch with given $M_{c,max}$ and $p_{h,max}$ is:

$$p_h = \frac{M_c}{M_{c,max}} p_{h,max} \tag{22}$$

The relation is shown in figure 23.
A normally closed clutch has a spring that acts to compress the clutch pack, while the piston acts against the spring, opening the clutch. The axial clutch force is then

$$F_c = F_s - F_p = F_s - p_h A_p \tag{23}$$

where F_s is the spring force. F_s and A_p are chosen so that the clutch is fully opened when $p_h = p_{h,max}$. The spring force is assumed to be constant, since there is no displacement of the spring depending on the hydraulic pressure, if clutch elasticity is neglected.

$$F_s = p_{h,max} A_p \Rightarrow M_c = (p_{h,max} - p_h) C_{design} \tag{24}$$

Together with equation 21, the result for the normally closed clutch becomes:

$$p_h = (1 - \frac{M_c}{M_{c,max}}) p_{h,max} \tag{25}$$

The relation is shown in figure 23. In the simulation, the clutch torques are first calculated, and then the hydraulic pressure is calculated from that, depending on clutch capacity and type. The pressure is therefor described as a function of the torque, and not vice versa.

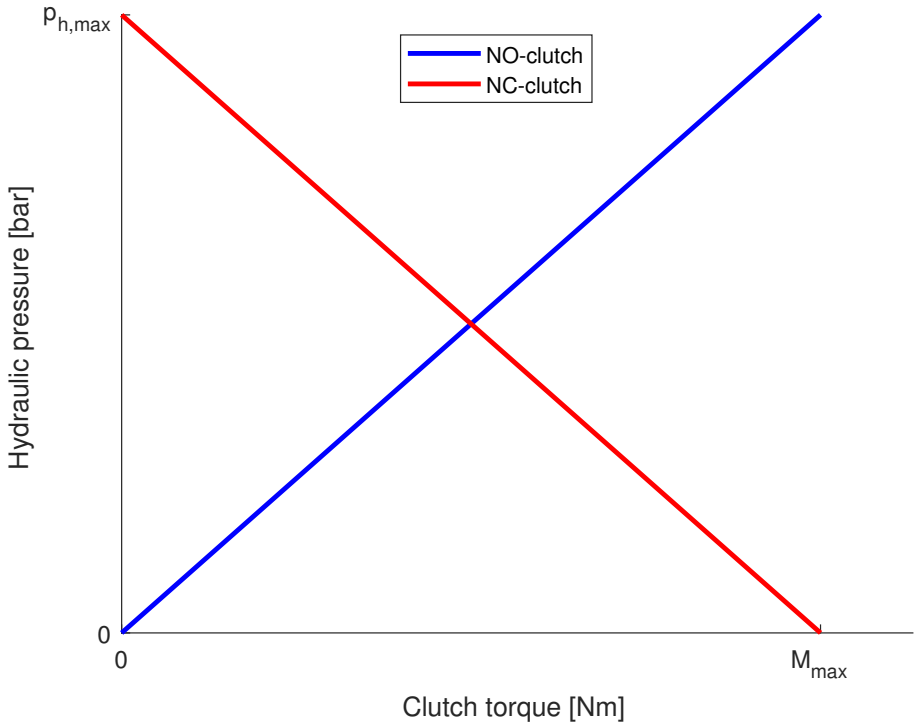

Figure 23: *Characteristics of the NO and NC clutch*

7.1.3 Torque vectoring model

No control algorithm was existing for the clutches at the time when the analysis was made. Therefor an approximation of the desired control had to be made. The chosen control model is based on equation 7 which gives the optimal vectoring force as a function of requested longitudinal force by the driver and grip on the outer wheel. It was then approximated that the requested longitudinal force F_T (which is per tire) was the same as the grip on the inner wheel, as illustrated in figure 4. This resulted in:

$$M_{w,out} = \frac{M_{w,tot}}{2} + M_{TV} = \frac{M_{w,tot}}{2} + F_{TV} r_w = \frac{M_{w,tot}}{2} + \frac{R_{in}(R_{out} - R_{in})}{R_{out} + R_{in}} r_w \tag{26}$$

$$M_{w,in} = \frac{M_{w,tot}}{2} - M_{TV} = \frac{M_{w,tot}}{2} - F_{TV} r_w = \frac{M_{w,tot}}{2} - \frac{R_{in}(R_{out} - R_{in})}{R_{out} + R_{in}} r_w \tag{27}$$

Where R_{out} and R_{in} were calculated as follows:

$$R_{out} = \mu_{x,out}(F_{z,out}) * F_{z,out} \tag{28}$$

$$R_{in} = \mu_{x,in}(F_{z,in}) * F_{z,in} \tag{29}$$

The tire model in the simulation uses different friction coefficients for the longitudinal and lateral directions which means that the friction circle in section 3.2 is not a circle anymore, but

an ellipse. To make calculations simpler, it was assumed that it was a circle. It was seen that the impact on the results was negligible when μ_y was used instead of μ_x in equations 28 and 29.

7.1.4 Loss models

Power losses had to be modeled in order to calculate system efficiency and required cooling power. The losses that were considered to be of highest significance were clutch slip losses, actuator losses, and thrust bearing losses. These were modeled according to the equations presented below. Other losses that were considered to be smaller were not modeled in order to save time. These were other bearing losses, oil drag losses and seal drag losses. Instead they were just lumped together to a guessed loss, which is hopefully closer to the real loss than to not account for them at all. Note again that the simulation does not know what is left and right, only what is inner and outer side. The losses can not be tied to a specific component (clutch, thrust bearing, actuator) because the inner and outer side is switching, depending on which direction the car turns in. However, this does not affect the loss analysis.

The simulation assumes that the tires are not slipping. Therefor the outer wheel will always have a higher rotational speed than the inner wheel. An assumption was made about the dual clutch control. The outer wheel clutch slip is always zero, while the inner wheel clutch is slipping, and transferring less torque to the inner wheel. All clutch slip losses will therefor be on the inner wheel, and all losses are turned into heat.

$$P_{loss,slip} = M_{w,in}(\omega_{w,out} - \omega_{w,in}) = M_{w,in}\Delta\omega_w \tag{30}$$

There are two hydraulic actuators (hydraulic pumps), one per clutch. They build the pressure behind the pistons to create the force that actuates the clutch. All of the electric power that the actuators consume is assumed to turn into heat because they do not create any net work. The consumed electrical power as a function of steady state hydraulic pressure have been measured at BorgWarner. The data can unfortunately not be presented due to confidentiality. The pressure p_h is known from equations 22 or 25 together with 26 and 27.

$$P_{loss,actuators} = P_{el,actuators} = P_{el,actuator,out}(p_{h,out}) + P_{el,actuator,in}(p_{h,in}) \tag{31}$$

The needle roller thrust bearings transfer the piston forces from the piston to the clutch pack (or clutch springs if it is NC) and they transfer the force from the clutch drum to the housing. Four bearings are used, two per clutch (see figures 19 to 21). The bearings can only take compressive forces. The piston bearing force is the same as the piston force F_p, both for the NO and NC clutch. The two pistons are pushing the clutch drum in opposite directions so the piston forces acting on the clutch drum partly cancel each other out. The housing bearings take up the force that is not cancelled out by the pistons. The housing bearing force is:

$$F_{thrust,housing} = abs(F_{thrust,out} - F_{thrust,in}) \tag{32}$$

For the NO-clutch, both forces will in general be $\neq 0$. For the NC-clutch, $F_{thrust,out}$ is assumed to always be zero. The bearing losses are calculated with a friction torque model provided by SKF [16]. According to SKF, the model is approximative, but relatively accurate under "normal operating conditions" if lubrication is good and the bearing load is over 10% of the rated bearing load.

$$M_{loss,thrust} = 0,5 * f_l((F_{thrust,out} + F_{thrust,in})d_{m,pistonbearing} + F_{thrust,housing}d_{m,housingbearing}) \tag{33}$$

Where $f_l = 0,005$ for needle roller thrust bearings.

The clutch drum is always rotating with the input speed, which is the same as the outer wheel speed because the outer clutch is not slipping.

$$P_{loss,thrust} = M_{loss,thrust}\omega_{w,out} \tag{34}$$

7.2 Vehicle data input

7.2.1 Engine and chassis

Two cars were simulated, one with a combustion powertrain and one with an electric powertrain. The input data is based on the LFS-19 car target, combined with achieved numbers on the LFS-18 car. The chassis parameters are shown in table 2.

Mass	310 kg (including driver)
Center of gravity position	Height: 300 mm, 47% front weight distribution
Driving wheels	Rear wheel drive
Wheelbase	1590 mm
Trackwidth	1190 mm
Drag coefficient	Cd*A = 1,4 (140 N @46 km/h)
Downforce coefficient	Cl*A = 3,7 (370 N @46 km/h)
Center of pressure	At center of gravity
Tires	Hoosier R25B 10"x18"x7,5"
Wheel radius	0,22 m (loaded radius for 18 inch OD tires)

Table 2: *Vehicle input parameters, excluding powertrain*

The combustion powertrain power curve comes from wheel hub dyno measurements done on the LFS-18. The electric powertrain power curve comes from the Emrax 228 motor, a commonly used motor in single motor FS-cars. It has been limited to 80 kW peak power which is required by the rules. The powertrain input data is shown in tables 3 and 4 and figures 24 and 25.

Engine	Honda CB 600F					
Max engine power and torque	50 kW @ 10000 rpm / 52 Nm @ 9000 rpm					
Number of gears	6					
Primary gear ratio	2,111					
Gearbox ratios	2,75	1,938	1,556	1,348	1,208	1,095
Final drive ratio	4,00					

Table 3: *Combustion powertrain input parameters*

Engine	Emrax 228
Base speed	3200 rpm
Base torque	238,7 Nm
Peak power	80 kW
Number of gears	1
Final drive ratio	3,52

Table 4: *Electric powertrain input parameters*

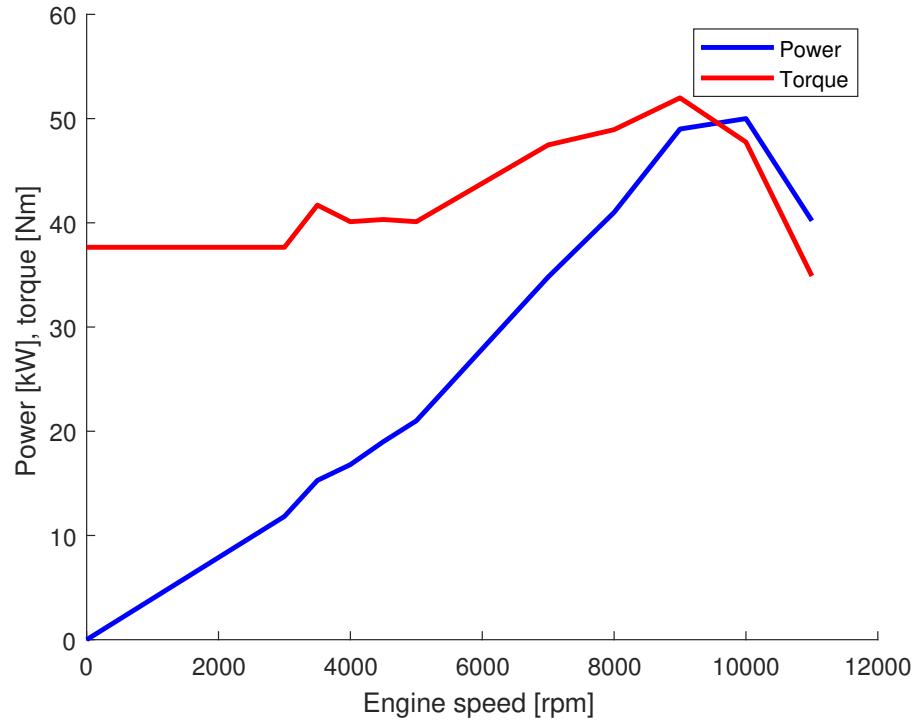

Figure 24: *Combustion engine power and torque*

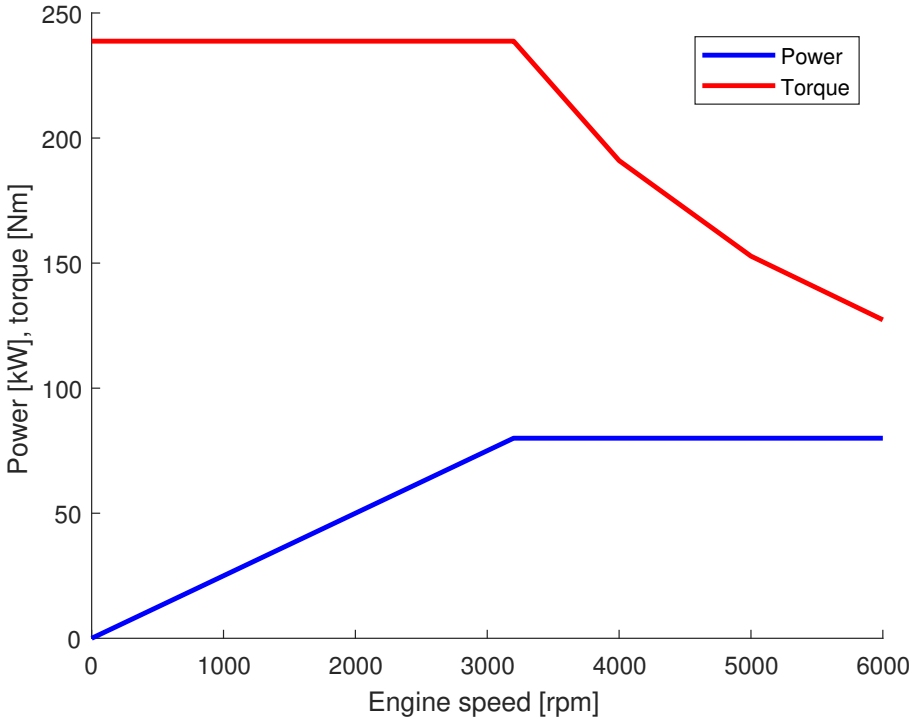

Figure 25: *Electric powertrain power and torque*

7.2.2 Tire data

The tire friction coefficient input deserved some extra attention because it was expected to influence the output significantly. It is a science on its own to model tires due to the many parameters

that influence the behaviour. Just to give an example, the lateral force, (F_y) ,produced by the tire is a function of normal force, longitudinal force, inclination angle (camber), slip angle, air pressure, temperature and surely even more parameters. All of this is not accounted for in this simplified simulation. The input to the program consists of two functions, one for longitudinal friction coefficient, $\mu_x(F_z)$, and one for lateral friction coefficient, $\mu_y(F_z)$.

Tire data from the Formula SAE Tire Test Consortium (FSAE TTC) and the Calspan Tire Research Facility (TIRF) is used by the Lund Formula Student team and was therefor available. The raw data has been processed and re-scaled to match realistic asphalt friction. The tire data shown in figures 26 and 27 is used as input to the simulation model.

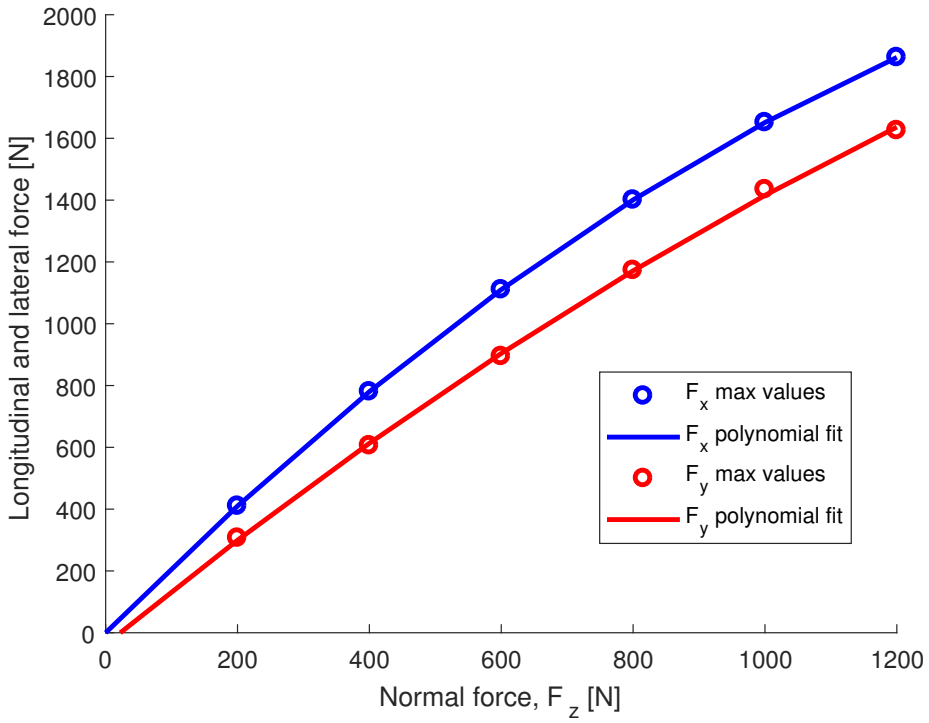

Figure 26: *Tire grip*

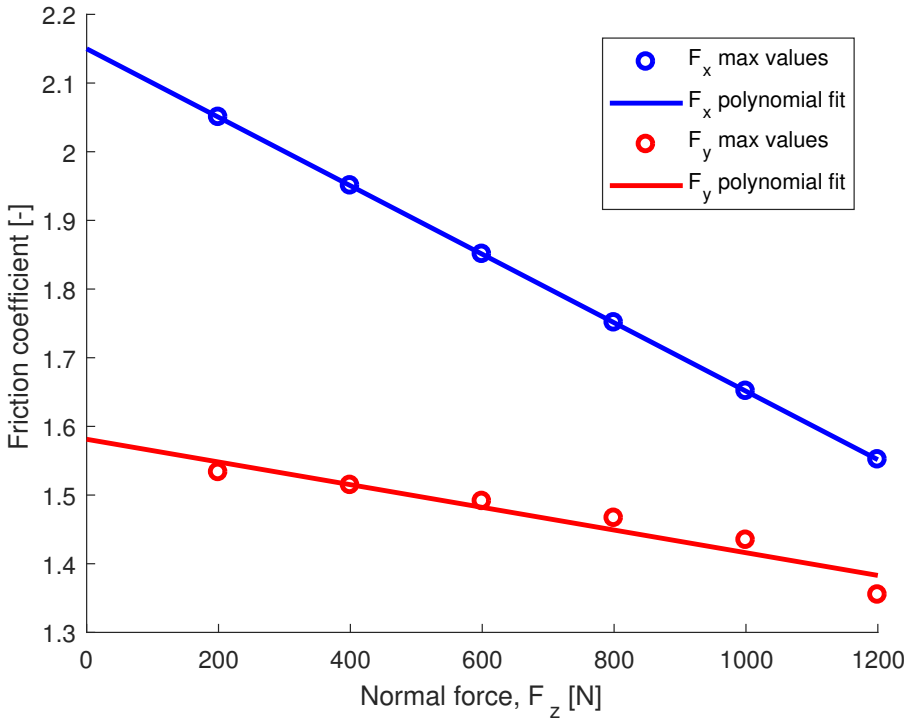

Figure 27: *Tire friction coefficients*

7.3 Track data

The track used in the simulations comes from the autocross event in Formula Student Germany, year 2012. It represents a typical formula student track well. The track length is 1,27 km and it is shown in figure 28.

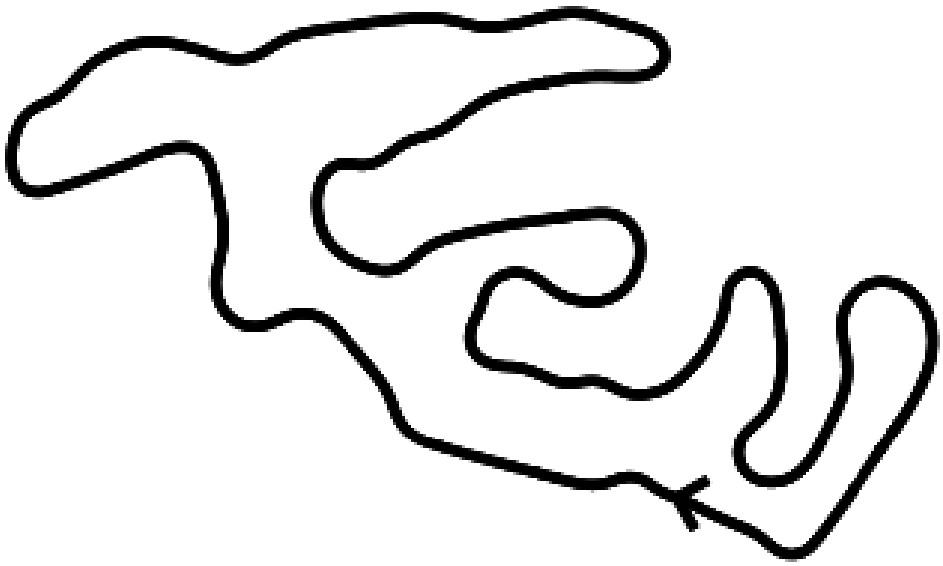

Figure 28: *FSG 2012 autocross track*

7.4 Results

Four different setup combinations were simulated. Electrical and combustion powertrains with normally open and normally closed clutches respectively. The figures shown are only from the electrical powertrain. The combustion powertrain figures look very similar. The most relevant differences are presented in tables 5 and 6. The results in the figures shown are zoomed in at the time span 10 to 20 seconds in order to better visualize the data. For reference, the whole lap took 73,67 seconds with the electrical powertrain.

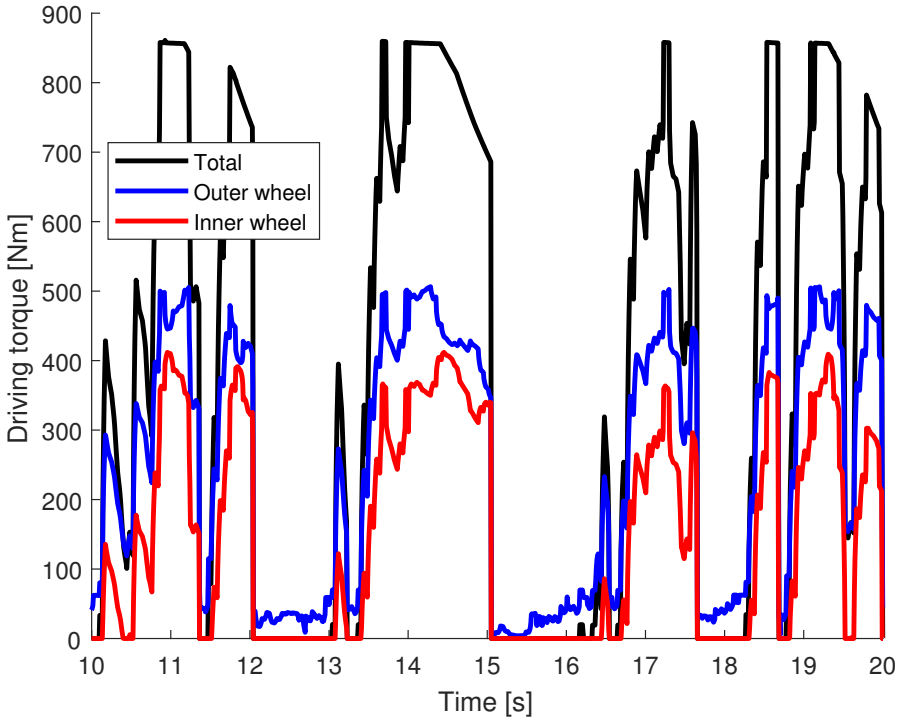

Figure 29: *Wheel torques*

Engine	Emrax 228	Honda CB 600F
Total wheel torque peak [Nm]	865	862
Outer wheel torque peak [Nm]	509	490
Inner wheel torque peak [Nm]	426	420

Table 5: *Wheel torque peaks*

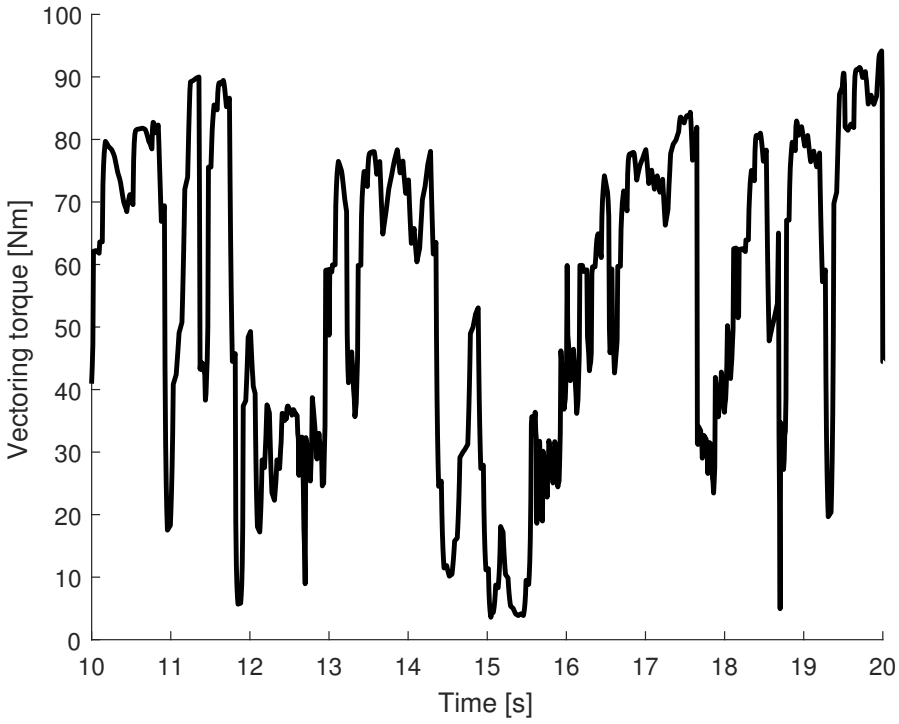

Figure 30: Vectoring torque M_{TV}

Corner radius larger than 100 m is shown as 100 m for better visualization.

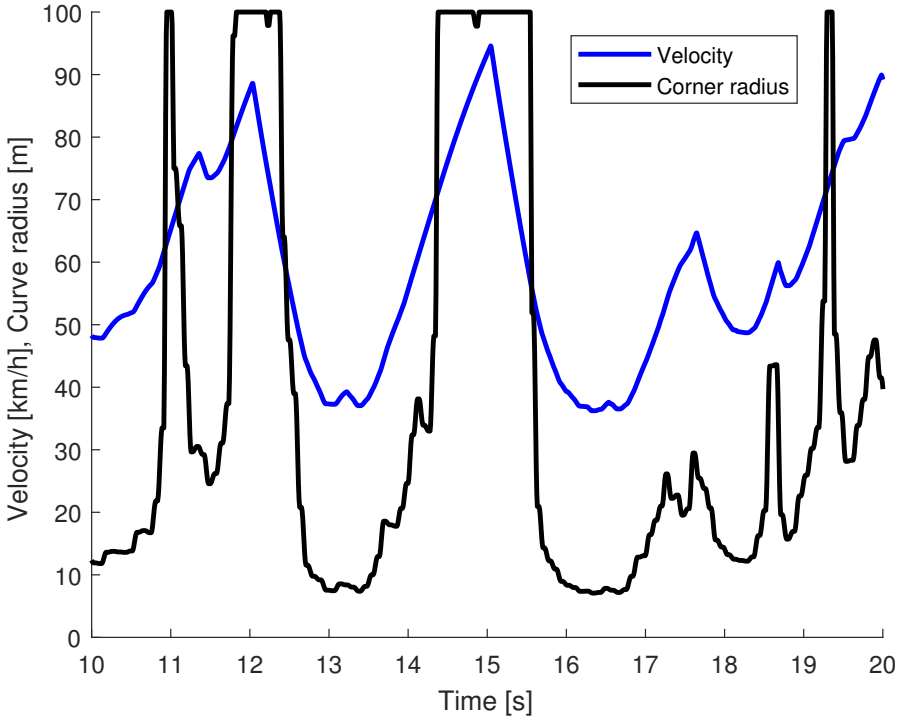

Figure 31: *Car velocity and corner radius*

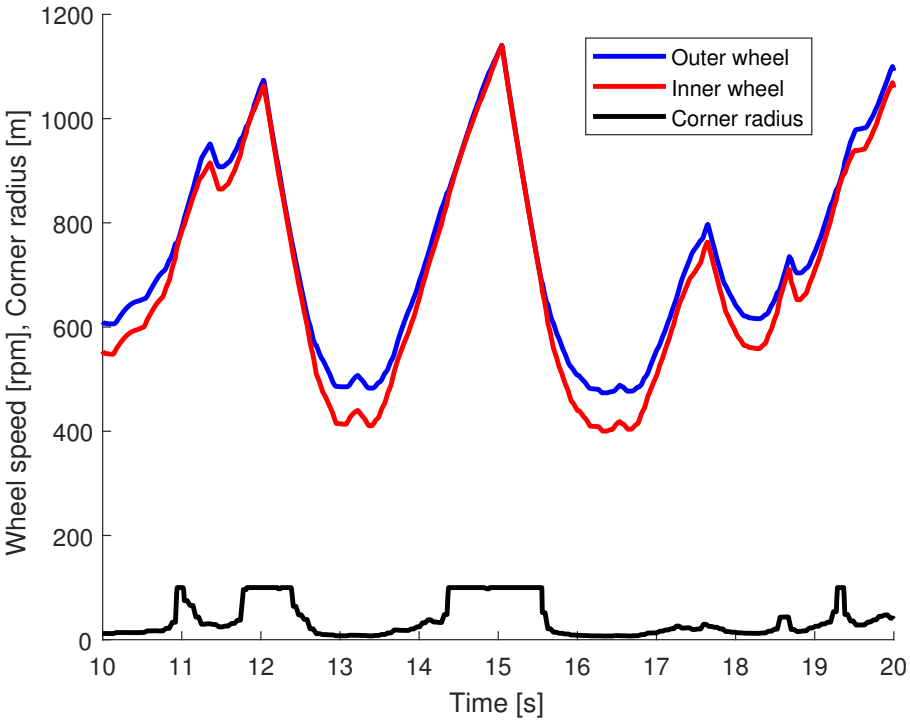

Figure 32: *Wheel speeds*

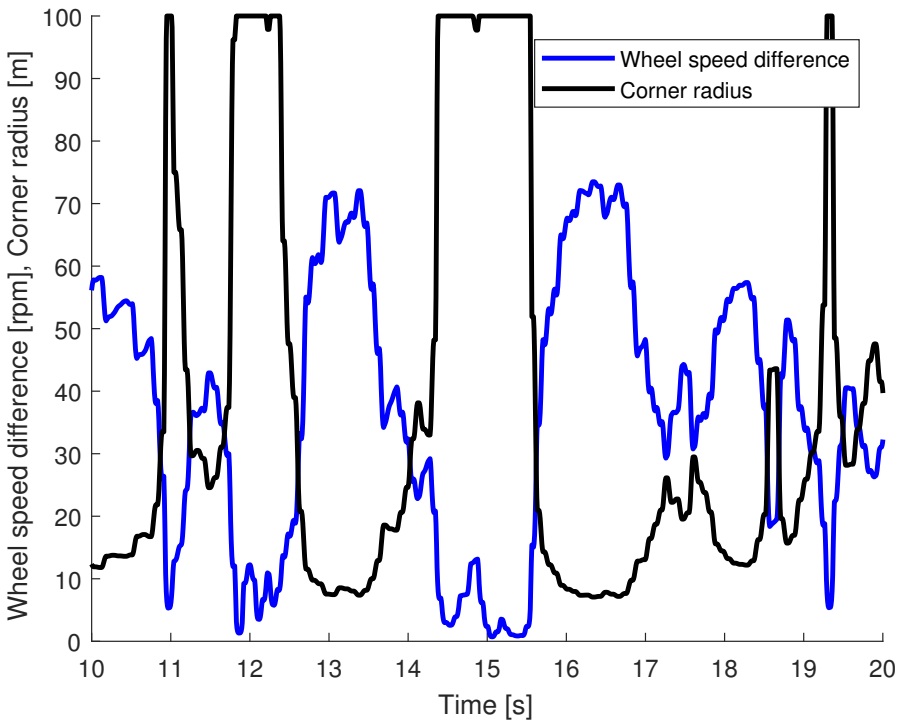

Figure 33: *Wheel speed difference*

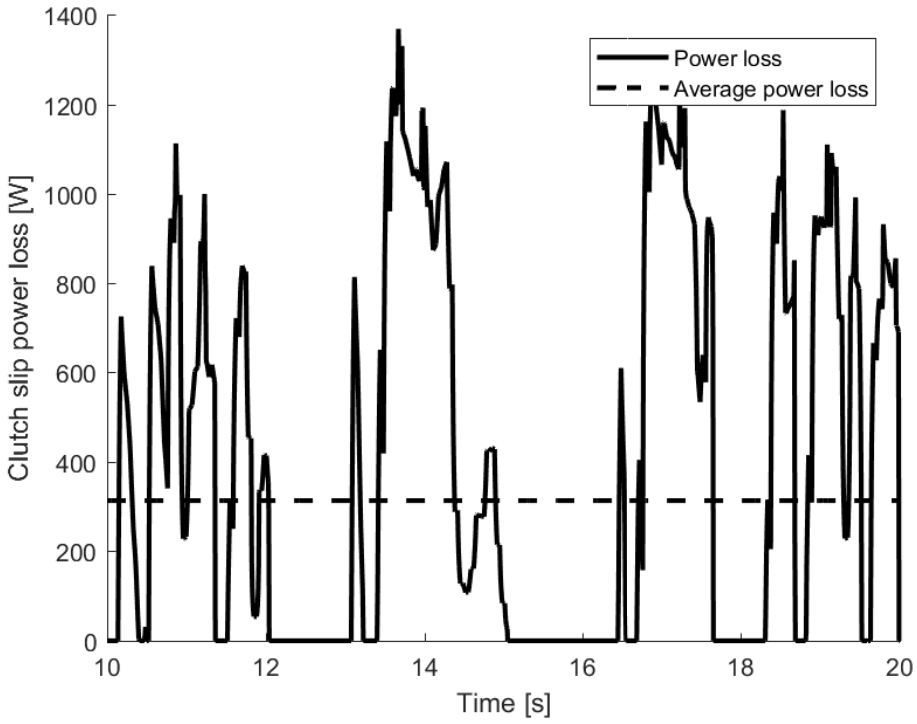

Figure 34: *Power loss from clutch slip*

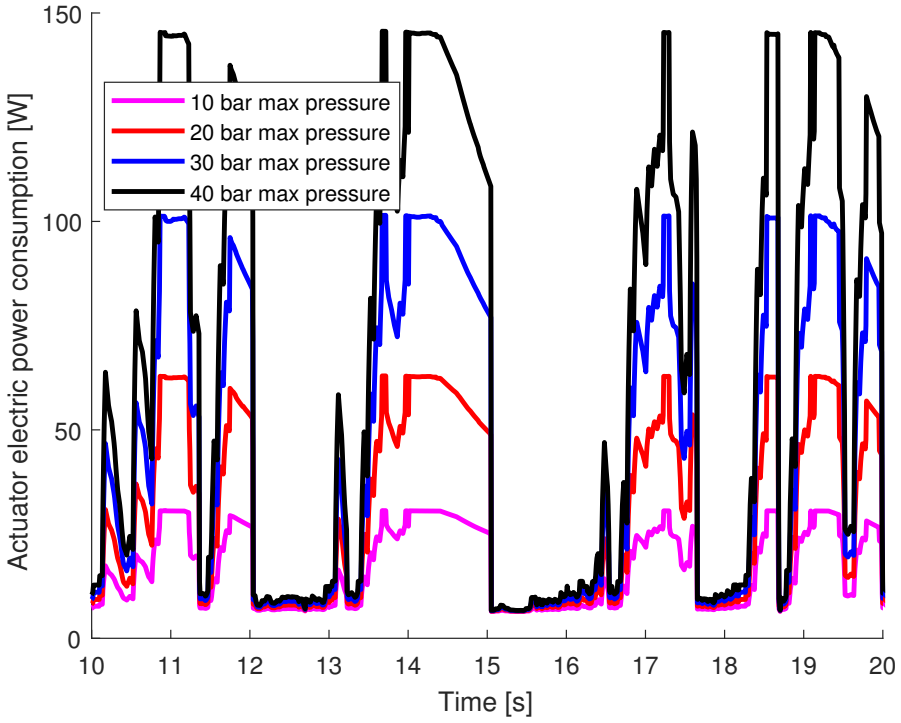

Figure 35: *Electric power consumption at different chosen hydraulic max pressures for normally open clutch*

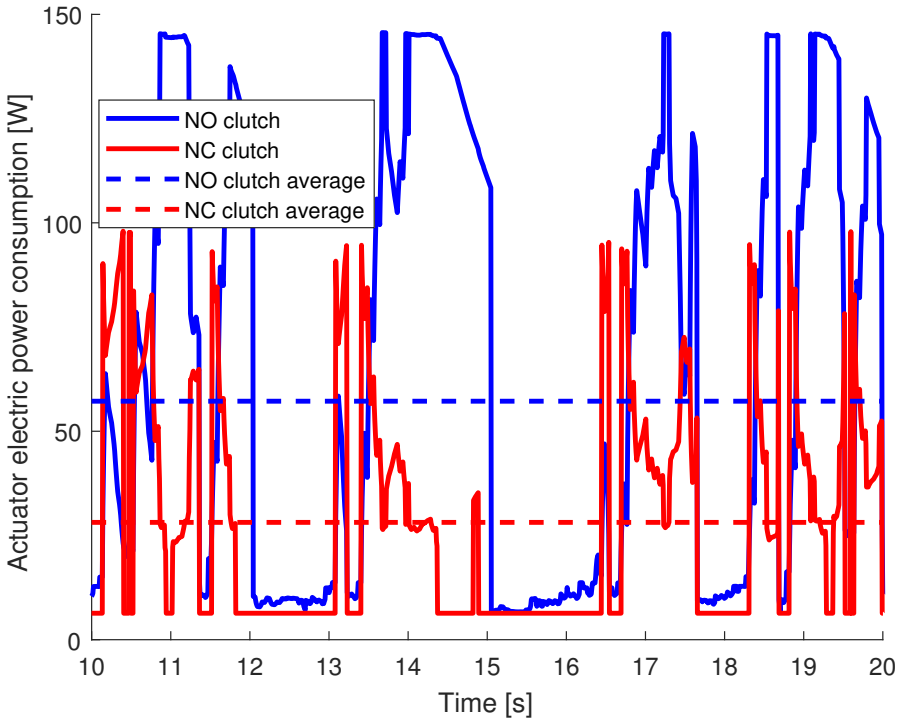

Figure 36: *Electric power consumption at 40 bar hydraulic max pressure for normally open and normally closed clutches*

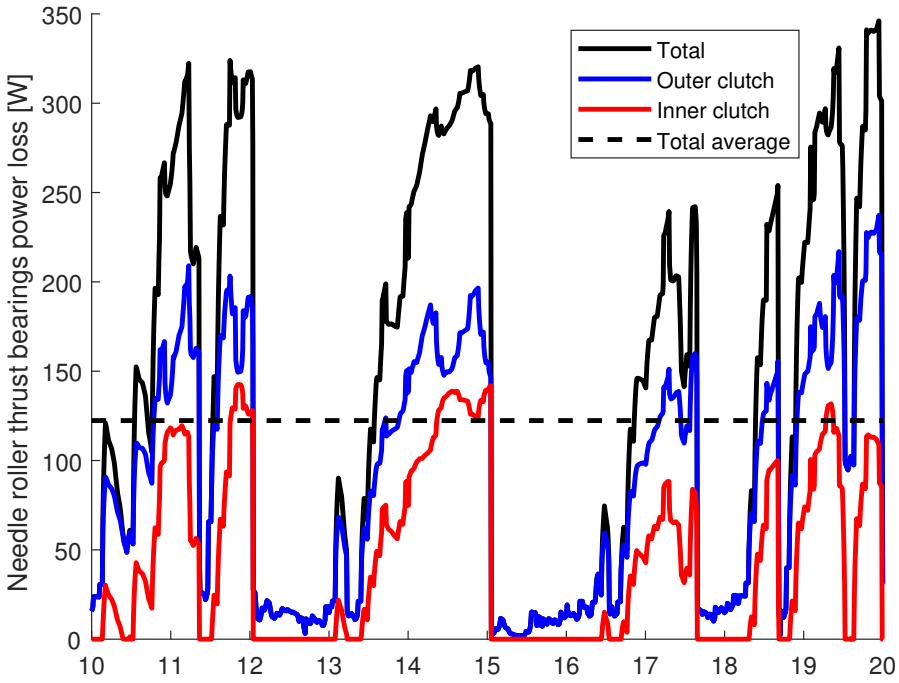

Figure 37: *Needle roller thrust bearing power losses for normally open clutch*

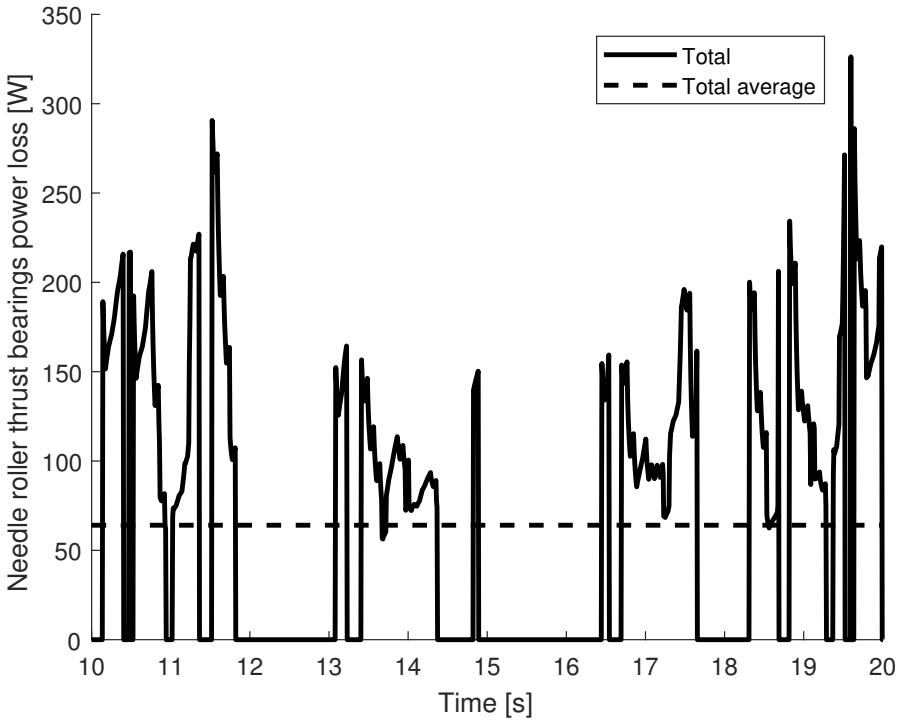

Figure 38: *Needle roller thrust bearing power losses for normally closed clutch*

Engine	Emrax 228		Honda CB 600F	
Clutch type	NO	NC	NO	NC
Clutch slip [W]	313	313	282	282
Actuators [W]	57	28	49	31
Thrust bearings [W]	122	64	105	74
Other losses (estimated) [W]	150	150	150	150
Total losses [W]	642	555	586	537
Average transfered power [kW]	29,5		24,7	
Transmission efficiency	97,8%	98,1%	97,6%	97,8%

Table 6: *Heat losses and efficiency*

7.5 Discussion

The main concern with the dual clutch concept before the analysis was done was the efficiency loss and heat generation due to clutch slip, because one clutch is always slipping. A system efficiency of around 98% is not so bad with that in mind. An average heat loss of around 550 W should also be manageable. It should be possible to manage with air cooling. Using water cooling would increase the design and manufacturing complexity a lot. As a qualitative analysis, the heat loss can be put in relation to how much cooling power an air cooled combustion engine has. It is usually in the same region as the produced mechanical power. So a small air cooled 10 kW motorcycle engine which is roughly the same size as a dual clutch transmission could be, would need to cool around 10 kW which is 18 times more.

The electric powertrain is more powerful than the combustion powertrain which is why it has higher wheel torque peaks. However, the difference is not a very large, which means that the available tire grip, and not the available engine torque, is what mostly defines the peak torque. The conclusion is that the required clutch capacity will be roughly the same, even if a stronger powertrain would be used in the car in the future.

It can be observed that the NC-clutch version is more efficient than the NO-clutch version. The clutch slip loss is the same, because it is assumed that the torque vectoring control is identical. The NC-clutch version needs less actuation though, due to its nature. It transfers full torque when not actuated at all. Less actuation leads to lower actuator losses and lower electrical consumption which is very positive because it lowers the demand on the alternator in the combustion powertrain and electric consumption from the battery in the electric powertrain. The alternator is already working at high capacity on the LFS cars and it is not easy to find a solution to increase the capacity. The lower amount of actuation also leads to lower thrust bearing losses.

The engine power has less influence on the total losses on the NC version than on the NO version because on the NC version, actuation decreases with increased torque while clutch slip losses increase. On the NO version all losses increase when torque is increased. This means that the losses will be more constant so the NC dual clutch will not heat up much more when the car is pushed hard compared to when driving easily. That can also be a problem for the NC version if the cooling is not dimensioned properly. It will not help to drive slower if the clutch is overheating.

There are many approximations made in the analysis in order to save time because the analysis in itself was not meant to be the largest part of the thesis. This could of course have an effect on the outcome. However, focus was put on modeling what was believed to be the largest influencing factors.

The largest approximation in the analysis is believed to be the torque vectoring model and the control strategy for the actuators which is very simple. A lap time simulation software that takes yaw moment into account, with a yaw control strategy for the torque vectoring together with a tire model that takes longitudinal and lateral slip into account would increase the accuracy of the analysis.

7.6 Conclusions

The most important conclusion that was drawn was that a dual clutch is feasible to use in a Formula Student car, in terms of efficiency and heat losses. Also the understanding of the difference in characteristics of the NO and NC versions have increased. It was chosen to continue with the mechanical development of the NC dual clutch. One reason was because of the lower losses which reduce the cooling requirements. An other reason is the lower electrical consumption. A third, maybe more important reason, is that an NC clutch has a much better failure mode. If it would stop working for some reason, the car would end up with a locked rear axle. With an NO clutch in the same situation, the car would not move a meter more. A fourth reason is that the NO clutch concept already exists in other applications, while an application with NC clutch could not be found and would be unique and exciting.

8 System requirements specification

The system requirements specification describes the targets and criterias for the dual clutch. It is based on the results from the feasibility analysis and experience from the LFS-team and Borg-Warner, combined with some assumptions. The purpose of the SRS is to serve as a base for calculations and design choices, but also to provide an overview of the targeted product specification.

General functional description
The dual clutch unit should consist of two normally closed clutches. It should fit a rear wheel driven Formula Student car with either combustion engine or single electric motor. It should be possible to control the driving torque distribution between the rear wheels so that the yaw moment, and through that, the yaw rate, can be controlled. It should be possible to use it for launch control, for example by controlling the slip ratio of the driving wheels individually when doing a full acceleration start from standstill.

Mechanical interface
The LFS-19 car was chosen as a testing platform for the unit. All mechanical interfaces should therefor be adapted to the LFS-19 car. It should be possible to relatively easy adapt the unit to other cars. The housing has to be mounted to either chassis or engine. The mounts should be possible to change without remanufacturing the whole housing. Chain slack adjustment possibility should be included somewhere in the design, for example using the same design as the LFS-19.
Chain and sprockets are used as final drive transmission. It should be possible to mount a chain guard according to FS-rules (reference [3]). Driveshafts are used to transmit the torque from the unit to the wheels via a constant velocity joint (tripod joint).

Serviceability requirements
The rear final drive sprocket should be possible to mount and dismount without a major disassembly of the unit. It should be possible to change clutch discs and oil. The unit has to be oiltight even when the tripod housings are removed in order to simplify handling.

Load capacity
The unit should be able to transfer at least 530 Nm per wheel at 130°C oil temperature without clutch slip. It should be able to transfer at least 890 Nm in total to both wheels. These numbers are based on the results in table 5, with a small added safety factor. It was decided that the minimum allowable rear sprocket size is 32 tooth for 520-chain ($r_{sprocket} = \frac{\frac{5}{8} * 25{,}4 * 32}{2\pi} = 80,85mm$), which with equation 35 leads to a dimensioning chain force of 11132 N.

$$F_{chain} = \frac{M_{tot}}{r_{sprocket}} \tag{35}$$

The maximum allowed angle between the driveshaft axis and the output axis of the unit was set to 12 degrees, according to limits determined by LFS. In CV-joints, this angle gives rise to a bending moment acting on the tripod housing according to equation 36. From this, it is given that the dimensioning bending moment is 55,7 Nm.

$$M_{cv,bending} = M_w tan(\frac{\alpha_{cv}}{2}) \tag{36}$$

A dynamic load factor of 1,7 should be used on the chain force, due to the pulsating torque output of the combustion engine and transmission. Further a safety factor of 1,2 against yield strength should be used for the structural integrity of all components.

Speed
The maximum speed of the car is assumed to be 130 km/h, based on expecience from LFS. With a wheel radius of 0,22 m, that leads to an angular wheel speed of 1568 rpm. The maximum clutch slip speed in normal use was set to 100 rpm based on the results of wheel speed difference from the feasibility analysis, assuming that the inner clutch slip speed is the same as the wheel speed difference, which it is if the outer clutch is not slipping. The clutch slip speed may be several times higher when used as launch control with both clutches slipping, but that is only during very short

intervals, on the order of one second.

Heat and energy absorption
The total average heat losses were set to 600 W for calculations. It is based on the feasibility analysis results in table 6, but a small safety factor of 45 W or 8% was added. A peak oil temperature of 130°C is allowed.

Mass target
The mass target was set to 9 kg for the unit with mounts, oil and tripod housings, without sprocket. It was based on preliminary sizing calculations and on the mass of the LFS-18 drivetrain assembly.

Fatigue, lifespan and safety factors
Fatigue life for the system should be at least 10000 km of autocross driving. A safety factor of 1,5 towards number of cycles should be used on this, which results in a dimensioning fatigue life of 15000 km. Some service demand is acceptable during this period, for example oil change and replacement of cheap and easily accessible components, for example seals or bearings. A compromise of the fatigue life can be acceptable if significant performance can be gained by reducing the fatigue life of a certain component that is replaceable, for example reducing bearing size to reduce mass.

Failure mode
It should be possible to turn off the electricity supply to the unit and still have the ability to drive the car. The purposes of this requirement is that car testing should not be stopped in case of problems with the electronics or software. Also, if a problem would occur at the endurance event, for example overheating of the unit, it should be possible to make it to the finish anyway.

Environmental demands
The unit should work in heavy rain. It should resist petroleum and alcohol based chemical solvents used for degreasing and washing. It should work in an ambient temperature of between 0°C and 40°C.

Sensors
The unit should have an oil temperature sensor so that friction disc temperature can be estimated in order to estimate the friction, which changes with friction disc temperature. It is also useful to know the oil temperature to identify overheating problems. A hydraulic pressure sensor should be used for each of the clutches so that the clutch compression force can be estimated.

For the reader's convenience: The sensor signals that are available on the LFS-19 and can be used as input for the control algorithm are wheel speed, accelerometer (x,y,z), yaw/roll/pitch rate, throttle position, current gear, engine clutch position, brake pressure and steering wheel angle.

Max electric power consumption
The calculated average electric power consumption of the actuators and their ECU:s is 65W, based on the feasibility analysis results and data from BorgWarner.

Electronics and control
Specifications of the control system, electric interfaces and similar are outside the scope for this thesis.

9 Dual clutch design

This section covers the major concept and design choices. The reasoning behind the design is explained and the results are discussed. The design is not fully finished in some cases. The final outcome can be seen in appendix B and it can be helpful to take a look at it before reading this section, to better understand what is discussed.

9.1 Calculations input

9.1.1 Load cases

The dimensioning load cases, defined from the SRS are presented in tables 7 and 8. They are used as a basis for dimensioning calculations.

Load case	**Straight full acceleration**		**Straight full acceleration angled driveshafts**		**Cornering full acceleration angled driveshafts**	
	Nominal	With d.f	Nominal	With d.f	Nominal	With d.f
$M_{w,tot}$ [Nm]	890	1513	890	1513	890	1513
$M_{w,1}$ [Nm]	445	756,5	445	756,5	530	901
$M_{w,2}$ [Nm]	445	756,5	445	756,5	360	612
F_{chain} [N]	11000	18700	11000	18700	11000	18700
$F_{r,b1}$ [N]	13971	23751	13971	23751	13971	23751
$F_{r,b2}$ [N]	2971	5051	2971	5051	2971	5051
$M_{b,h1}$ [Nm]	0	0	47	80	56	95
$M_{b,h2}$ [Nm]	0	0	47	80	38	64
α_{cv} [°]	0	0	12	12	12	12
$F_{p,1}$ [N]	-	-	-	-	-	-
$F_{p,2}$ [N]	-	-	-	-	-	-

Table 7: *Driving load cases*

Load case	**Piston 1 de-airing**	**Piston 2 de-airing**	**Both pistons de-airing**
$F_{p,1}$ [N]	17635	0	17635
$F_{p,2}$ [N]	0	17635	17635
$p_{h,1}$ [bar]	44	0	44
$p_{h,2}$ [bar]	0	44	44

Table 8: *De-airing load cases*

9.2 Friction system

9.2.1 Description and targets

The friction system is here defined as the parts that directly affect the torque transmission from input to either wheel. These parts are inner and outer friction discs, friction disc springs, pushrods, pushrod carriers and pistons.

The targets for the friction system are:

- Be able to transfer a wheel torque of 530 Nm at no slip at high temperature (130 °C)
- Low response time for applying and reducing torque
- Not too sensitive for manufacturing tolerances
- As small size as possible to keep the system weight low

The constraints are:

- Standard disc springs have to be used, to reduce price and design time.
- Friction disc material and oil combination already used by BorgWarner have to be used due to availability of data and to reduce design complexity.

It was considered too time consuming for the scope of this thesis to quantify the last three targets and to do the analysis to confirm that they have been met. Nevertheless, they had to be kept in mind when the friction system was designed.

9.2.2 Friction discs and springs

This subsection shows the analysis and reasoning for friction disc material choice, disc dimensioning and spring choice.

The outer friction discs are in this case in steel, as in most BorgWarner clutch products. For the inner friction discs there are different types of materials that are commonly used in wet clutches. The choice was between sintered bronze or paper discs because they have been used in clutches from BorgWarner and therefor test data was available for them. Carbon discs have also been used in some products, but those were ruled out due to high cost. It is crucial to have test data on friction coefficient at different disc temperatures for a certain disc and oil combination in order to properly dimension and control a clutch. It was considered to use discs from an untested supplier due to lower price for low volume orders, but that alternative was ruled out due to the lack of friction data with a known disc and oil combination. Friction testing is out of scope for this thesis, and therefor only available friction data was used. Using a proven combination of disc and oil also reduces the risk of problems occuring due to a bad combination.

The paper discs consist of raw paper (cotton linter or cellulose fibers) in combination with a thermosetting (organic or phenolic resin). They have a high friction coefficient in general, and they have a positive slope $\mu - v$ curve, which reduces the risk of clutch judder and noise, vibration and harshness (NVH) problems [14]. On the other hand, the friction coefficient is quickly reduced at high temperatures, and they have low thermal conductivity, which in combination may lead to severe friction loss when the slipping power is high. They have a maximum allowed disc pressure of 5 Mpa, compared to 8 Mpa (60% higher) for the sintered discs, which is negative in terms of torque capacity.

The sintered bronze discs have comparatively high friction at high temperatures, good heat conduction, and higher maximum disc pressure than the paper discs. They are stiffer than the paper discs which decreases response time. The piston has to travel less when the piston force is changed and thus less volume of oil has to be pumped, hence the reduced response time. The clutch pack can be made smaller with sintered discs due to their significantly higher torque capacity at high temperatures. The downside is that the occurrence of a negative slope on the $\mu - v$ curve makes stick-slip problems possible with sintered bronze discs.

Friction tests have been performed for the discs. Figures 39 and 40 show that the friction coefficient is slightly higher for the paper discs than the sintered discs in general. The sintered discs have higher static friction at high temperature though, which is the limiting factor for dimensioning in this case. It can be seen that friction is decreasing when temperature is increasing. The temperature will increase during the test when the speed difference is swept, from low to high value, which means that the friction shown in the test will decrease for higher slip speed differences. This temperature effect has not been compensated for in figures 39 and 40. The curves will be almost horizontal if compensation is added.

A second order polynomial was fitted to the data for extrapolation because the test data only covers up to 100 °C, see figure 41. The friction coefficient at 130 °C is 0,0509 for the paper discs compared to 0,0652 (28% higher) for the sintered discs. That results in a 105% higher torque capacity for a sintered disc at no slip and 130 °C if two discs of the same size are compared. A paper disc clutch therefor needs to either have more discs or a larger mean radius, leading to a larger and heavier unit. When the response time and heat characteristics are also taken into

account, it stands clear that the sintered discs are the best for this application and were therefor chosen.

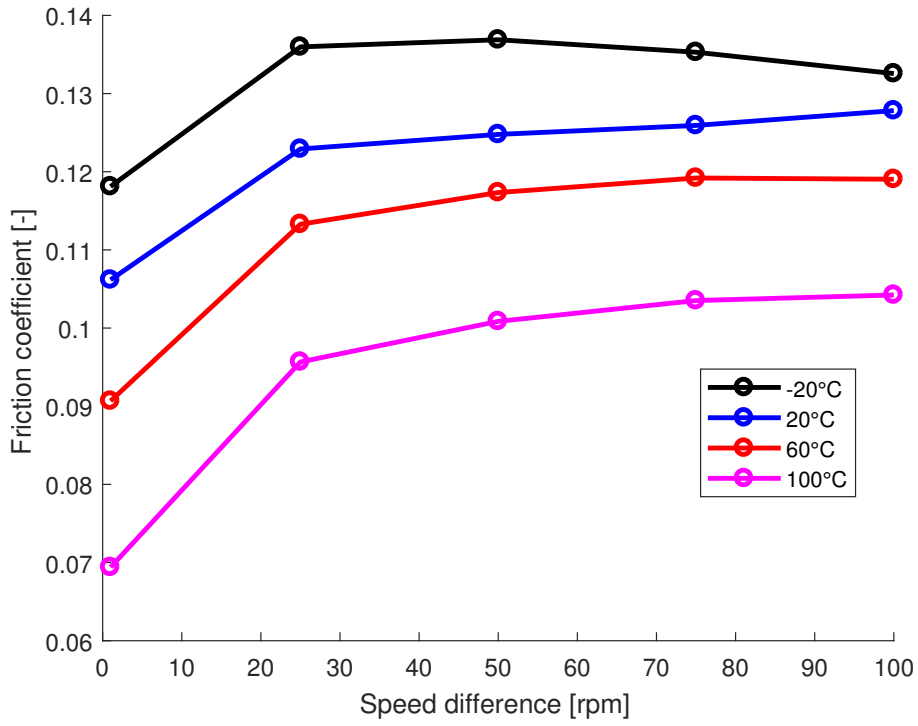

Figure 39: Friction-velocity curves for organic discs

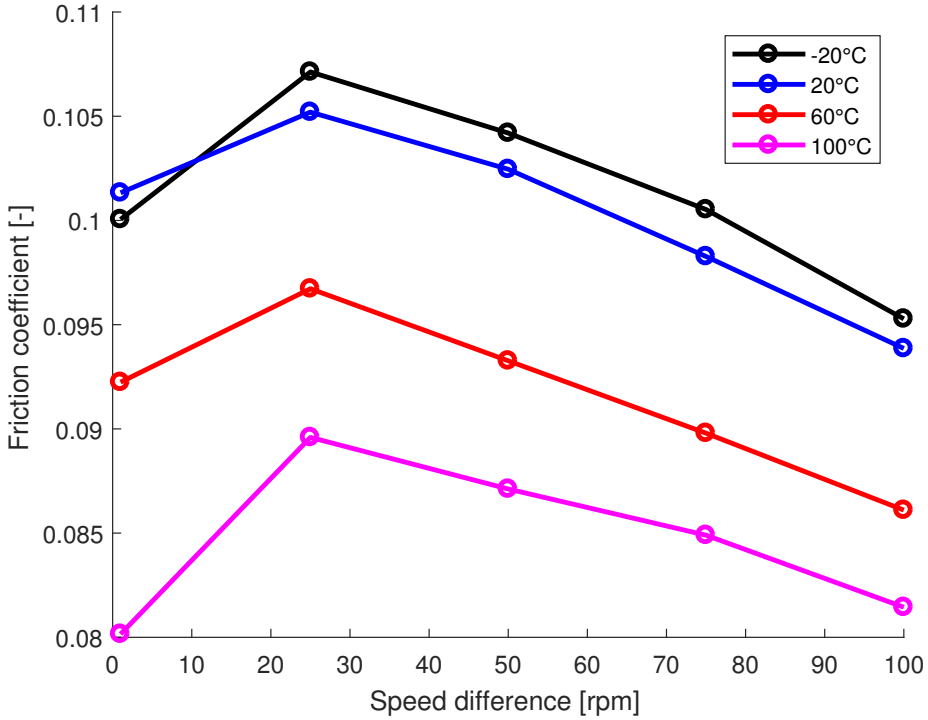

Figure 40: Friction-velocity curves for sintered discs

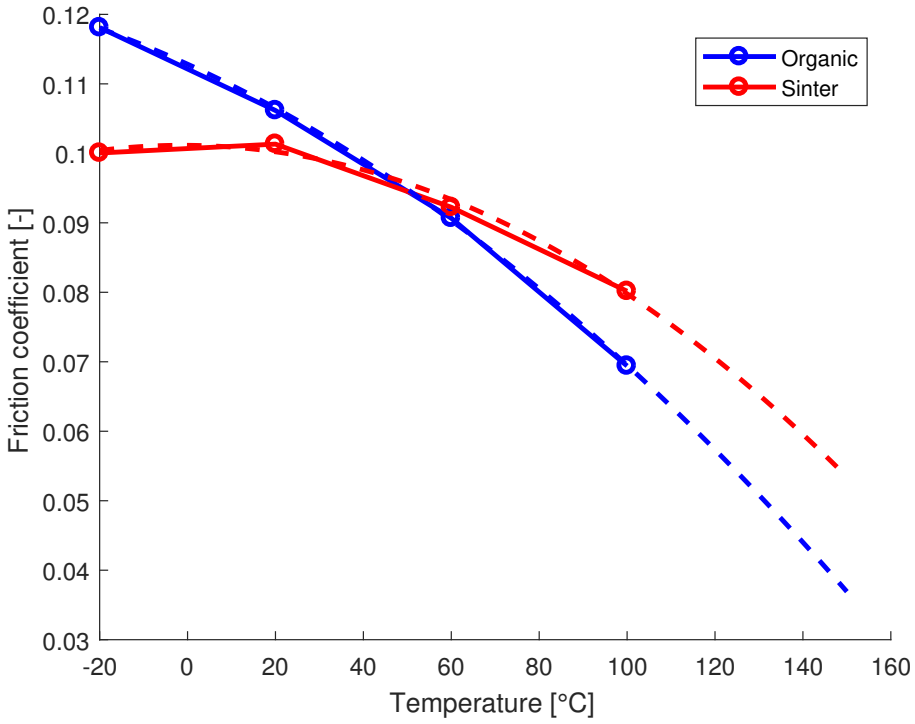

Figure 41: Static friction coefficients with second order polynomial extrapolation

The next step was to determine the number of discs, their inner and outer diameter, spring size and spring preload. All these parameters are connected and have their constraints so a trial and error approach was unavoidable in order to meet the objectives.

Equation 13 was used to plot the torque capacity per friction disc (= per two friction surfaces) as a function of inner and outer diameter in figure 42. It is assumed that the discs are fully used (p_{max} = 8 Mpa), and the friction coefficient is according to static friction for sintered discs at 130 °C ($\mu = 0,0652$). The inner diameter is expressed as multiples of the outer diameter. The horizontal lines represent the number of discs required to meet the torque capacity requirement of 530 Nm. Every cross between the lines is listed as a parameter combination in table 9.

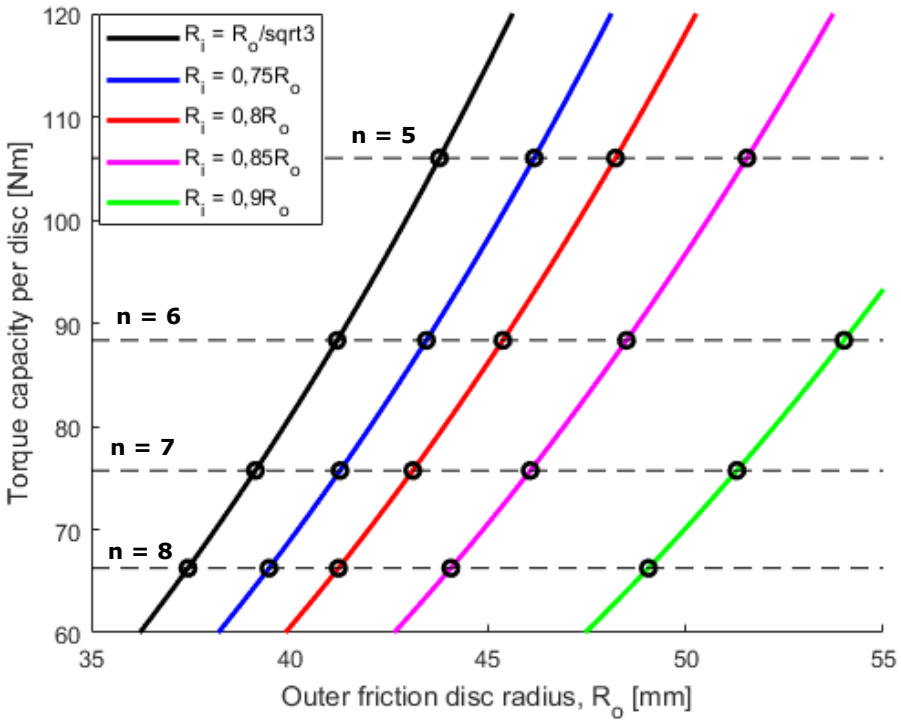

Figure 42: Feasible friction disc parameter combinations

It was decided that disc springs according to DIN 2093 standard should be used because of their availability. It is possible to make custom sized springs as well, but that was ruled out due to cost and time constraints. The next step was to find a good match between springs and discs.

The available springs in the size and force range that matches the friction discs in table 9 are presented in table 10. They are taken from appendix D.

Alternative number	R_o	R_i	R_i **- ratio**	**number of discs**	**F**
1	49,1	44,2	0,90	8	10893
2	51,3	46,2	0,90	7	11907
3	44,1	37,5	0,85	8	12454
4	54,0	48,6	0,90	6	13196
5	46,1	39,2	0,85	7	13613
6	41,2	33,0	0,80	8	13680
7	39,5	29,6	0,75	8	14696
8	43,1	34,5	0,80	7	14954
9	48,5	41,2	0,85	6	15086
10	41,3	31,0	0,75	7	16065
11	45,4	36,3	0,80	6	16573
12	51,6	43,8	0,85	5	17036
13	37,4	21,6	0,577	8	17196
14	43,5	32,6	0,75	6	17803
15	48,2	38,6	0,80	5	18714
16	39,1	22,6	0,577	7	18797
17	46,2	34,6	0,75	5	20104
18	41,2	23,8	0,577	6	20831
19	43,8	25,3	0,577	5	23524

Table 9: *Friction disc sizing combinations*

						s = 0,25 h0		s = 0,5 h0		s = 0,75 h0		s = h0		
De	**Di**	**t**	**Lo**	**ho**	**ho/t**	**s**	**F**	**s**	**F**	**s**	**F**	**s**	**F**	**art.nr**
80	41	3	5,3	2,3	0,766	0,575	4450	1,15	7838	1,725	10518	2,3	12844	4397
80	41	4	6,2	2,2	0,55	0,55	8726	1,1	16213	1,65	22874	2,2	29122	4398
80	41	5	6,7	1,7	0,34	0,425	11821	0,85	22928	1,275	33559	1,7	43952	4399
90	46	3,5	6	2,5	0,714	0,625	5836	1,25	10416	1,875	14161	2,5	17487	4401
90	46	5	7	2	0,4	0,5	11267	1	21617	1,5	31354	2	40786	4402
100	41	4	7,2	3,2	0,8	0,8	8715	1,6	15219	2,4	20251	3,2	24547	4403
100	41	5	7,75	2,75	0,55	0,687	12345	1,375	22937	2,062	32361	2,75	41201	4404

Table 10: *DIN 2093 feasible disc springs*

Now there was still a wide variety of alternatives left to choose from. Therefor a couple of constraints and targets had to be introduced. According to the DIN 2093 standard, springs that are loaded dynamically should not be compressed more than $s = 0,75h0$. In the application, the springs will be preloaded to a certain value. The variation of piston force will affect the spring load slightly, but not very much. When piston force is applied, the clutch force will decrease. The clutch pack has a certain axial stiffness, although very high, but it will expand a bit, leading to some spring travel. Whether that is considered to be dynamical loading or not, was not looked into. Instead, the constraint $s \leq 0,75$ was introduced to be safe.

An important target for the dual clutch is to keep down the mass. The clutch drum and housing will have to grow with growing outer disc diameter, which leads to a large mass increase. Therefore the outer diameter had to be relatively small. On the other hand, with the packaging of the chosen concept there is a limit when the pistons, clutch drum shafts and thrust bearings together drive the housing diameter instead of the clutch drum. An other factor that affects the mass is the required spring preload force. A higher force will require stronger and stiffer housing, axially stiffer clutch drum assembly and larger pistons, which increases the mass. It would also worsen the response time, due to the larger pistons. It is therefor highly desirable to keep down the required force. That can be done by increasing the amount of discs and by increasing the mean diameter, which is the same as increasing the diameter ratio for a given outer diameter. That also lowers the mass in itself due to the decrease in friction disc area.

Without any extensive analysis done, it was concluded that the outer diameter of the spring should be within the friction disc area, in other words larger than R_i and smaller than R_o. The reason is that the distribution of the spring force should be somewhat even over the friction disc surface. A larger outer spring diameter would lead to bending of the thick outer steel disc and a more uneven force distribution that could lead to excessive friction disc wear along R_o. On the other hand, the outer spring diameter needs to be relatively close to R_o in order to avoid bending of the thick steel disc when the pushrods are pushing to disconnect the clutch. Bending will increase stresses in the steel disc and also worsen the response time due to the required increase in piston travel when actuating the clutch.

The spring stiffness was an other aspect that was looked into. A characteristic of the disc spring is the decrease in spring stiffness with displacement. The thinner the spring (lower t), the more pronounced is the characteristic. It is highly desired to have a low spring stiffness at the preloaded displacement in order to increase the accuracy of the predicted preload. Manufacturing tolerances and inaccuracy in the axial clutch drum stiffness calculations will affect the actually obtained preload, which will affect the clutch capacity.

It was also found that it is desirable to have a large inner diameter of the spring due to the challenge of packaging the oil channel inside the spring, which is discussed more in detail later.

All this was weighed together with the pushrod design and available spline dimensions for the friction discs. It lead to a dimension very close to alternative 5 and disc spring number 4401. The final specification presented in table 11. The spring characteristics and preload is shown in figure 43 which has been calculated with a spreadsheet from [6]

R_i [mm]	46
R_o [mm]	38,375
n_{discs}	7
p_{max} [Mpa]	7,49
p_{max} safety margin	6,43%
$M_{c,max}$ at 130 °C [Nm]	530
Spring number	4401
$F_{s,preload}$ [N]	13763
Spring deflection at preload [mm]	1,805 (=0,722 h0)
Spring stiffness at preload [N/mm]	5800
M_c change per 1/100 mm spring displacement [Nm]	2,23
M_c % change per 1/100 mm spring displacement	0,42%

Table 11: *Clutch specification*

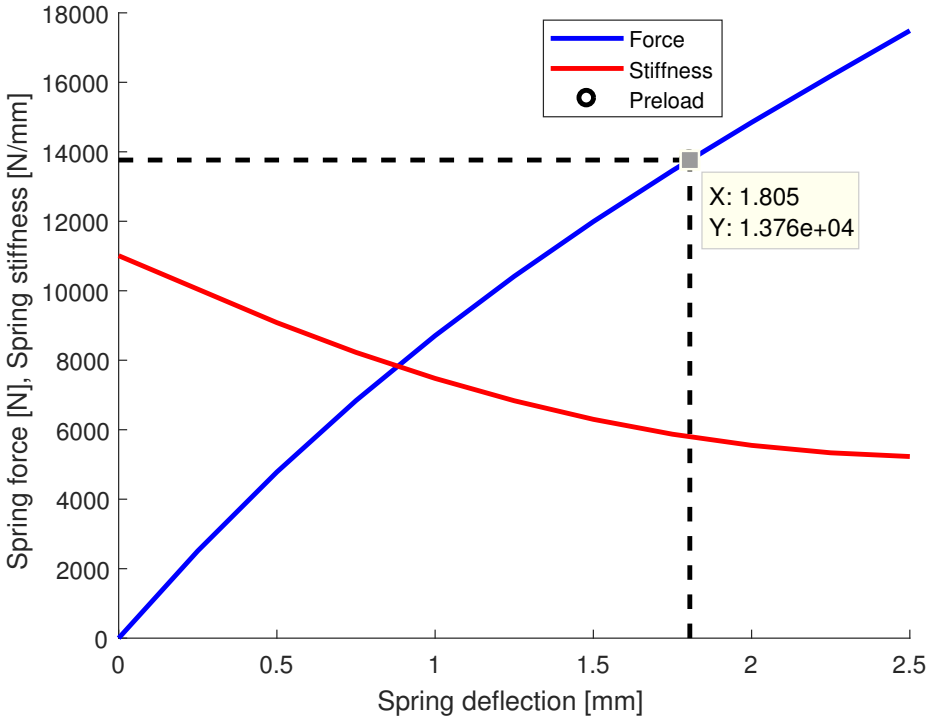

Figure 43: Force-deflection and stiffness curve for spring 4401

Friction disc wear was calculated, based on the laptime simulations and tested data from BorgWarner. It was concluded that the wear is insignificant, even over a lifespan of 10 000 km. The calculations are not presented due to confidentiality.

9.2.3 Pistons and pushrods

The piston area is critical because it directly affects the force that can be produced by the piston, according to equation 23. A larger area can give more force for the same pressure, but it also worsens the response time because a larger volume of hydraulic oil will have to be pumped for a given piston force change. The only reason why the piston moves is due to flex in the components, as mentioned before. The piston area was chosen to be as small as possible, without risking not being able to release the clutch pressure completely. The disc spring has a force tolerance of +10%/-5% at $s = 0,75h0$ according to Further, some extra force is required as a safety margin for friction and other tolerances. The same de-airing valve (overpressure valve) is used as in other BorgWarner clutches and that is what limits the hydraulic pressure. The valve opens at 44 bar and

the maximum working pressure is 40 bar. This means that the piston must be able to fully open the clutch at 40 bar. The inner and outer diameter of the piston was chosen so that it matches the chosen thrust bearing which has 85 mm inner diameter and 110 mm outer diameter. The bearing size was chosen to match the position of the pushrods. The chosen piston specification is shown in table 12. The safety margin is defined as $\frac{F_{p,40}-F_{s,preload}}{F_{s,preload}}$. The piston is shown in figures 44 and 45. Aluminium 7075 T6 was chosen as piston material due to its machinability.

$d_{p,i}$ [mm]	81
$d_{p,o}$ [mm]	108
A_p $[mm^2]$	4008
$F_{p,40}$ [N]	16032
$F_{p,44}$ [N]	17635
Safety margin	16,5%
Material	Aluminium 7075 T6
Mass [g]	103

Table 12: *Piston specification*

It was chosen to use cylindrical rods in combination with a pushrod carrier that holds the rods towards the thrust bearing instead of the push cage that was used in the conceptual model. The push cage would be very difficult to manufacture.

It was realized that if the clutch drum spline was made very large, then every other tooth on the outer friction discs could be removed. That space could then be used to fit a pushrod instead. A large module was chosen for the clutch drum spline in order to fit as large pushrods as possible inside. An even tooth number was chosen so that a symmetrical setup could be achieved. 32 teeth in total made it possible to use 16 teeth for the friction discs and 16 for the pushrods, 8 in each direction. The pushrods are supported by a plastic bushing that is pressed into the clutch drum shafts. It can be seen on figure 44 that the load path from pushrod to outer diameter of the disc spring is relatively straight which is desirable in order to avoid bending of the thick outer friction disc.

The pushrods must be able to take the maximal piston force without failing in buckling or crushing. The were checked for uniaxial stress and Euler buckling according to equation 37 and figure 79 in appendix E. The results are presented in table 13. It was assumed that three rods would take all load in the worst case, which means that the compressive force in each rod is $\frac{F_{p,44}}{3}$.

$$\sigma = \frac{F}{A} = \frac{F_{p,44}}{3}\frac{4}{\pi d_{pushrod}^2} \tag{37}$$

$d_{pushrod}$ [mm]	3,5
$L_{pushrod}$ [mm]	59,2
E [Gpa]	206
Axial force [N]	5878
Buckling load 1 [N]	4273
Buckling load 2 [N]	17093
Buckling load 3 [N]	8760
σ [Mpa]	611

Table 13: *Pushrod structural calculation results*

Only the relevant buckling cases were checked. They are numbered starting from the left in figure 79. The only buckling case that was failed was the first one, which is very conservative in this case. The pushrod is guided by the bushing and by the spline. Somewhere between case two and three is a better approximation of the reality, hence buckling is not a problem. There are many steels with yield strength higher than the compressive stress as well. Even if three pushrods

can take all load it is beneficial to have more of them in order to distribute the load on the thick outer friction disc and on the thrust bearing. Steel was decided as pushrod material, but the alloy is not yet specified. The pushrod carrier will be in 7075 T6 for the same reasons as the piston and the bushings will be in POM plastic.

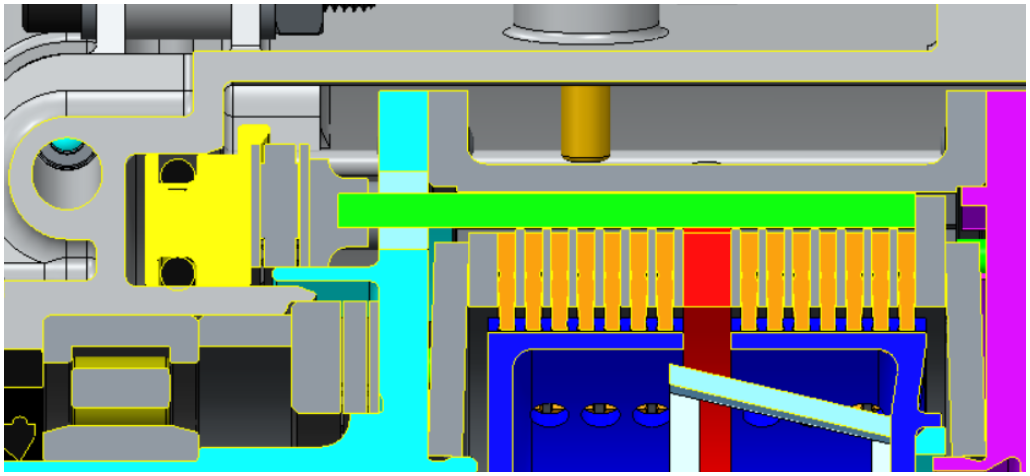

Figure 44: Piston and pushrods cross section

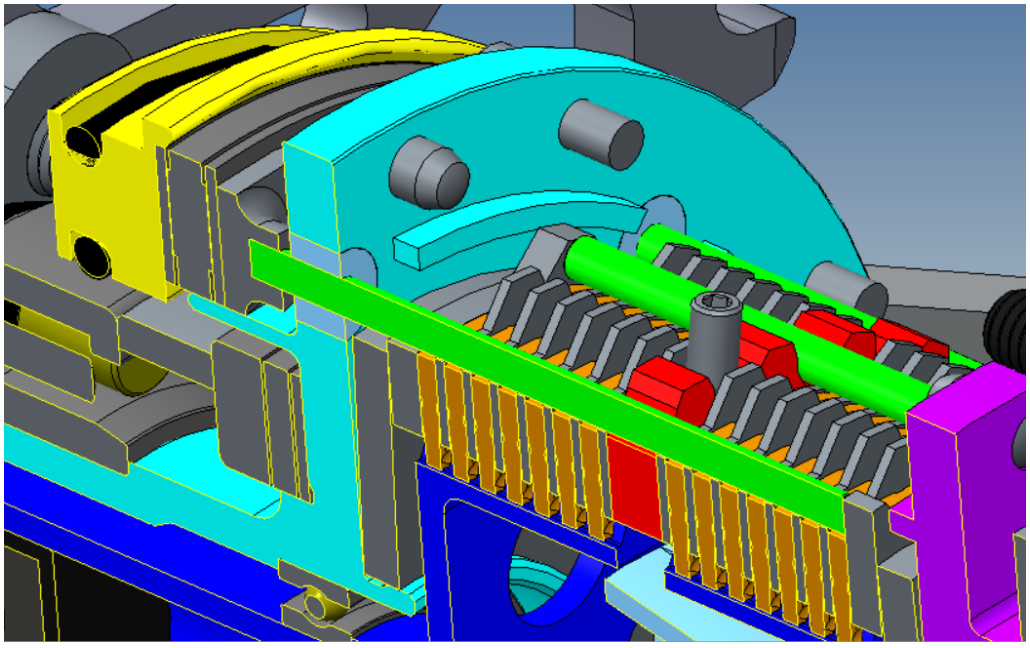

Figure 45: Piston and pushrods with hidden clutch drum and housing

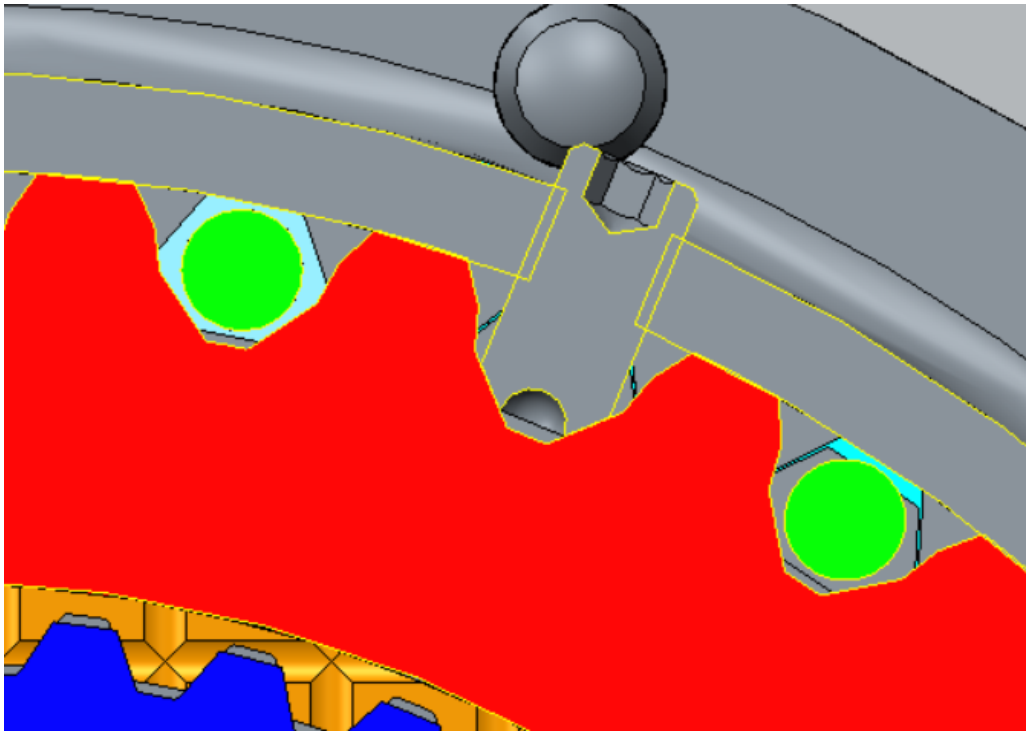

Figure 46: Pushrods at mid disc section

9.3 Shafts

9.3.1 Clutch drum assembly

The clutch drum assembly consists of a clutch drum, two clutch drum shafts and the mid disc. Its main purpose is to transfer the input torque to the outer friction discs. It has to provide room for pushrods, disc springs and hub bearings and support the load from them. There has to be a possibility for oil to flow to the clutch center. This has to be taken in consideration because the oil inevitably has to pass through the clutch drum assembly in some way. It is radially fixed by the two main bearings and axially fixed by the two needle thrust bearings that rest toward the housing. It has to be stiff in the axial direction between the end walls of the drum to reduce axial deformation variation when the pistons are actuated. Excessive axial deformation will lead to long torque response time. The assembly also needs to be stiff in bending due to the large chain force that applies a bending moment. The bending deflection has to be kept low in order to not damage the main bearings and the thrust bearings due to excessive misalignment. The weight has to be low in order to reach the system weight target. That is achieved through good choice of material and material treatment and through designing for good load paths, for example by using large diameter shafts to reach high strength/weight and stiffness/weight ratios.

The targets for the clutch drum assembly are:

- Enough bending stiffness to keep bearing misalignment under 2 mrad.
- Less than 0,2 mm axial deformation between clutch drum end walls when only disc spring preload force is applied (no piston force).
- Easy to assemble
- As low weight as possible

The first iteration of the clutch drum assembly is shown in figures 47 and 48. It is a compact concept, but difficult to manufacture because the tool for spline manufacturing can not pass through the clutch drum due to the closed end. It is also tricky to assemble. One spring and clutch pack have to be inserted first, then the mid disc has to be inserted and rotated to the locking position while being pushed to compress the spring. The same procedure has to be done

for the other clutch pack and the purple drum shaft. Note that rotational locking for the mid disc and the drum shaft is necessary but missing in the figures. This concept was ruled out due to lack of robustness and difficult manufacturing and assembly.

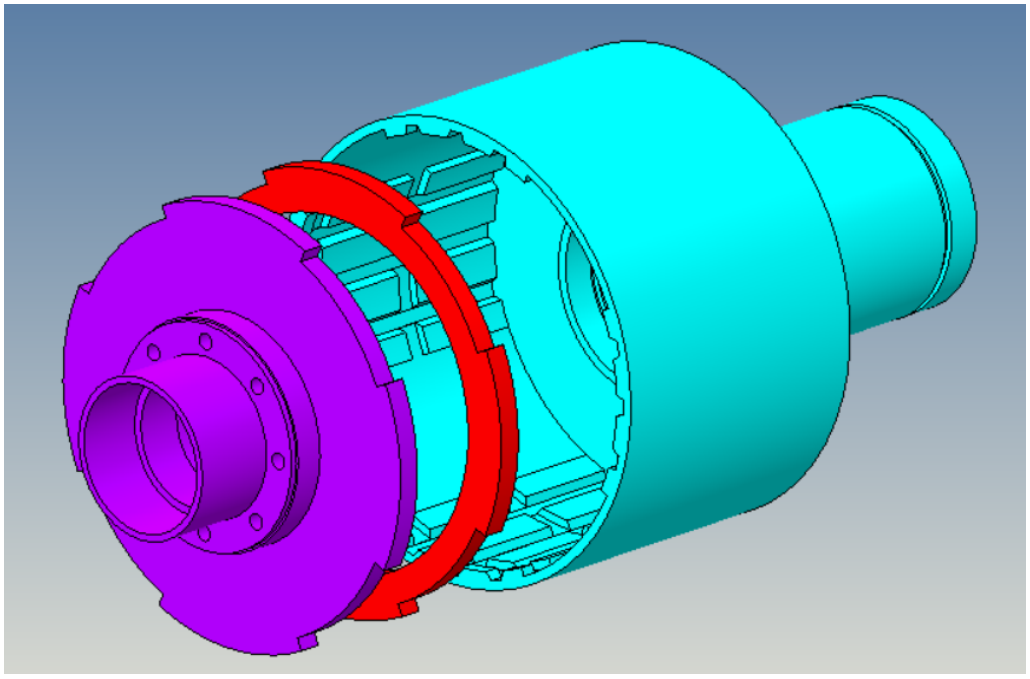

Figure 47: Clutch drum concept in the early stage

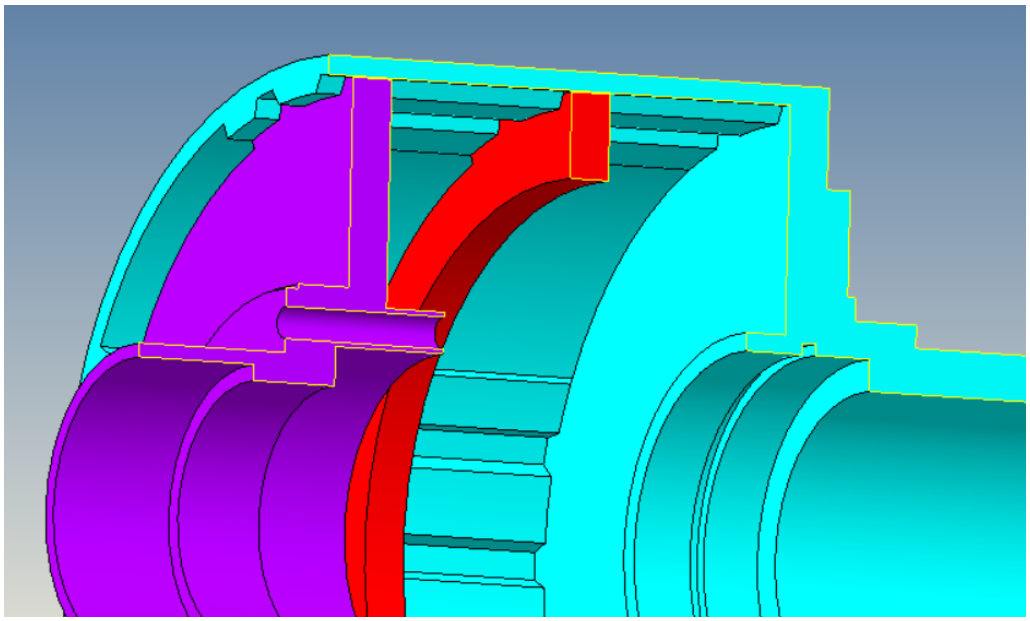

Figure 48: Clutch drum concept in the early stage, cross section

The chosen concept has a separate clutch drum and uses screw flanges to connect both shafts. The final design is shown in figures 49 and 50. It is easier to produce the splines, the interface between the purple drum shaft and the drum is more robust (no risk for play) and it is much easier to assemble compared to the concept above. The mid disc is first mounted and secured with four screws. Then the clutch pack and springs can be mounted from each side. The springs can be compressed by tightening the flange screws in a criss-cross pattern. A downside with the concept

is that the outer diameter increases due to the flange.

One alternative would be to weld the shafts onto the drum to save space, but that would be very impractical because the welding would have to be done with all components in place and compressed springs. It would also make it difficult to open up for clutch disc replacement or if there is a need for shimming of the disc springs. Therefor that alternative was also ruled out.

When the concept was chosen effort was spent on the details. One of the important design aspects was to maximize the diameter of the clutch drum shaft on the input side in order to reach the needed bending stiffness. It is also the most stressed part of the clutch drum assembly because it is subjected to the input torque and the bending moment peak for the whole assembly is located where the left main bearing is. It ended up with a 45 mm outer diameter. It would have been difficult to fit a larger left main bearing due to the piston that also needs place. The distance between the input sprocket and the bearing was important to reduce as much as possible since that is the lever arm that creates the bending moment in the whole clutch drum assembly.

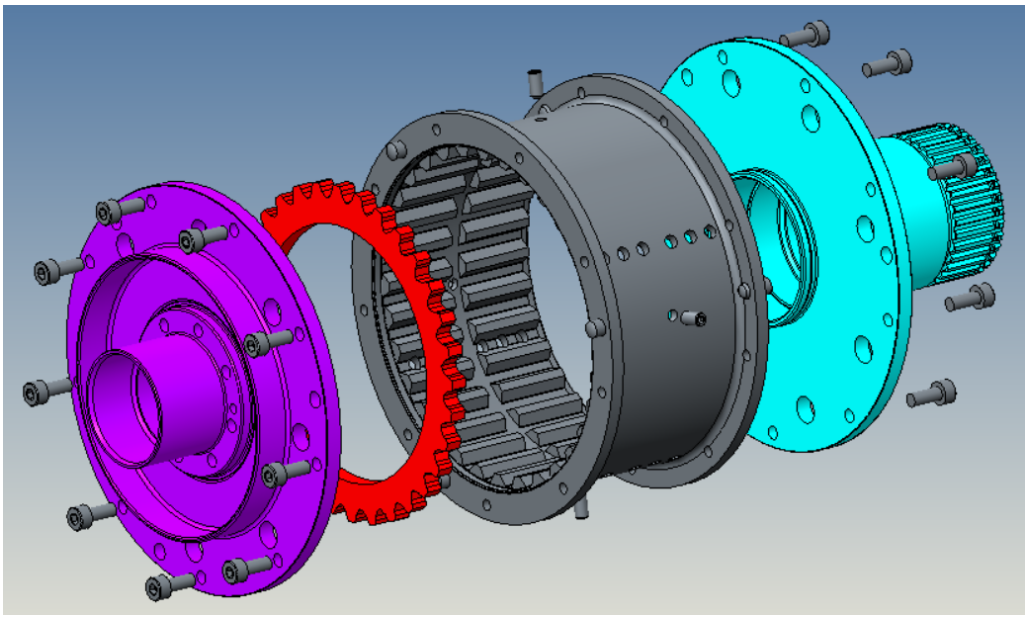

Figure 49: Final clutch drum design, cross section

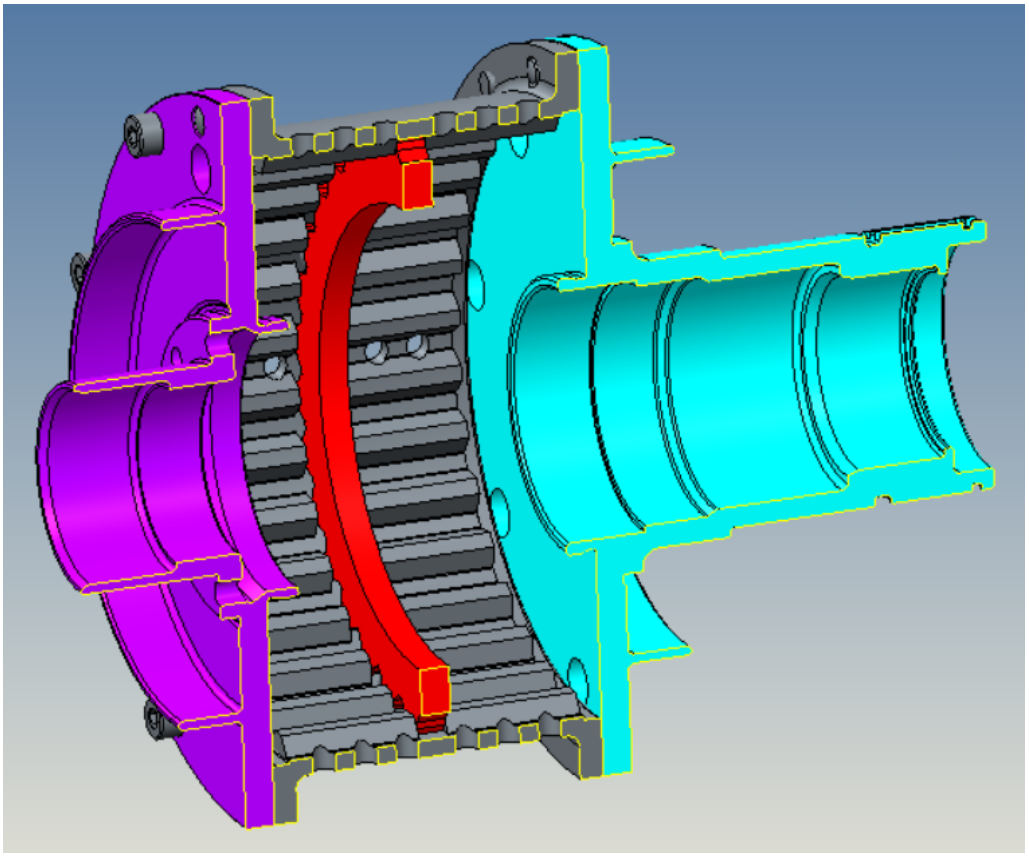

Figure 50: Final clutch drum design

Structural FEA was performed with load case 1. The setup and results are shown in figures 55 to 58. The stresses are in general not problematically high, but there are some stress concentrations that deserve a closer look. The peak stress is in the undercut at the left thrust bearing surface. It can be seen in figure 58 that the stress is decreasing very quickly towards the core of the material. 1270 Mpa is a high stress, but can be coped with if a good material and material treatment is chosen. For example quenched, tempered and nitrided 34CrNiMo6 steel. It has a yield strength 7-900 Mpa when quenched and tempered [5]. Nitriding gives a surface hardness of 600-800 HV [7], which corresponds to at least 1995 Mpa tensile strength according to DIN 50150 hardness to strength conversion [1].

The left axial bearing misalignment was measured to 1,06 mrad along the outer seat diameter and 2,46 mrad along the inner seat. The axial bearing is not loaded in this analysis. In reality, when it is loaded, the clutch drum assembly and housing will deform so that the misalignment is reduced, because the of the force distribution due to the misalignment. The misalignment at the left main bearing is 4,36 mrad if housing deformation is not taken into account. That is relatively much will definitely lead to reduced bearing life. On the other hand, it will only occur at peak load, the housing deformation will decrease the misalignment, and it is calculated with a relatively large dynamic factor. The allowed misalignment is discussed in section 9.4.

9.3.2 Hubs and tripod housings

The function of the hubs and tripod housings is to transfer the torque from the inner friction discs to the driveshafts. One important requirement is that oil has to be able to pass through the hubs in order to reach the friction discs. The LFS-team has used tripod joints (a constant velocity joint) in previous cars and is intending to keep the design in the future as well. The existing tripod housing design has therefor been copied and adapted to fit with the hub.

The hubs have to be fixed axially to the clutch drum assembly and also guided properly so that they can take up bending torque from the CV-joints. They also have to be well centered to

the drum so that they rotate co-axially in order to avoid NVH problems from the friction discs, and possibly from other sources as well. The hubs are therefor connected to each other through a ball bearing. The bearing transfers rightward axial force acting on the left hub to the axial washer of the right hub and it transfers leftward axial force acting on the right hub to the ball bearing of the left hub. It also transfers bending torque acting on the right hub, to the left hub which has bearings that together can take up bending torque. The point of using this bearing constellation is to avoid using a ball bearing on the right hub where space is very limited due to the oil channels that go through the clutch drum shaft. Instead only an axial washer could be used.

The tripod housings are fastened axially to the hubs with circular cross section snaprings in order to avoid long screws and complex, heavy design with threads in the hub. It is a design commonly used for axial fastening driveshafts in cars.

FEA analysis of the right hub is shown in appendix A. The worst load case was used; outer wheel in full acceleration cornering with angled driveshafts. Torque was applied on a tripod housing dummy, where the x-component is the driving torque and the y-component is the bending torque. A friction disc dummy with tangential cylindrical support was used to take up the driving torque. Two radial cylindrical supports were used as bearings and two compression only supports were used as axial bearings, which represents the real setup well (see appendix B).

High stresses were observed in one of the radiuses and in the spline root of the tripod spline. A submodel was created of the most stressed area. A very fine mesh could be used, without being too large because only a small part of the geometry is modeled. The nodal displacements of the full model analysis were used as a "load". In that way, the stress calculation becomes more accurate thanks to the fine mesh. It could be seen that the stresses should be possible to handle if the same material and heat treatment is used as for the clutch drum assembly.

One thing that is quite concerning is the relatively large radial deformation at the spline towards the tripod housing. It needs to be further investigated if it is a problem and in that case, what can be done about it.

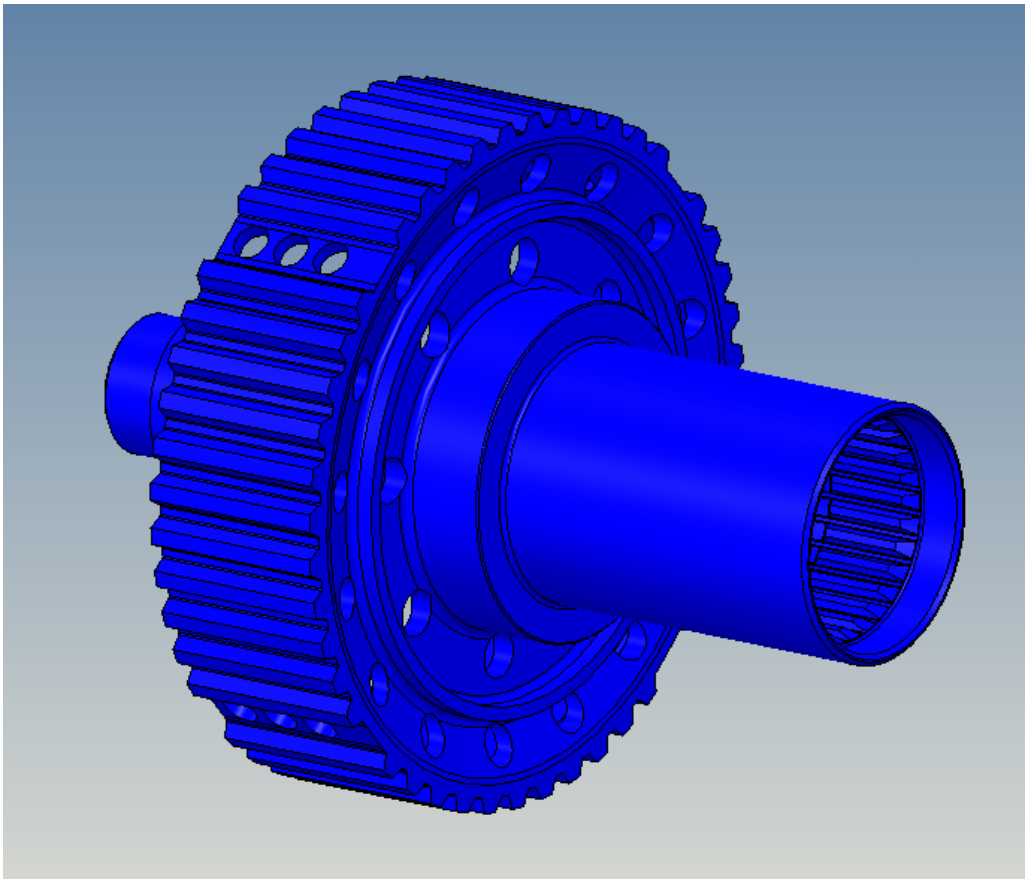

Figure 51: Right hub final design

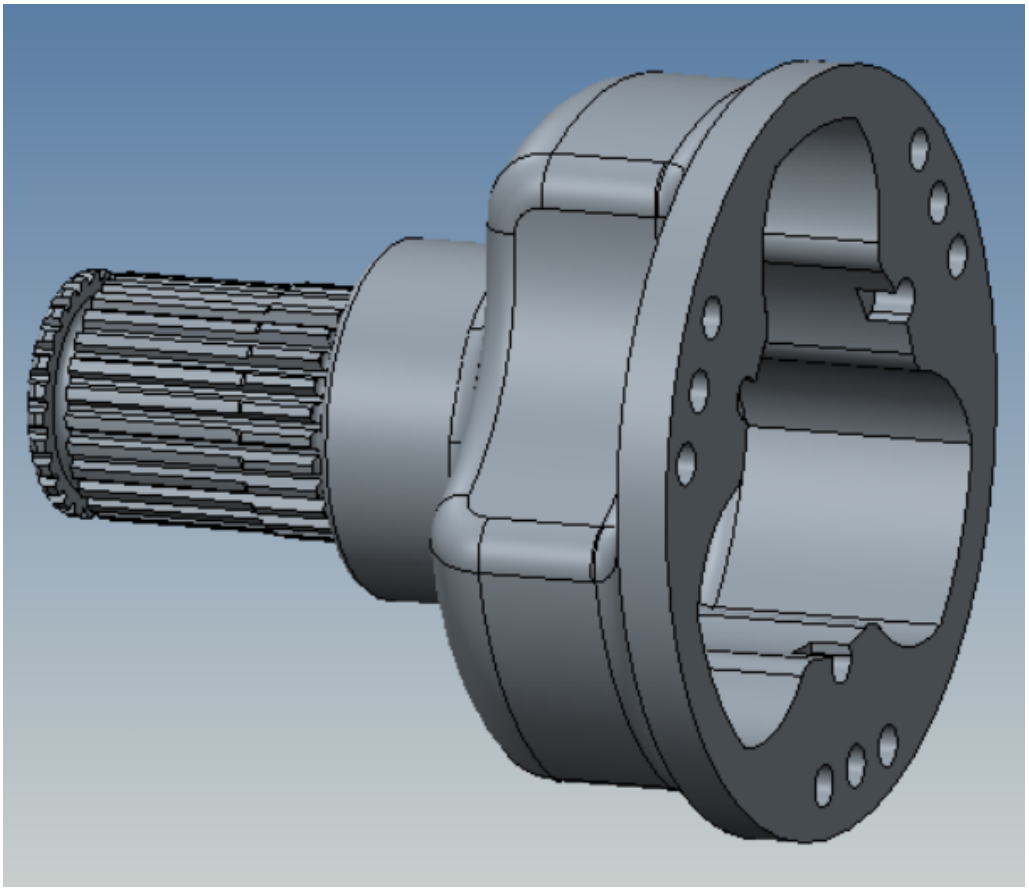

Figure 52: Right tripod housing

9.4 Bearings

Two bearing concepts were considered for the bearings that hold the clutch drum assembly in the housing. One was with two tapered roller bearings that take up the radial and axial forces. It could be a space efficient solution because only two bearings are needed. The downside is that the design becomes more complex because they have to be preloaded and that would put high demand on the axial stiffness characteristics of the clutch drum assembly in order to make sure that the correct preload is obtained at all piston force combinations. This concept was therefor not looked into further. The other concept was with two main bearings (ball or roller bearings) and two axial bearings. The main bearings take the radial force, and the axial bearings take the axial force. This was chosen due to simplicity and because axial needle bearings are used in BorgWarners clutches, which makes it a safer choice.

The targets for the bearings were to keep them as small and light as possible while having a life expectancy of 10 000 km. A very simple approach was taken for initial dimensioning. It was based on the nominal life expectancy L_{10} according to equation 38 from ISO 281, using the peak loads as input (with dynamic factor for the main bearings). The left main bearing takes a much larger force than the right one. It was found that a size and weight could be kept down if using a roller bearing on the left side instead of a ball bearing. The downside with a roller bearing is that it is more sensitive to angular misalignment. It is difficult to find exact numbers for maximum misalignment because it depends on many factors, like how it is mounted and loaded. Too large misalignment leads to a shorter life expectancy. The maximum misalignment is 0,6 - 2,9 milliradians for ball bearings and 0,9 milliradians for roller bearings according to the SKF catalogue [16].

The axial needle bearings were chosen based on what could be fitted. The chosen bearings are presented in table 14.

$$L_{10} = \left(\frac{C}{P}\right)^p \tag{38}$$

Where $p = 3$ for ball bearings and $p = \frac{10}{3}$ for roller bearings.

Bearing use	**Left main bearing**	**Right main bearing**	**Left axial bearing**	**Right axial bearing**	**Piston bearing**
Bearing name	NU1009ECP	61907	AXK5578	AXK5070	AXK85110
C [N]	44600	10800	34500	28500	52000
P [N]	23751	5051	17635	17635	17635
L_{10} [Millions of revolutions]	8,17	9,78	9,36	4,95	36,76
Driving distance [km]	11286	13506	12938	6844	50794

Table 14: *Bearing life expectancy*

It is very conservative to only take the peak loads into account, but it is also a large approximation to only look at the nominal life expectancy and not take oil viscosity and contamination into account. It would be desirable to do a system analysis in SMT Masta where oil viscosity, contamination, load spectras and misalignment due to deformation of shafts and housing can be taken into account. Unfortunately there was not enough time to do this.

The ball bearings and plain bearings inside the clutch drum assembly take up relatively small loads. The only loads are due to bending torque from the CV-joints, lateral acceleration of the car, and static load when mounting and dismounting the tripod housings due to the snaprings. Only a quick analysis was made on this and the work was unfortunately not documented but the conclusion was that they will not fail due to the loads.

9.5 Housing and mounts

The housing and mounts are supposed to hold everything together. The housing needs to be stiff, light and dissipate heat well from the oil to the ambient air. It has to provide room for an oil reservoir, pressure and temperature sensors and a breather. The mounts need to be removable so that the unit can be adapted to different vehicles or test rigs without making changes to the whole housing.

Load paths are the most important aspect to consider in the housing design, in order to achieve high stiffness, structural integrity and low mass. The load cases in tables 7 and 8 were kept in mind when designing the housing. The chain force has to be led to the mounting points toward the car frame, and the piston forces have to be led from one housing half, through the clutch drum assembly to the other housing half, and then back through both housing halves. The key is to keep the load paths as straight as possible in order to reduce bending loads and through that increase the stiffness and strength relative to the mass.

The left main bearing takes a large radial force due to the chain force. It was therefor made sure that there are straight walls leading from the bearing to the four left mounting points, which can be seen in the cross section figure in appendix B. The right main bearing takes a much smaller radial load so the load path is not as critical and therefor less effort was put on it. It is still relatively good thanks to the radial ribs on the right housing that lead the force from the bearing to the wall behind the piston, which then leads the force to the four right mounting points. The direction of the bearing forces can be seen in figure 66 in appendix A.

When the pistons are actuated, there will be a force that wants to separate the housing halves. It will also tend to deform the housing sidewalls in the axial direction which can be seen as "axisymmetric bending". Ribs that go in the radial direction towards the screws in the housing flange were used to increase the sidewall bending stiffness on both housing halves. This deformation is important to keep low in order to decrease response time. One of the benefits of having opposed

pistons instead of two pistons on the same side is that the maximum axial force acting on the housing is halved.

Cooling fins were added around the oil reservoir in order to increase the heat convection area of the housing. The structural ribs also help to increase the area. Cooling is further discussed in section 9.5.1.

Two dowel pins are used in the flange to align the housings. 12.9-grade screws were chosen to hold the housings together in order to save weight. Four of the nine screws are also used for the right mounts. Double shear joints were chosen for the left mounts, which have to take a large force. Single shear joints were chosen for the right mounts to increase the manufacturability of the right housing.

Aluminium was chosen as material for housing and mounts. It has good heat transfer properties compared to steel and is commonly used in housing applications, both by BorgWarner and other manufacturers. Since this is a prototype, the housing will be milled from a solid block and not cast. Therefor the 7075-T6 alloy was chosen. It has high strength to weight ratio, stiffness to weight ratio and machinability. An extruded round bar of 7075-T6 with 150-200 mm in diameter has a yield strength of 400 Mpa and tensile strength of 440 Mpa according to Alumeco [4]. That results in a maximum allowed stress of $\frac{400}{1,2}$ = 333 Mpa. A problem with hardened aluminium is that the mechanical properties are worse for larger dimensions of material because the temperature distribution becomes more uneven throughout the material piece in the hardening process. The left housing has to be made from a piece that is at least 180x180x120 mm.

FE analysis was performed for the straight full acceleration load case and for right piston de-airing and is presented in appendix A. The other de-airing cases were also analyzed but the analysis is not presented because the results were similar to the first case. The conclusion in general is that the housing and mounts are relatively good, but need some changes in order to reduce stresses in some areas, and deformations in some other areas. A second iteration of the housing has been made, but an analysis of that has not been made because the time ran out. The presented analysis is for the first iteration. The second iteration design is shown in figure 53.

In the acceleration load case, the largest problem was around the left actuator sump. The are high stresses on the radius where the pump supply channel meets the actuator sump, over 510 Mpa. It would probably not be a problem if a larger radius was used, but unfortunately the CAD-program did not allow that. The geometry of the channel was changed for the second iteration of the housing design in order to allow a larger radius of 4 mm instead of 1 mm. Another problem was the large deformation of the actuator sump, due to the force in the lower arm of the lower left mount. It could lead to leakage past the sealing rings of the actuator. In reality, the deformation is most probably not that large, because the actuator will stiffen up the sump. Nevertheless, a change was made to the angle of the arm that supports the sump, in order to increase stiffness. Including the pump part of the actuator in the analysis would increase the accuracy in the analysis in this area of the housing.

High stresses could also be found at the upper left mount, reaching 630 Mpa. The geometry of the "ears" was changed for the second iteration and the thickness was increased from 3 to 4 mm. The stress peak could also partly be due to the way the boundary condition of the joint is applied. Including the screw and sphere from the bearing would increase the accuracy of the analysis. There are stress peaks at the lower left mount near the points where it is fastened to the housing. These could arise due to the way the connection is defined, and therefor a new analysis would have to be made, where the screw is included in order to draw any conclusions.

A relatively large deformation of the left main bearing seating surface can be seen as well. It would probably be smaller if the bearing was included in the analysis because it would have a stiffening effect when press fitted in place. Nevertheless, it is important to look at this deformation because the housing could pinch the inner diameter of the piston. The conclusion is that the piston to housing clearance at the inner diameter should be slightly larger, and the piston should rather be guided by the outer diameter.

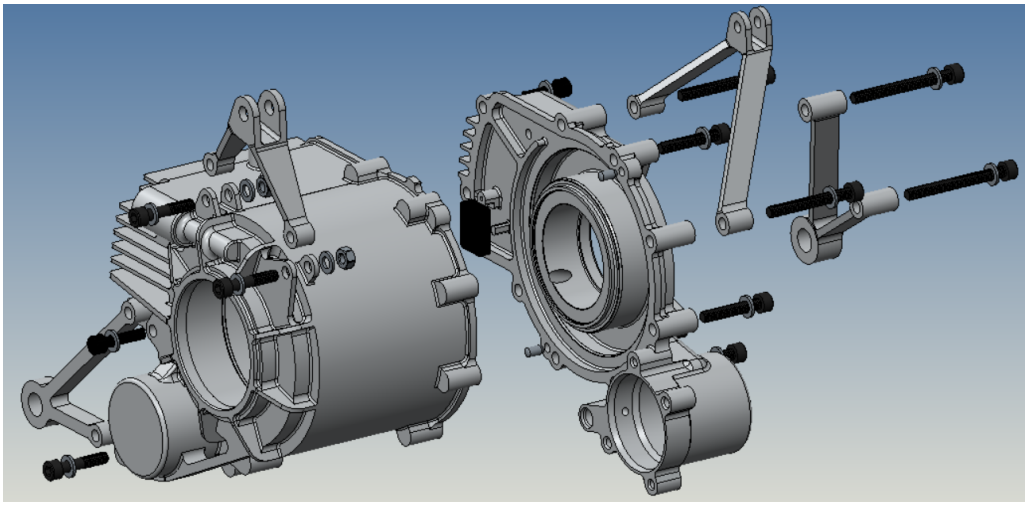

Figure 53: Housing and mounts

9.5.1 Heat analysis

Heat will be produced in the unit according to the feasibility analysis, therefor it has to be made sure that no component gets too hot. The clutch friction coefficient is decreasing rapidly with increased oil temperature. There is also a risk for overaging the aluminium of the highly stressed housing, but also pushrod carrier and pistons, which will lead to a decrease in material strength and eventually a failure. An other heat challenge is that the unit is placed right behind the engine, which is not really the coolest place on the car. On the other hand, new cold air is constantly blowing on the car as it is driving around.

It is complex to accurately model the heat flow and temperature because it depends on many parameters. The airflow around the unit and the oil flow inside, along with surface roughness, and materials will all have an effect on the results. It was out of the scope of the thesis to make a CFD-model or practical tests to base the heat calculations on. Instead a quicker and simpler approach was taken. The purpose was to evaluate if the cooling capacity would be approximately good enough with just air cooling, or if a higher capacity cooling system would be needed.

It was assumed that all produced heat goes to the oil, which then transfers the heat to the inside wall of the housing with convection. The heat goes through the housing wall by conduction. It goes from the outside housing wall to the ambient air by convection. No other heat transfer is included in the calculation. Steady state heat transfer is assumed, which means that the thermal capacity of the mediums is irrelevant for the analysis.

The input for the analysis is shown in table 15. The needed cooling power is based on the SRS, which is based on table 6. An ambient temperature which should correspond to a hot summer day was used. The maximum allowed oil temperature is based on experience from BorgWarner and the overaging effect on aluminium.

The inside and outside housing area and thickness was taken from the CAD-model. The conduction coefficient for aluminium was taken from [8]. The convection coefficients were more difficult to determine because they depend very much on the velocity of the flowing medium and the turbulence at the surface. In paper [15], forced convection from air to an aluminium fin (6063 alloy) of the same size order as the dual clutch is measured. Unfortunately, the air velocity is not mentioned. The resulting convection coefficient is 100-101 $\frac{W}{m^2K}$ depending on surface roughness. In paper [17] measurements have been performed on two different aluminium heat sinks. The results are varying quite much with reynolds number, but seems to be typically around 50-100 $\frac{W}{m^2K}$. A relatively conservative choice was made for the air-aluminium convection coefficient based on this. In paper [13] a theoretical CFD-study is done on an impinging oil jet for piston cooling of an internal combustion engine. The study results in a convection coefficient of around 6300 $\frac{W}{m^2K}$, which is compared to a theoretical formula that gives around 2600 $\frac{W}{m^2K}$. An impinging jet creates high turbulence and thus transfers heat well. The oil in the dual clutch will be mixed around, which is

also positive for heat transfer. A conservative choice was made for the oil-aluminium convection coefficent as well, based on this.

Equations 39 - 41 were used for convection and conduction to calculate the resulting temperatures and the results are presented in table 16.

T_a [°C]	45
$T_{oil,max}$ [°C]	130
Q [W]	600
$h_{c,air-aluminium}$ $[\frac{W}{m^2K}]$	60
$h_{c,oil-aluminium}$ $[\frac{W}{m^2K}]$	1000
$k_{aluminium}$ $[\frac{W}{mK}]$	164
$A_{housing,out}$ $[m^2]$	0,164
$A_{housing,in}$ $[m^2]$	0,1
$t_{housing}$ $[m]$	0,003

Table 15: *Heat analysis input data*

$$T_{housing,out} = \frac{Q}{h_{c,air-aluminium} A_{housing,out}} + T_a \tag{39}$$

$$T_{housing,in} = \frac{Q}{\frac{k_{aluminium}}{t_{housing}} A_{housing,in}} + T_{housing,out} \tag{40}$$

$$T_{oil} = \frac{Q}{h_{c,oil-aluminium} A_{housing,in}} + T_{housing,in} \tag{41}$$

$h_{c,air-aluminium}$ $[\frac{W}{m^2K}]$	**60**	**47**
$T_{housing,out}$ [°C]	106	122,8
$T_{housing,in}$ [°C]	106,1	123
T_{oil} [°C]	112,1	129

Table 16: *Heat analysis results*

First of all, it can be observed that the resulting oil temperature is below the maximum limit, which is very positive. It can be seen that the heat transfer is mostly limited by the aluminium - air convection. The temperature difference between the outside of the housing and the ambient air is 61 °C, compared to 0,1 °C between inside and outside, and 6 °C between oil and housing inside. The impact of the conduction and oil-aluminium convection coefficients on the result is not very large. The air-aluminium convection coefficient is affecting the result much more, therefor a sensitivity analysis was performed. It can be seen that a coefficient of 47 $[\frac{W}{m^2K}]$ results in an oil temperature approximately at the allowed limit. The neglection of conduction to driveshafts and car frame together with conservative coefficient choices makes the analysis conservative, but the neglection of sun radiation makes it more optimistic.

The conclusion is that the oil temperature will be possible to keep below the maximum allowed, and the housing temperature will be below the temperature where over aging can be a problem. If it is shown that the temperature of the unit is too high, cooling can be improved in several ways. A fan that directs cold air on the unit can be added. An other possible improvement could be to increase the surface roughness by for example sand blasting the housing.

9.6 Actuators and oil system

Two actuators are used in the design, one for each piston. The actuator is a BorgWarner product that is used in other applications as well. The Gen V actuator uses a DC-motor and an axial piston pump to produce the hydraulic pressure that actuates the piston. The Gen VI actuator

uses a brushless DC motor instead of a conventional one. They have a slightly different interface toward the housing and a slightly different size. The ECU is integrated in the Gen VI actuator while there is an external ECU for the Gen V. One kg of mass can be saved if Gen VI is used, but the motor control software is much easier to implement with Gen V. Therefor, the housing was designed to be able to fit both types so that the choice of actuator model can be made by the control and software designers.

One weight saving alternative could be to only use one actuator and a valve that controls which piston the actuator is connected to. This would be possible because normally only one piston has to be actuated at a time since the clutches are normally closed. On the other hand it would probably be difficult to achieve the same performance as with two actuators, especially when it comes to response time. The idea was quickly scrapped due to the already high enough complexity of the unit, but could be something to look into in the future.

There are three separate oil flow paths. One is the oil flow that lubricates and cools the friction discs, and the other two are the de-airing flow paths, one for each actuator. The flows are explained below. The lubricating and cooling flow path starts in the reservoir. The oil passes the magnet and continues through a channel in the right housing half. It comes out to the left of the right main bearing and is pumped through the clutch drum end wall by the oil scoop that is attached to the clutch drum shaft. It continues through the holes in the hub into the clutch center. There is a thin plastic ring that creates a seal between the hub and clutch drum end wall so that the oil does not escape that way due to the centrifugal force. Every other of the eight holes in the hub is connected to the oil distributor that throws the oil to the left hub. The centrifugal force then throws the oil through the radial holes in the hubs into the friction disc compartment. The inner friction discs have grooves through which the oil can flow to the clutch drum. The oil is then thrown out through the radial holes of the clutch drum, into the reservoir through the 10 mm high slot in the housing.

It has been in focus to get much oil to the friction discs in order to cool them well. A tough challenge was to find room for the oil to pass through the clutch drum end wall and the hub while going within the inside diameter (46 mm) of the disc spring. The oil can not be routed outside of the disc spring because then it would be thrown out through the clutch drum without passing through the friction discs. The other way would be to try to push the oil inside the hub shaft, but that would be a risky solution because it would have to work against the centrifugal force. It could maybe be done if an external pump was used but using a separate pump would increase complexity and mass, so it was avoided.

One more difficulty with the lubrication is that the oil will always be thrown towards the outside clutch when the car is cornering, but it is mostly the inside clutch that needs to slip and thus need the oil flow. The oil distributor is therefor especially needed in left hand corners and will hopefully help to distribute oil to the left clutch.

No quantitative analysis of the oil flow has been done due to time constraints. If more time was available a 3D printed prototype would have been used to measure the oil flow. An other alternative would be to do a CFD analysis.

10 Outcome

The outcome is presented in figure 54 and in appendix B. The resulting mass is 9561 g with Gen VI actuators and 10551 g with Gen V actuators, excluding oil and sprocket and including tripod housings, as seen in figure 54. The exact amount of oil has not been defined, but with 0,5 L the weight will be very close to 10 kg with the Gen VI actuators.

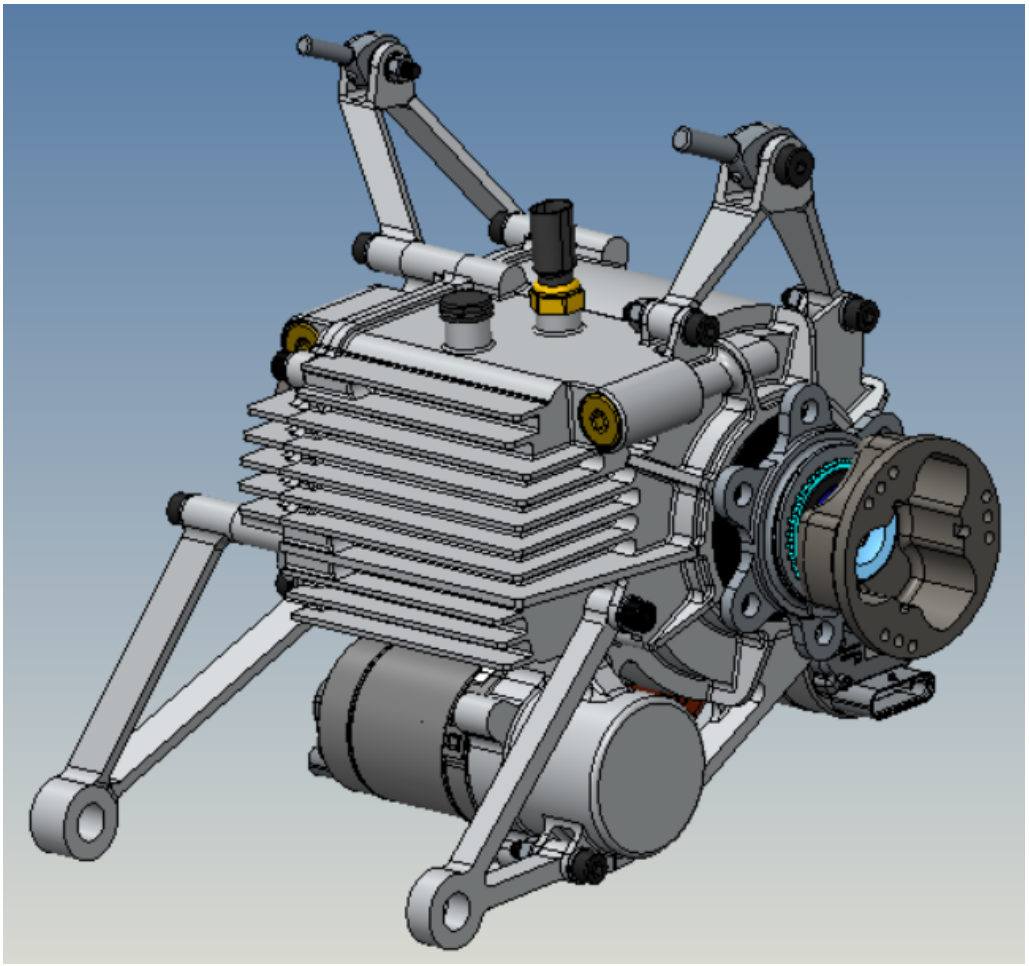

Figure 54: Complete assembly with Gen VI actuators

11 Discussion

The project turned out to be much larger than expected so the initial plan could not be completed within the timeframe of the thesis. The first three project goals were met, and the fourth was partially met because there is a 3D-model of the device, but it is not completely finished. The rest of the goals were not met, but nevertheless a lot of progress has been done and a good foundation has been set to make reality of a dual clutch torque vectoring device in the future.

It was decided early in the process that a lapsim analysis would be needed in order to evaluate if the dual clutch would be feasible to use as a permanent propelling device, or if it would be too bad in terms of efficiency and cooling requirements. It took more time than it was expected to find a way to do the analysis with the tools that were available, but in the end it was worth it because of all the results it led to, that could be used as input to the SRS. The quantitative comparison between the NO and NC concepts gave knowledge about the characteristics and differences between them. A quicker alternative would be to estimate the losses roughly with hand calculations instead and save 2-3 weeks of work. The accuracy would probably have been good enough to tell if the efficiency high enough for the concept to be useful, but it would not be accurate enough to be used as input to the SRS for cooling power demand and electric power consumption. The torque capacity demand could have been hand calculated with fairly good results.

It also took some time to get up to speed with all the tools that were used, but on the other hand that was unavoidable and it also felt very rewarding to become more confident in using different engineering software.

The higher complexity of the NO-concept compared to the NC-concept led to increased design time. The size and force capacity of the disc springs had to be matched with the size of the clutch packs and pistons, which is of course more complex than just dimensioning the clutch packs and pistons. The oil path to the clutch center became more complex due to the small inner diameter of the disc spring. It required much design time to find a good compromise between oil flow capacity (which was only qualitatively evaluated), structural integrity and manufacturability of the right clutch drum shaft and right hub. The NO-concept would most probably not need a flange on the clutch drum assembly, leading to a smaller housing as well. The axial length of the unit would also be smaller without disc springs and it would be possible to reduce the mass and meet the target of 9 kg. It can definitely be questioned whether the right choice was made when choosing the NC-concept, but in the authors opinion, it will not be possible to answer correctly until both concepts have been tried out in real testing on a race car. If time could be turned back and the choice could be made again, the same path would have been taken.

The question to answer with the thesis was: **Is it possible to make a transmission that allows independent driving wheel torque control on a combustion engine driven formula student car, without vastly exceeding mass and size of an LSD?**

The presented dual clutch unit replaces the LSD, sprocket carrier, two bearings, tripod housings and differential mounts in the LFS drivetrain. These parts weigh 5,45 kg together on the LFS-18, which is 4,55 kg lighter than the dual clutch, or almost half the weight. Considering a car that weighs 300 kg with driver, it is a 1,5% difference in total mass. The dual clutch is slightly larger, but not very much considering the added functionality. It has not been proven that this dual clutch works in reality, but the analysis and reasoning in this thesis hopefully points to that it is likely to work. Based on this, the subjective answer to the question is **YES**.

12 Future work

The purpose of this section is to investigate what would have been done if more time was available. It also serves as help for those who will continue with the work.

12.1 Needed for working unit - not started tasks

These are the major things that have not been done, but that have to be done in order to have a working product:

- Specify amount of oil.
- Choose gasket material and design the gasket between the housing halves.
- Specify heat treatment types, surface hardness and hardening depth for the clutch drum assembly, sprocket carrier and hubs.
- Create 2D-drawings and specify tolerances.
- Order all parts.
- Assemble the unit.
- Initial functional rig testing and tuning of control parameters in rig.
- Car testing - fine tuning of control parameters and reliability testing.

12.2 To finish and improve - unfinished tasks

The tensioning torque has to be specified for all screws. The dimensioning of the screw joints has been done by looking at required preload to prevent slippage at the joint. For the axially loaded screws (housing flange and clutch drum flange), preload was calculated so that at full axial load, the yield limit is not exceeded while still providing enough friction. The work was not documented so it needs to be re-done.

The oil distributor that is inside the clutch center needs to be designed. What can be seen in some figures is only the concept for how it could look. A 3D-printed plastic part that is screwed onto the right hub is proposed. In that case it has to be ensured that the plastic can cope with the high temperature of the oil and hub. The same has to be verified for the oil scoop that is also meant to be in 3D-printed plastic.

FEA has to be done on the second iteration of the housing with screw joints and pump part of the actuator included. The analysis has been set up, but has to be run on a computer with more than 16 GB of RAM, due to the mesh size and large number of connections. Over-aging of the aluminium has only been looked into very briefly, but it definitely deserves a closer look. If tempered aluminium is exposed to high temperatures for a long time, it will lose its strength. If the housing reaches 120 °C, it will probably be a problem that has to be dealt with. Either an other material can be chosen, or it has to be made sure that the housing never reaches those temperatures. A third alternative is to reduce the stresses in the housing so that it works with the strength of over-aged 7075.

The strange deformation of the hub in the FEA has to be looked into. It should be made sure that the results are realistic and the analysis should maybe be re-done.

The sprocket carrier needs to be verified with FEA to ensure that the stresses and deformations are reasonable.

Tip and root clearances and quality has to be specified for the splines between tripod housing and hub, and the splines between sprocket carrier and left clutch drum shaft. The numbers in the reports in appendix C are just the preset values by KISSsoft. (The friction disc splines have been fully specified).

12.3 Potential design improvements

It was noticed in a late stage that the sprocket could have been placed closer to the left main bearing if it was put on the right side of the sprocket carrier flange. In that case, the six screws that fasten the sprocket should be turned around so that a nut can be used on the left side. (This change could also be done with the current placement of the sprocket to gain more thread length without increasing mass significantly). Placing the sprocket closer to the bearing would decrease the bending moment lever arm from the chain force and lead to less bending of the clutch drum assembly and thus less bearing misalignment. Making this change would require changes to the housing. The chain would come too close to, or interfere with, the left actuator sump and the right actuator if a GenV actuator is used. The left mounts would have to be modified so that the same axial distance between the sprocket and the mounts is maintained in order to fit the LFS-19 car straight on.

The axial clearance between the mid disc and the spline side faces of the clutch drum is important to keep low, in order to achieve good torque accuracy. The disc will move axially every time the axial clutch force on one side becomes larger than on the other side if a clearance is present. This will lead to sudden torque changes which could lead to bad performance. In the current design there has to be a clearance, even if it probably can be kept down to around 0,01 mm with enough manufacturing precision. A solution that clamps the mid disc in place would be desirable, for example using some kind of wedge effect or making the mid disc in a material with higher thermal expansion coefficient than the clutch drum so that it is clamped in place at working temperature, but possible to assemble at room temperature.

The mass target was exceeded by 1 kg. It is difficult to see how the unit could be lightened that much, but a couple hundreds of grams should be possible. Material can be removed around the flange on the clutch drum assembly between the screws and pins. The pistons can be lightened by drilling blind holes in them, or by lathing a groove. The wall thickness of the side walls on the clutch drum shafts could maybe be decreased, or holes could be made in them, although this would reduce the stiffness and thus increase the deformation due to spring force.

12.4 Potential analysis improvements

The oil flow in the unit has not been quantified. A CFD analysis would be useful to do in order to see that the oil system is working. The analysis could be validated by making a 3D-printed plastic prototype and rotating the hub and clutch drum assembly with different speeds using a lathe and a drilling machine while measuring the oil flow.

CFD could be used to model the heat transfer from the unit to the ambient air and surrounding components in order to estimate the working temperatures of the different components of the unit.

No effort was spent on modeling the torque response time. It would be interesting to do it, especially because it is a NC-clutch, of which limited experience was available at BorgWarner. It could for example be done in Simcenter Amesim where hydraulic systems can be modeled.

A bearing life analysis in SMT Masta with a load spectra based on the lapsim results would be useful to do to ensure that the bearings have sufficient lifetime.

13 Appendix

13.1 Appendix A - FEA setups and results

13.1.1 Clutch drum assembly

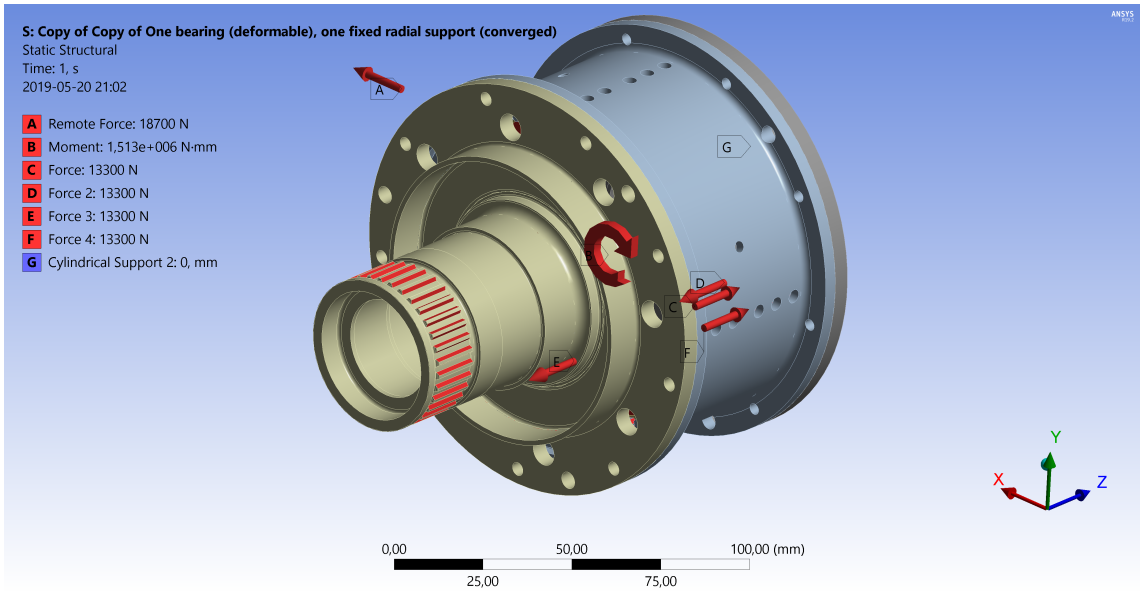

Figure 55: Clutch drum assembly FEA setup

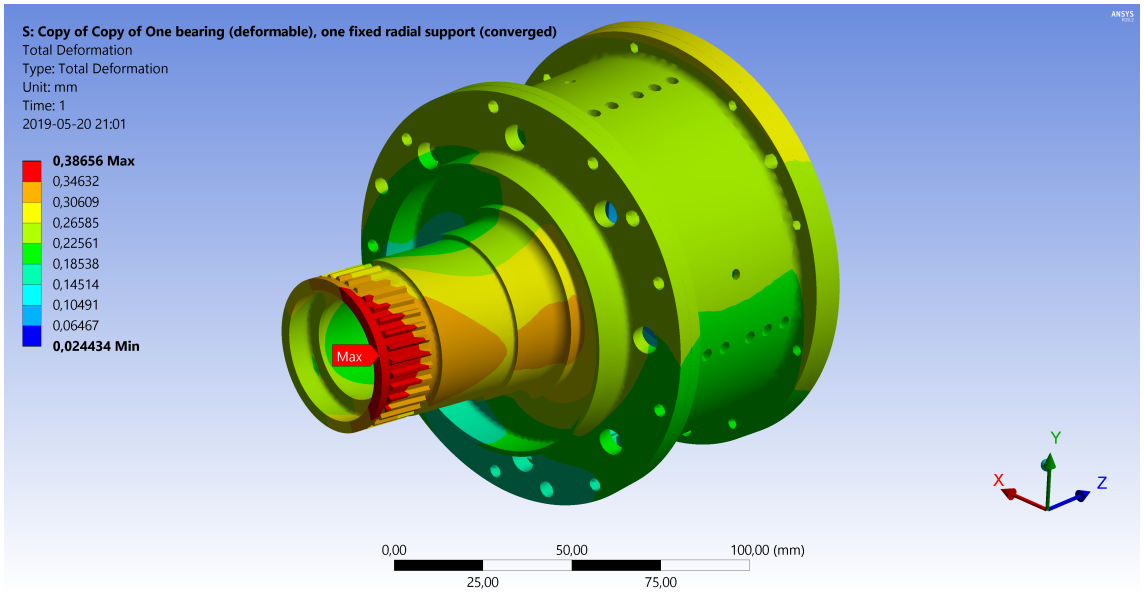

Figure 56: Clutch drum assembly deformation

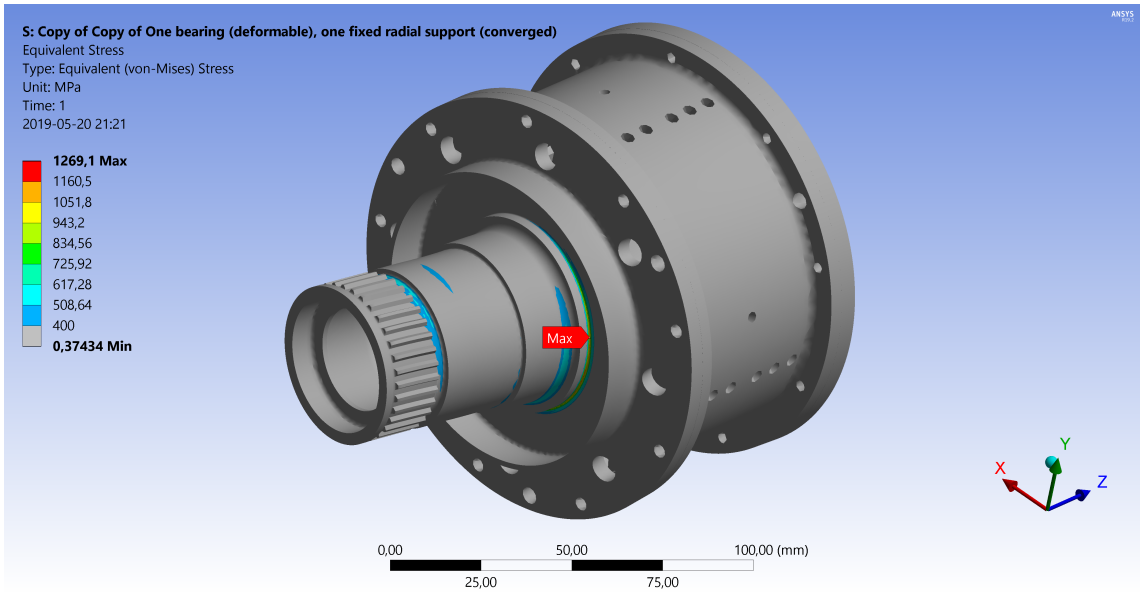

Figure 57: Clutch drum assembly Von Mises stress

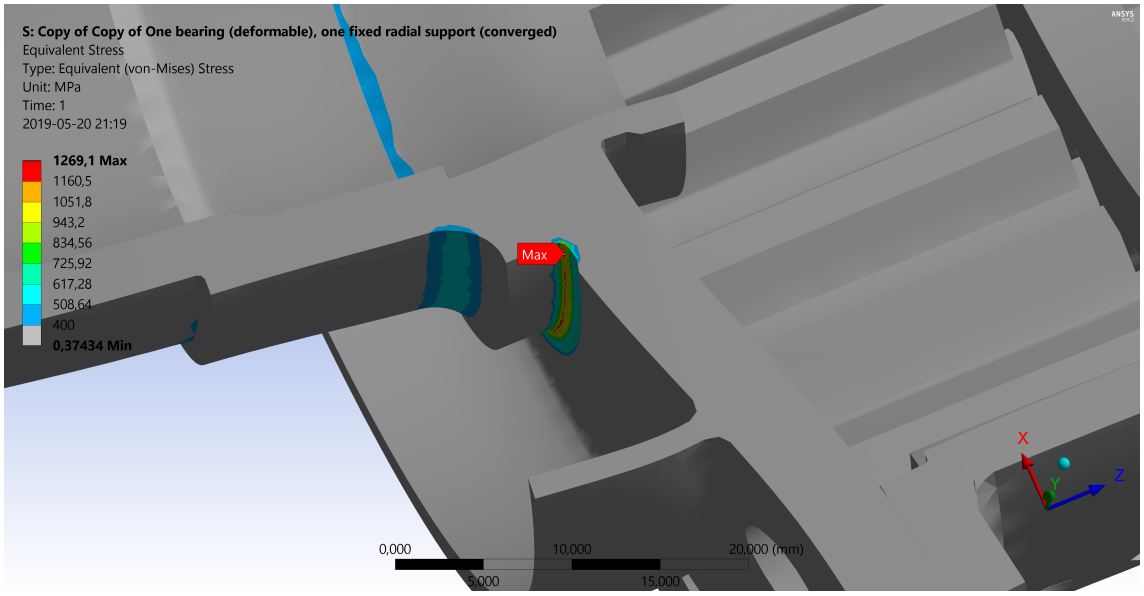

Figure 58: Clutch drum assembly Von Mises stress peak

13.1.2 Hubs

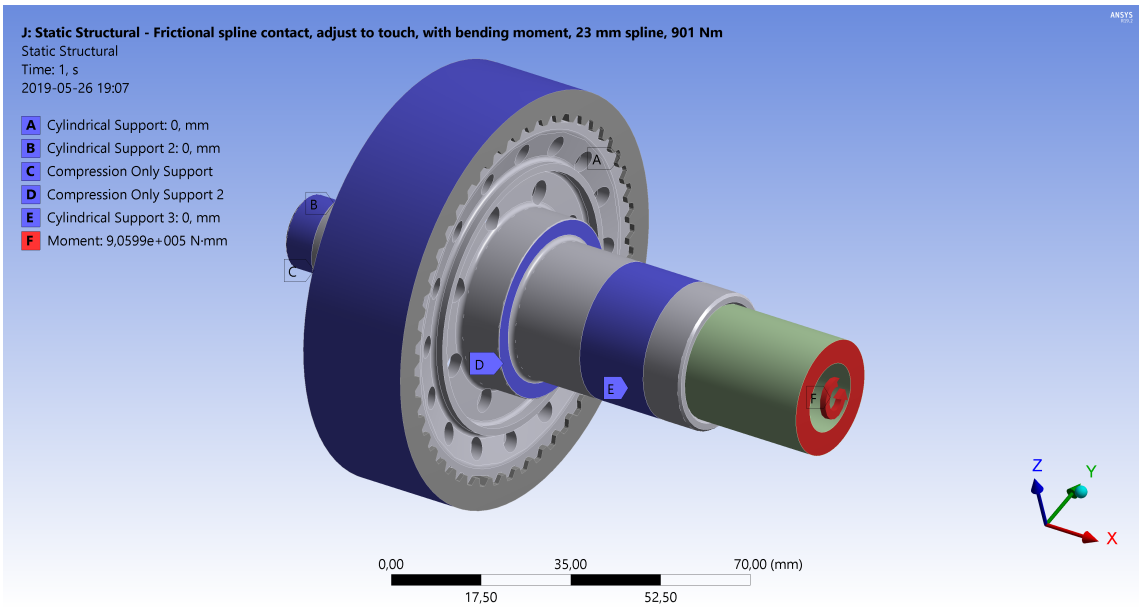

Figure 59: Right hub FEA setup

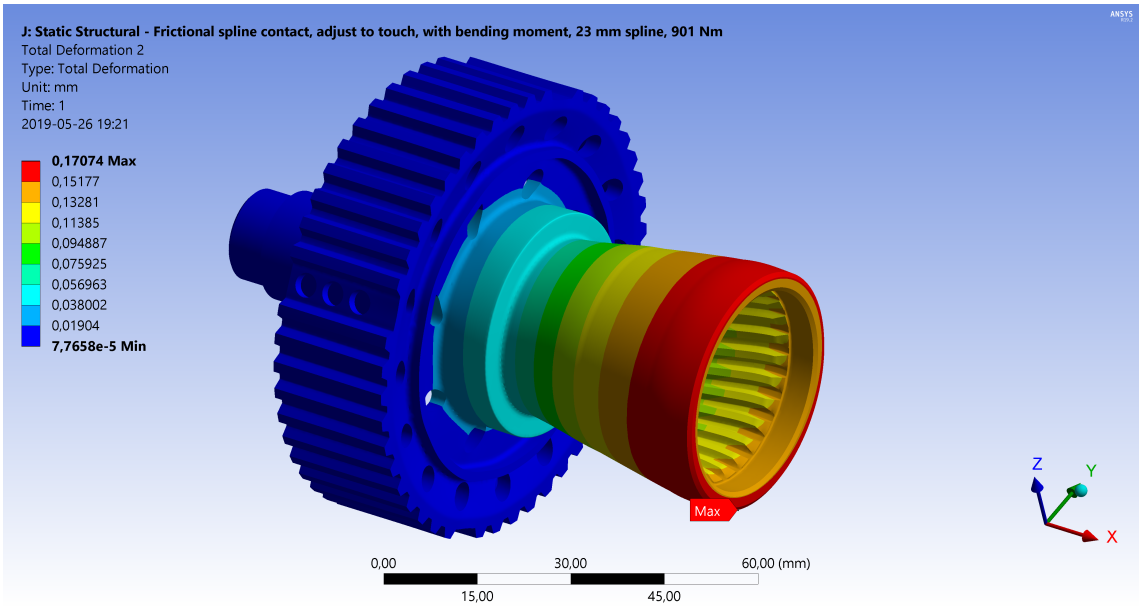

Figure 60: Right hub total deformation

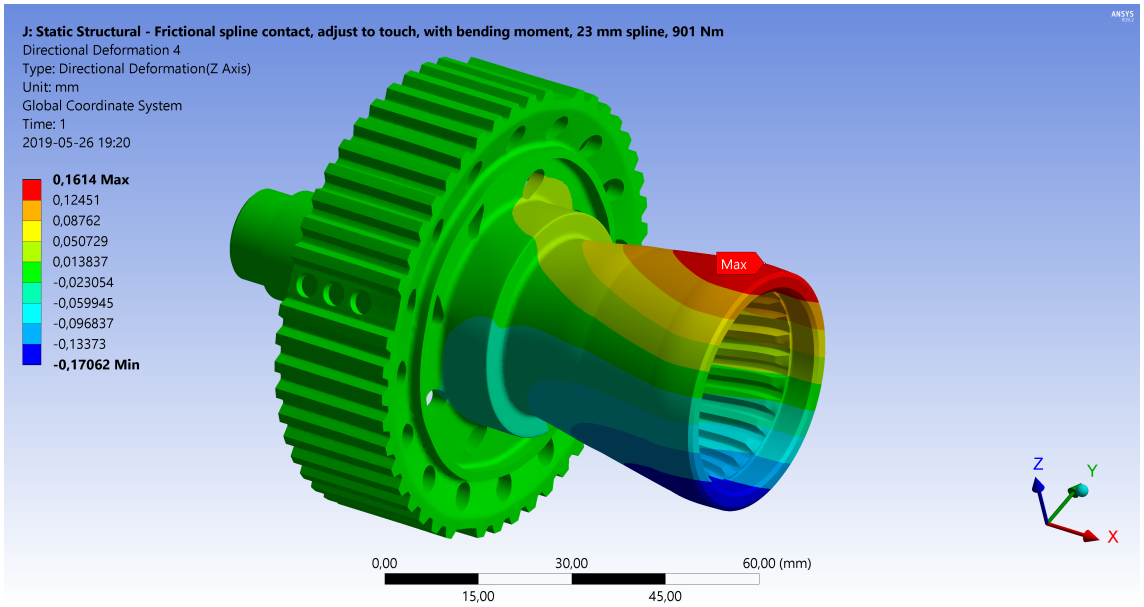

Figure 61: Right hub z-axis deformation

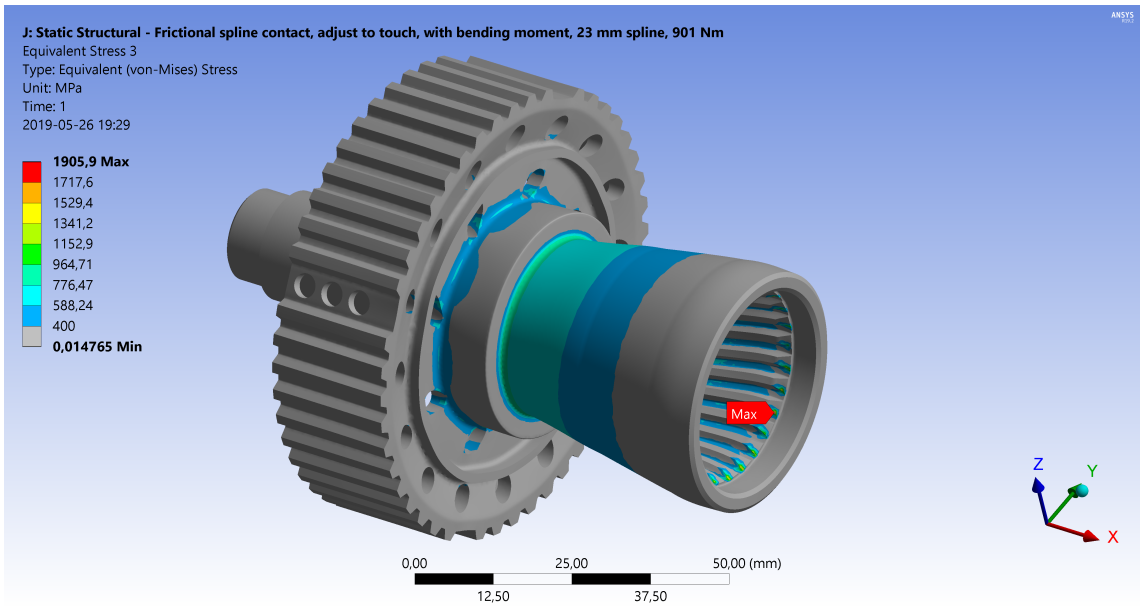

Figure 62: Right hub Von Mises stress

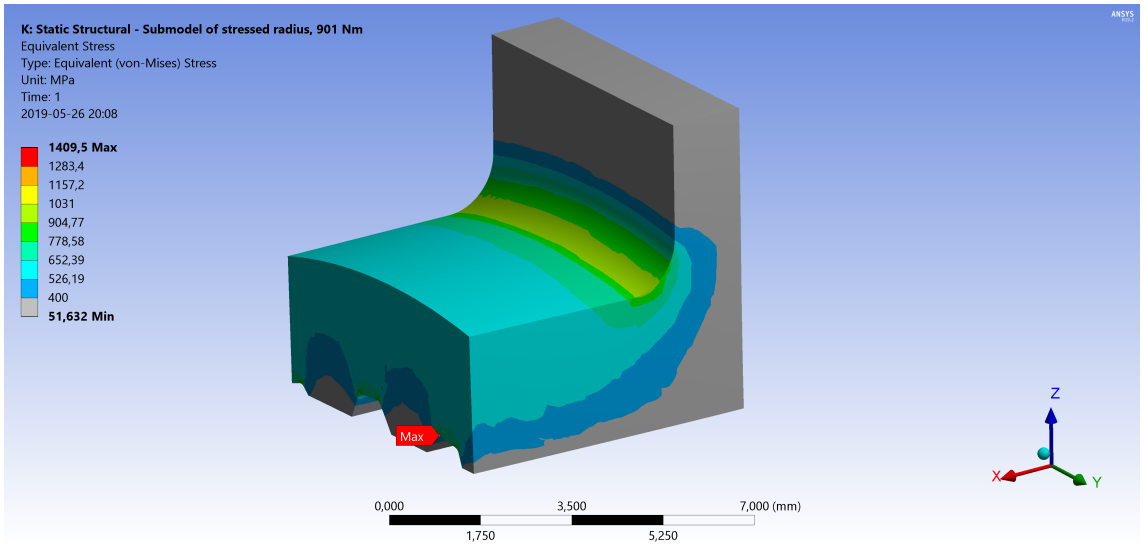

Figure 63: Right hub submodel Von Mises stress

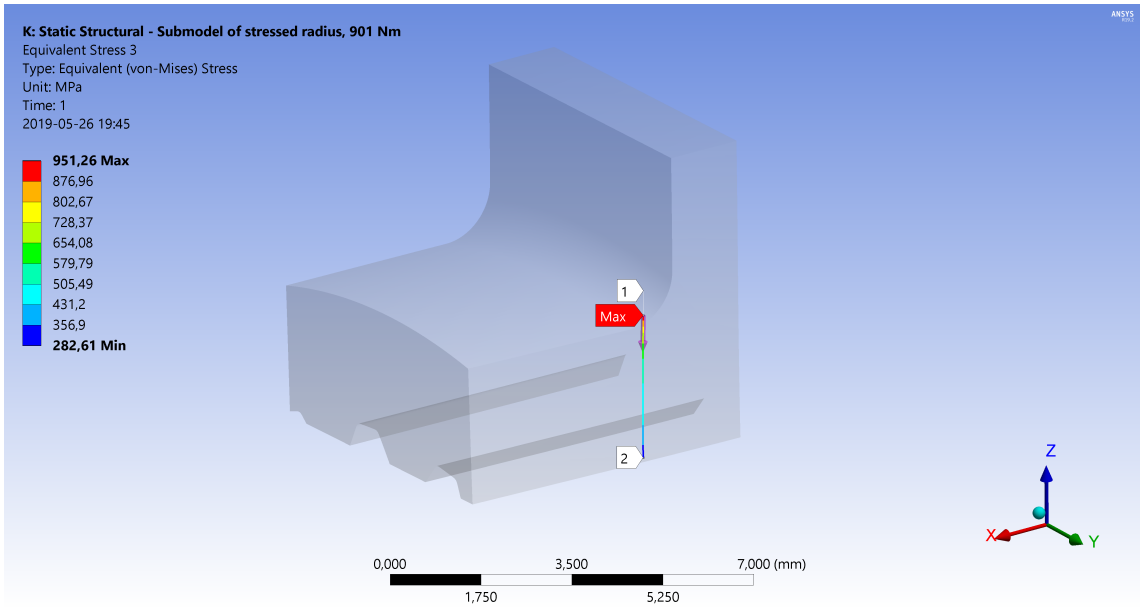

Figure 64: Right hub submodel Von Mises stress line

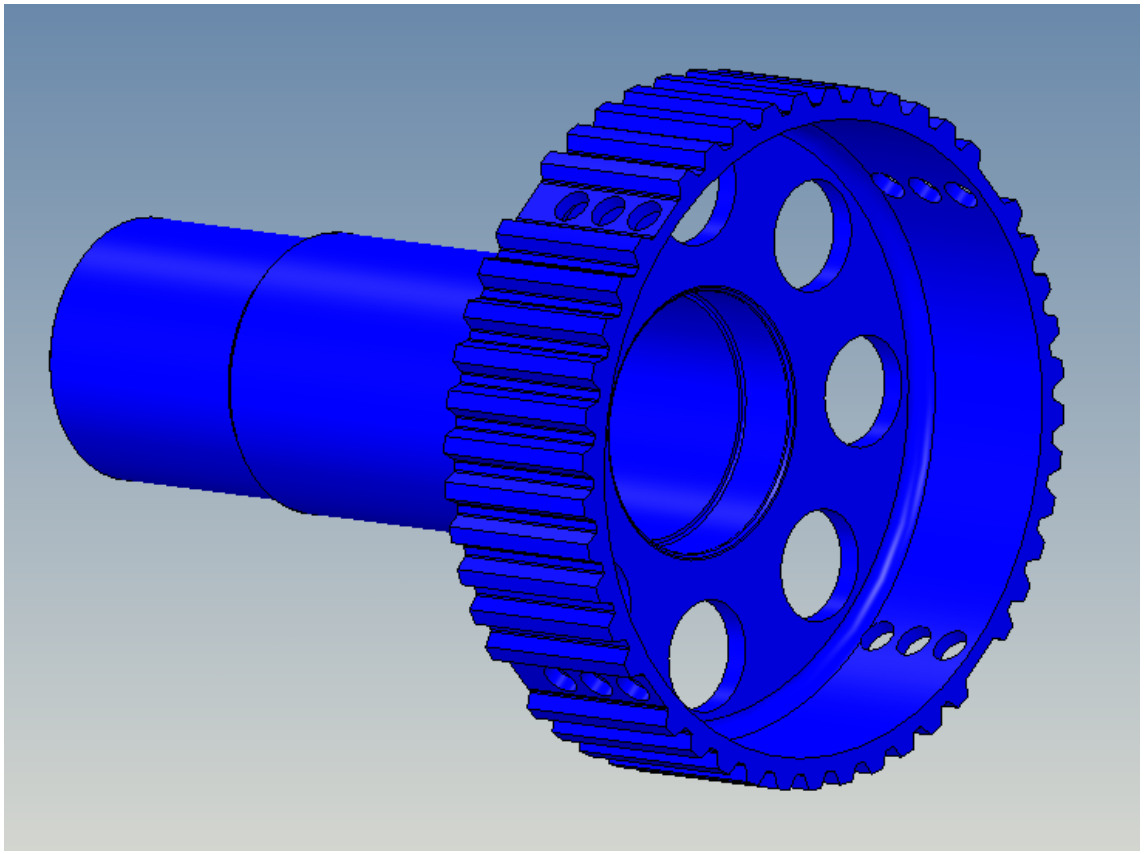

Figure 65: Left hub final design

13.1.3 Housing

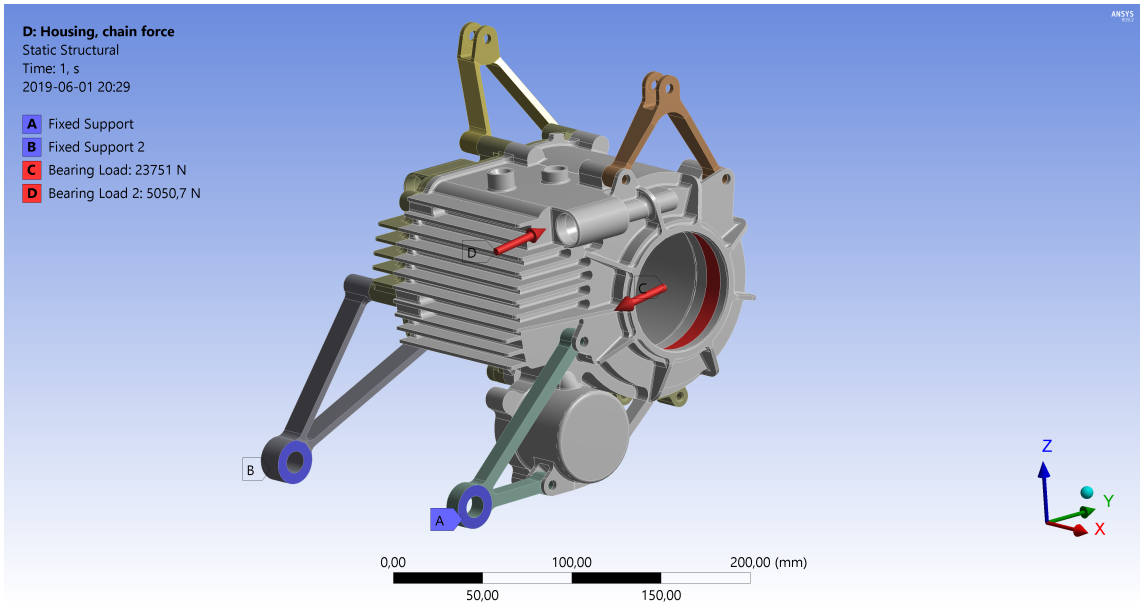

Figure 66: Housing chain force load case setup

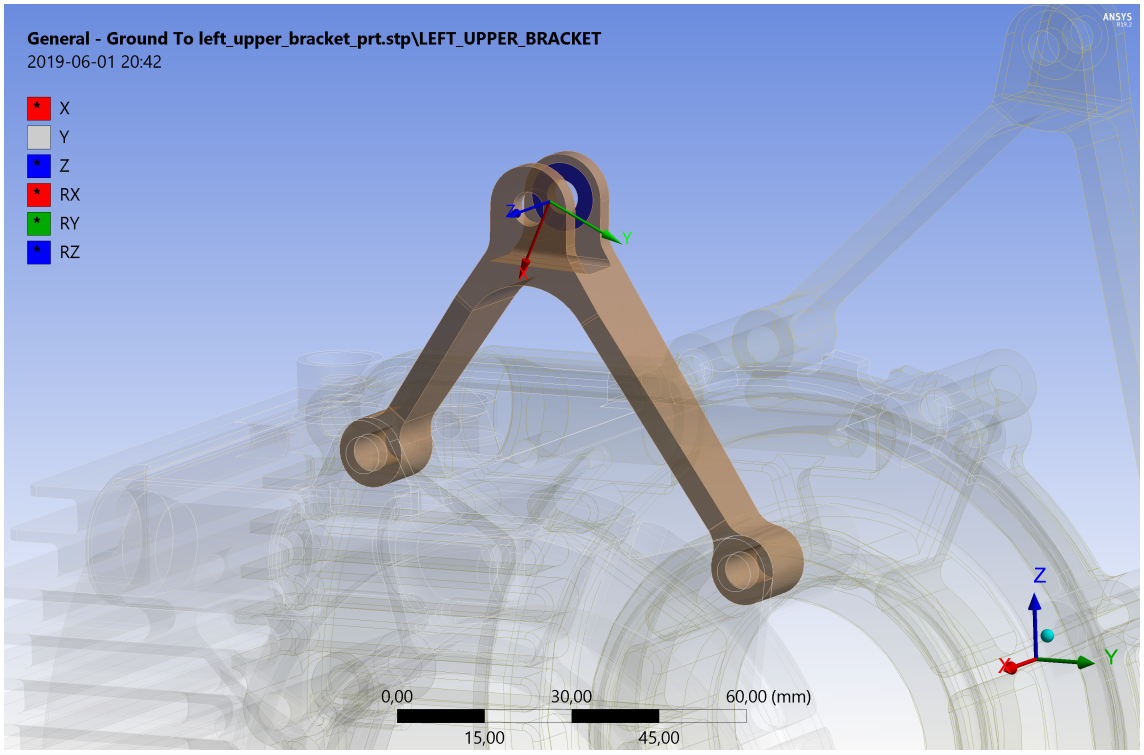

Figure 67: Housing chain force load case setup, joint

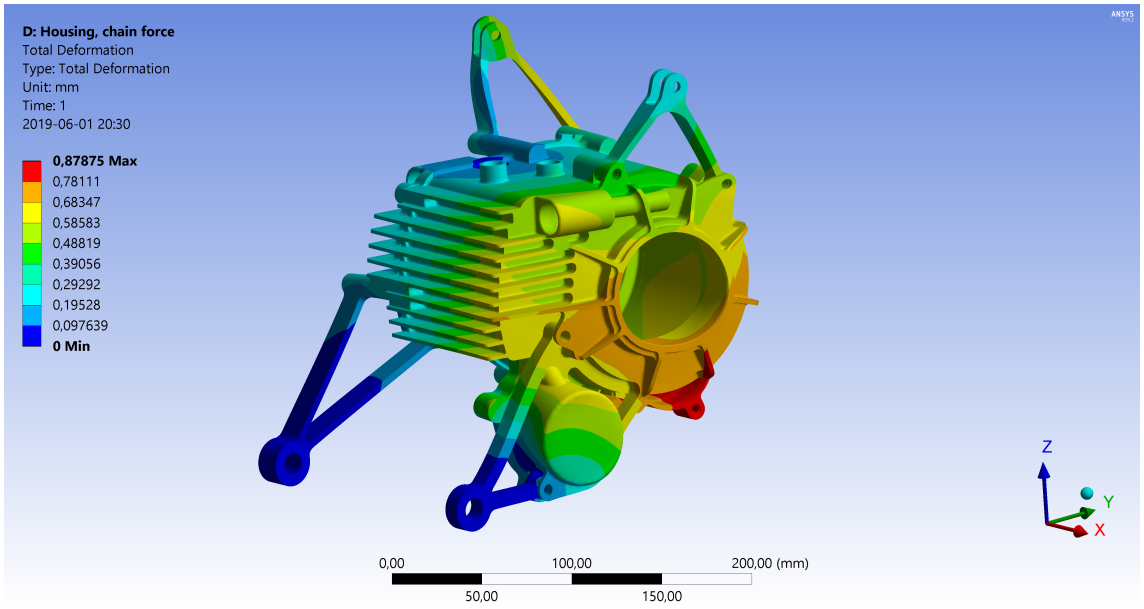

Figure 68: Housing chain force load case deformation

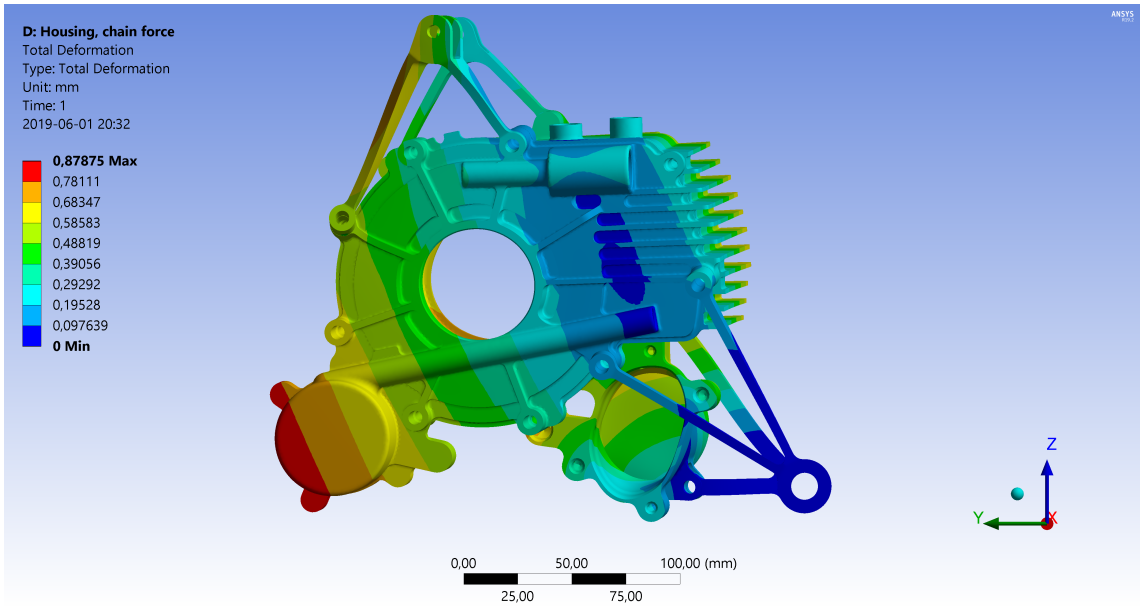

Figure 69: Housing chain force load case deformation

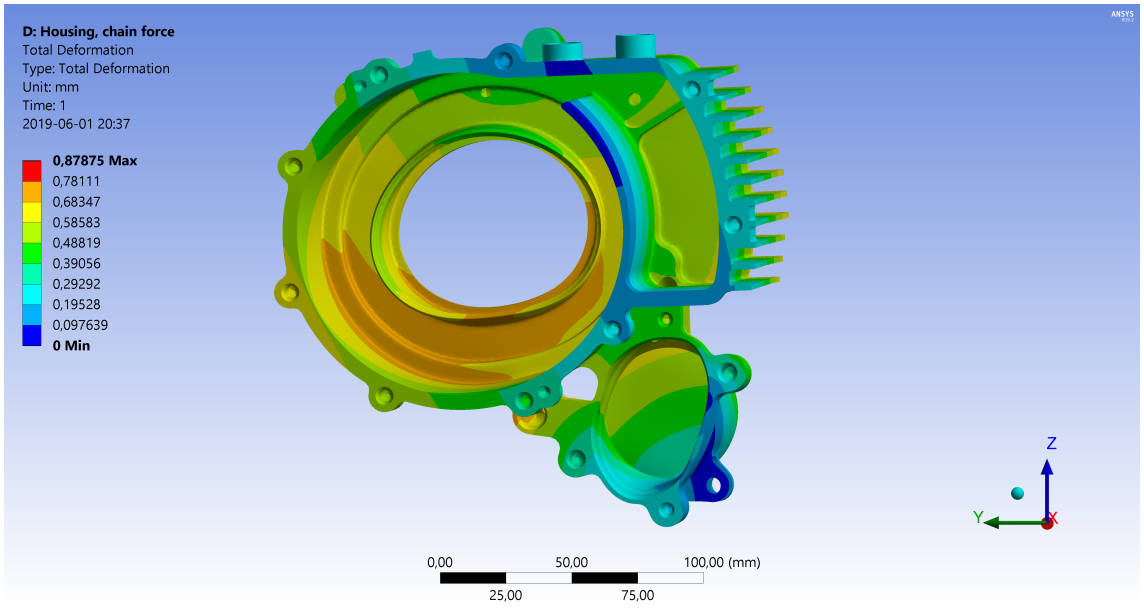

Figure 70: Housing chain force load case deformation

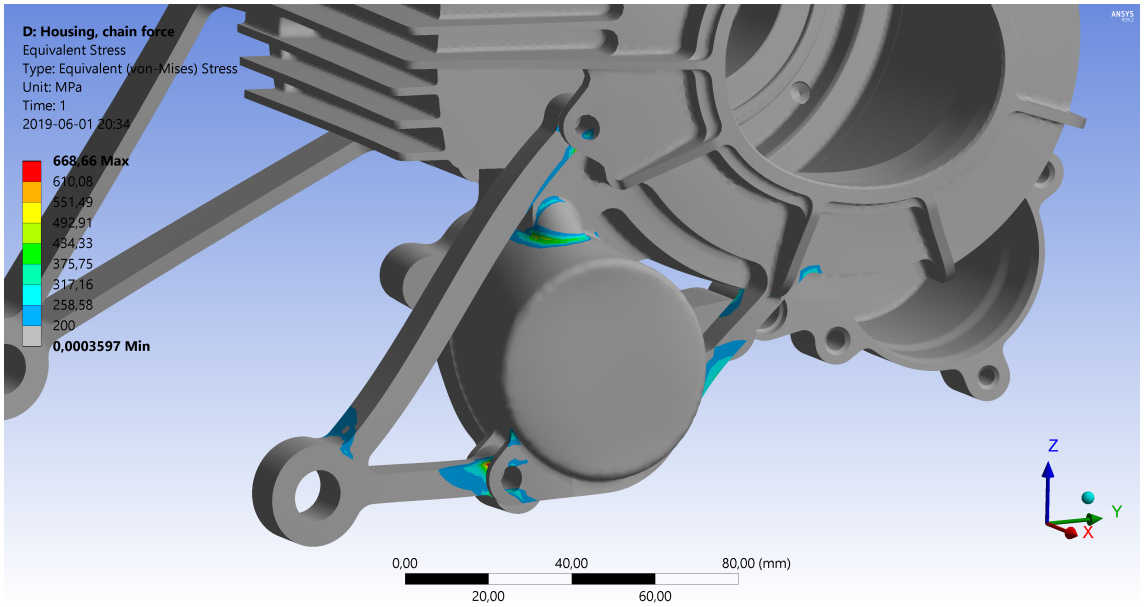

Figure 71: Housing chain force load case stress

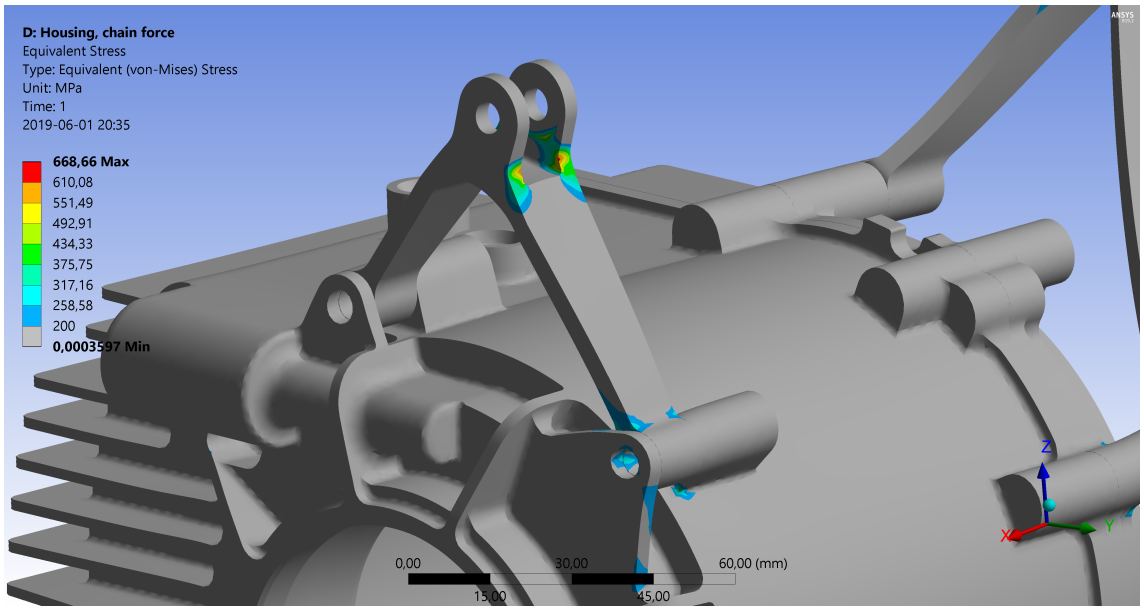

Figure 72: Housing chain force load case stress

13.2 Appendix B - Outcome figures

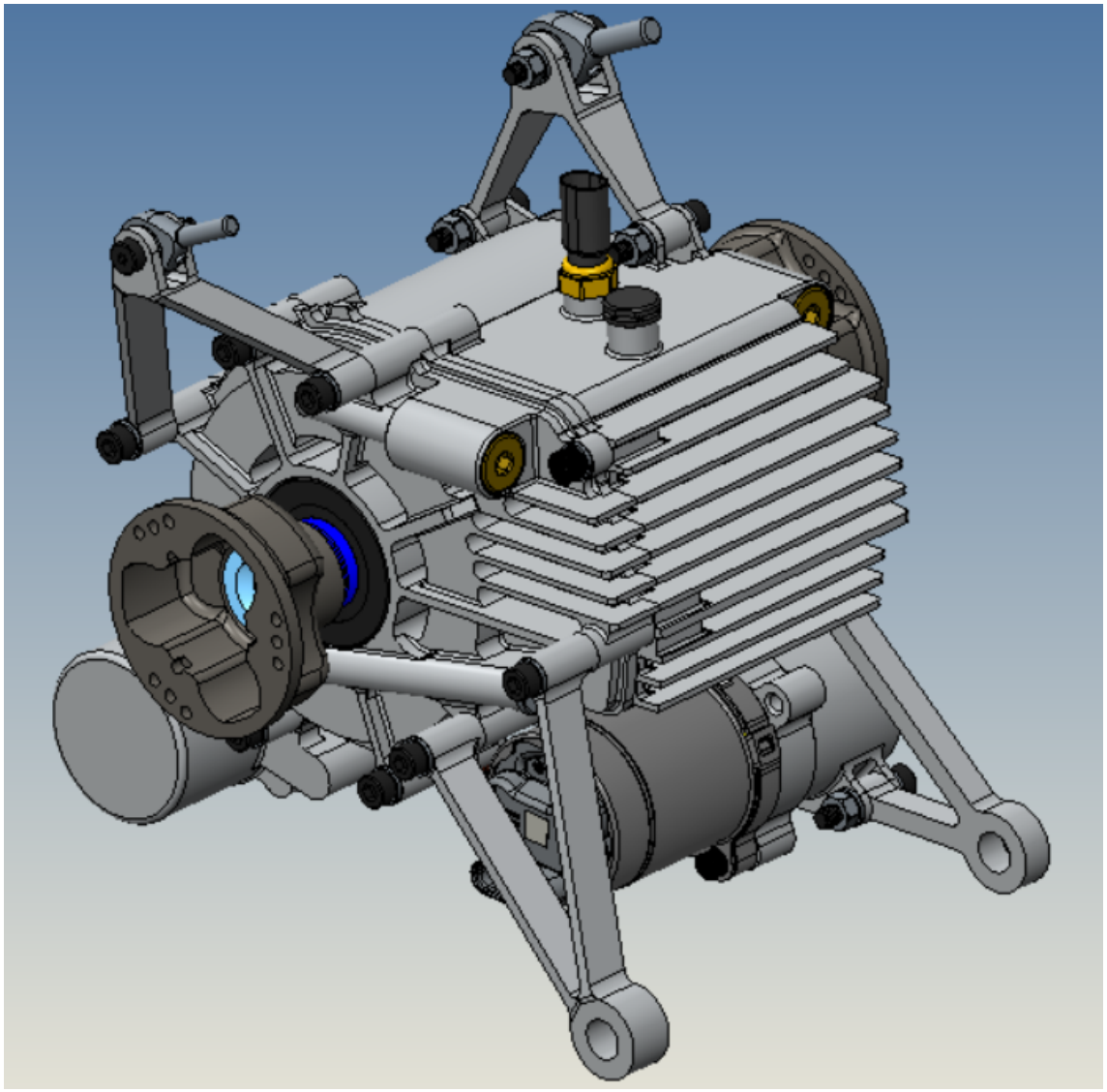

Figure 73: Complete assembly with Gen VI actuators

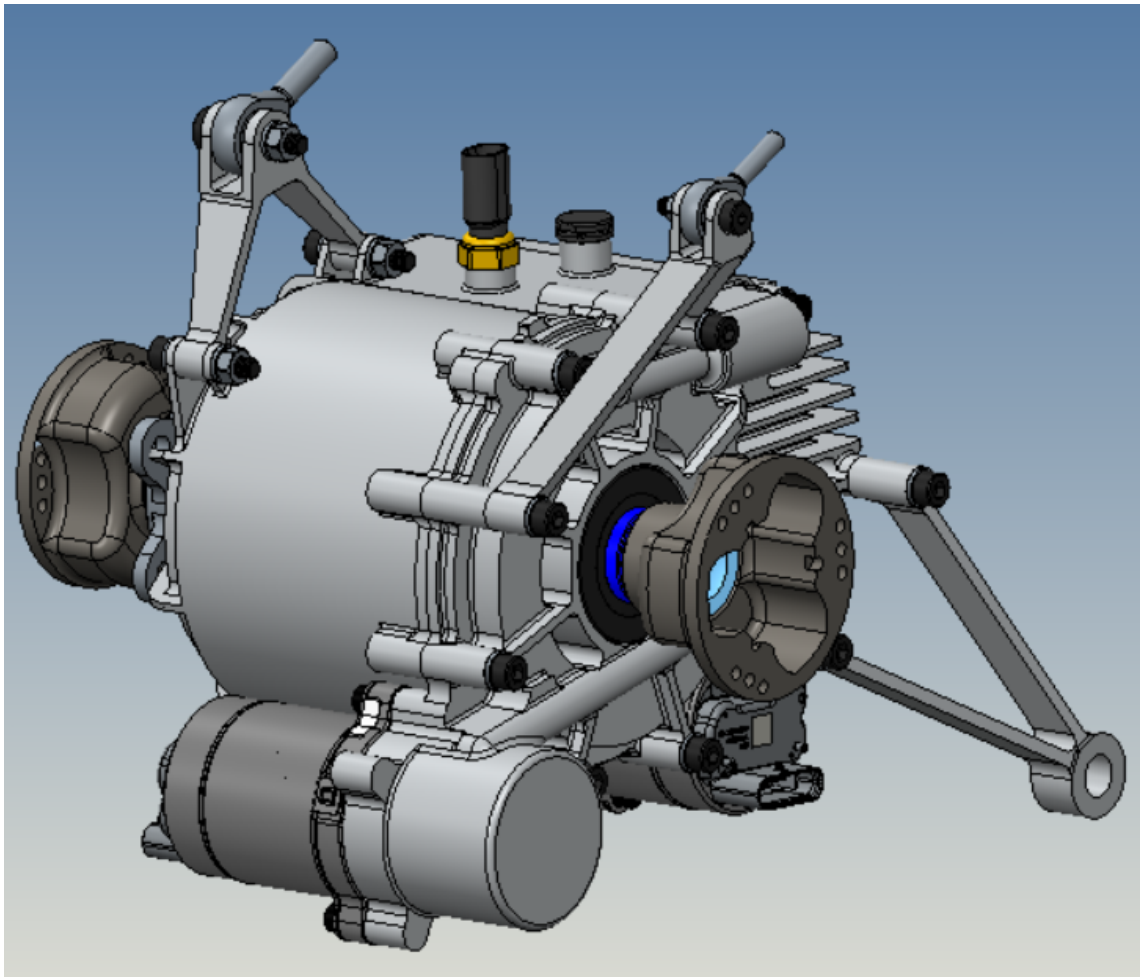

Figure 74: Complete assembly with Gen VI actuators

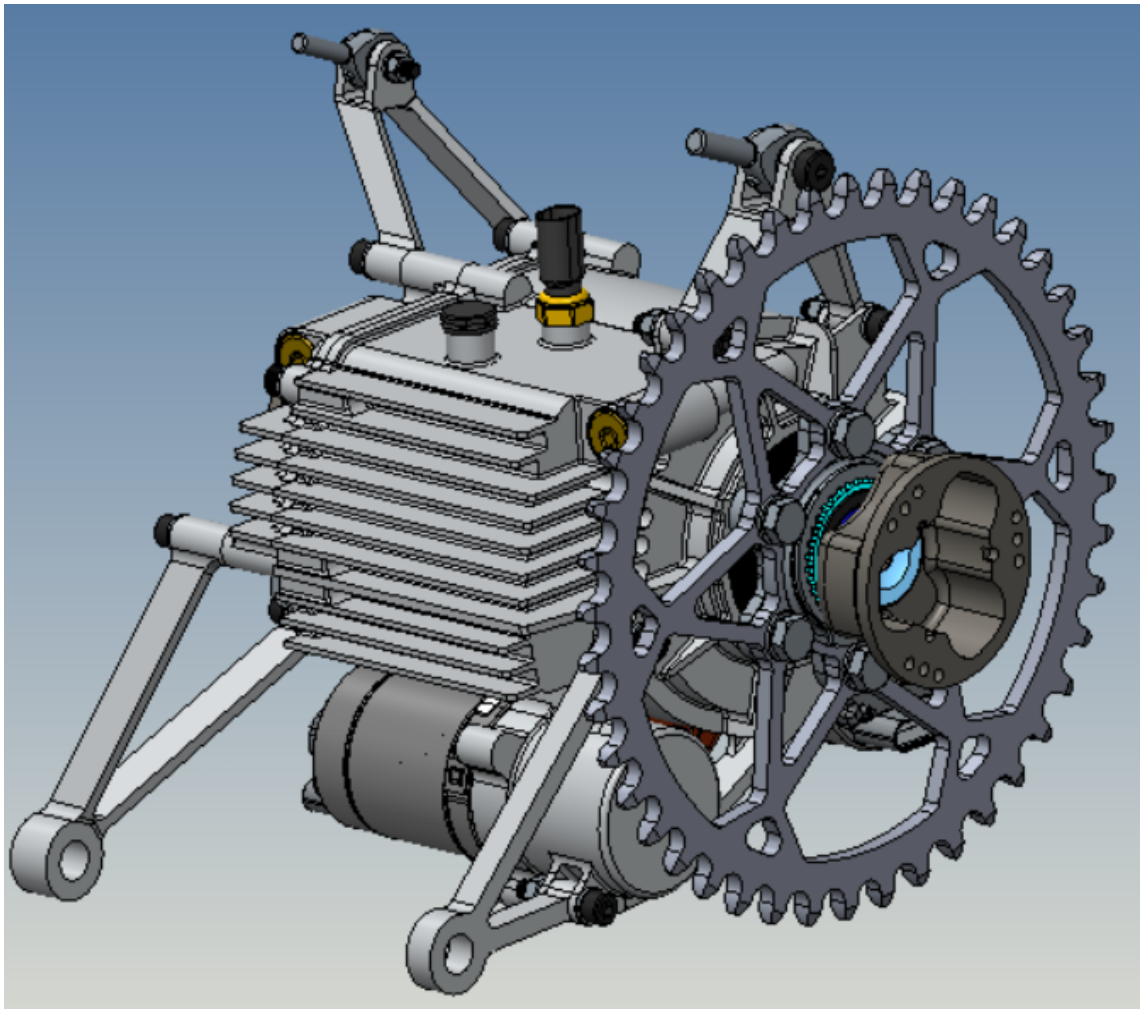

Figure 75: Complete assembly with Gen VI actuators and 44-tooth sprocket

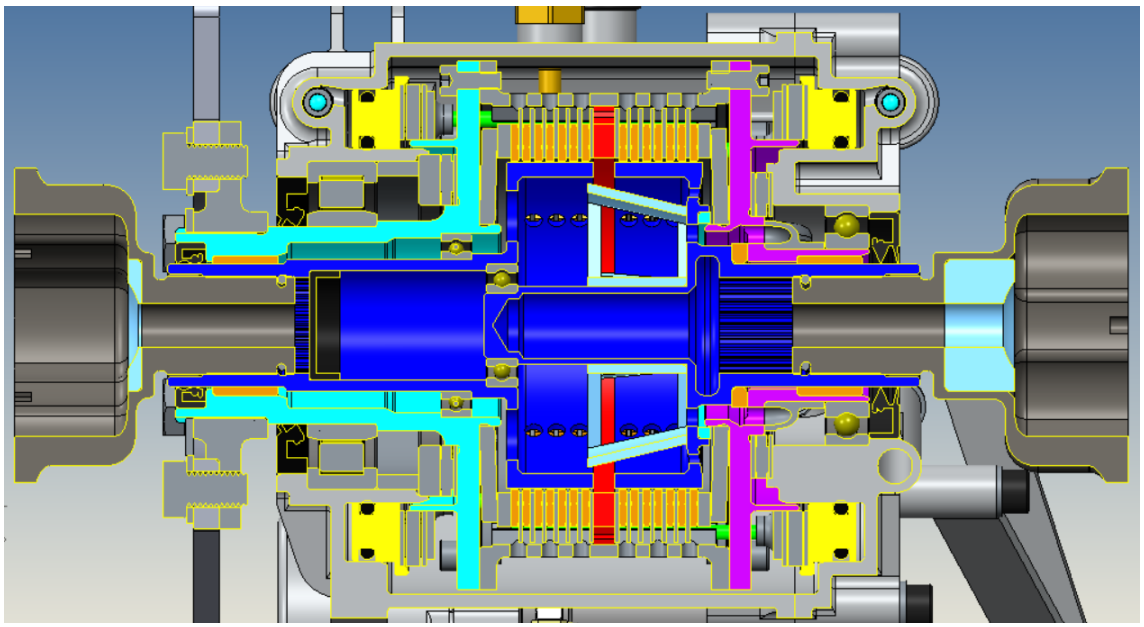

Figure 76: Complete assembly crossection

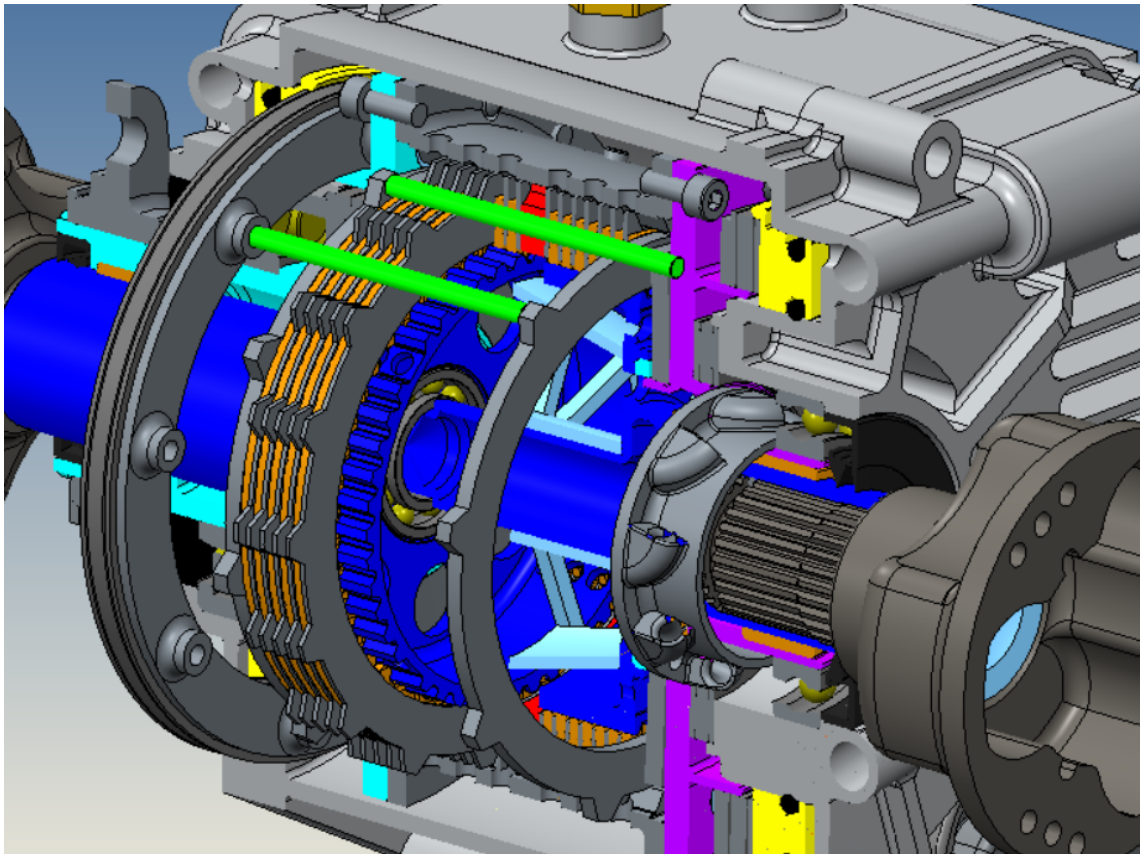

Figure 77: Complete assembly crossection

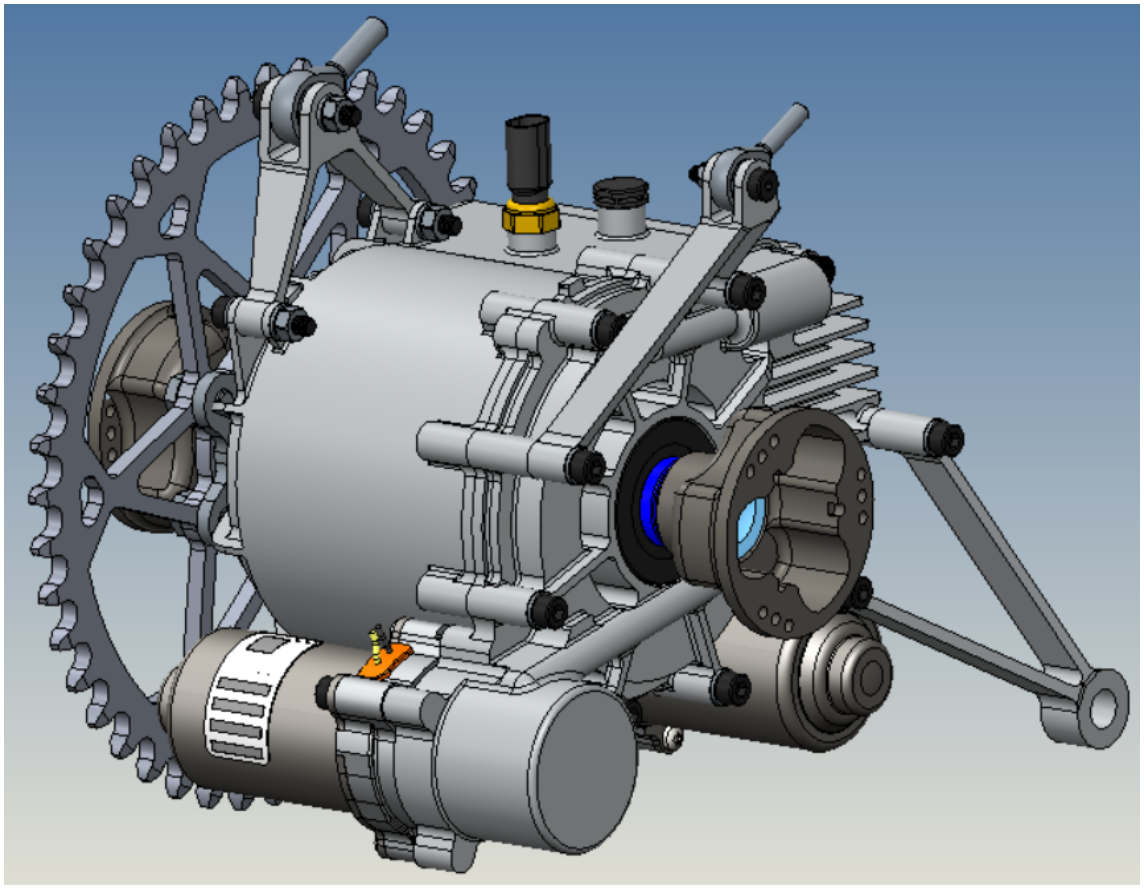

Figure 78: Complete assembly with Gen V actuators (ECU excluded)

13.3 Appendix C - Spline data

KISSsoft Release 03/2017 B

BorgWarner TTS, SE-Landskrona

File

Name : Friction_disc_inner_spline
Changed by: skalkan on: 09.06.2019 at: 15:42:45

Important hint: At least one warning has occurred during the calculation:

1-> Gear 1 :
Root circle deviation is much too large!

SPLINED JOINTS DIN 5480:2006

Shaft DIN5480 - W 75.00*1.50*48*11c
Hub DIN5480 - N 75.00*1.50*48*11H

Drawing or article number:
Shaft: 0.000.0
Hub: 0.000.0

1. TOOTH GEOMETRY AND MATERIAL

Normal module (mm)	[mn]	1.5000	
Nominal diameter DIN (mm)	[dB]	75.00	
Pressure angle at normal section (°)	[alfn]	30.000	
		------- SHAFT ---------	HUB --------
Number of teeth	[z]	48	-48
Helix angle at reference circle (°)	[beta]	0.0000	
Facewidth (mm)	[b]	20.00	0.80
Hand of gear	Spur gear		

Material
Gear 1: 34 CrNiMo 6 (3), Through hardened steel, nitrided
ISO 6336-5 Figure 13b/14b (MQ)
Gear 2: C60, Through hardened steel, unalloyed, through hardened
ISO 6336-5 Figure 5/6 (MQ)

		------- SHAFT ---------	HUB ----
Surface hardness		HV 650	HBW 220
Reference diameter material (mm)	[dB]	75	92
Tensile strength (N/mm²)	[σB]	1000.00	750.00
Yield point (N/mm²)	[σS]	800.00	450.00
Young's modulus (N/mm²)	[E]	206000	206000
Poisson's ratio	[v]	0.300	0.300
Roughness average value DS, flank (µm)	[RAH]	0.00	0.00
Roughness average value DS, root (µm)	[RAF]	0.00	0.00
Mean roughness height, Rz, flank (µm)	[RZH]	20.00	8.00
Mean roughness height, Rz, root (µm)	[RZF]	20.00	20.00

Gear reference profile 1 :
Reference profile DIN 5480:2006 0.55 / 0.16 / 0.45 Broaching

Dedendum coefficient	[hfP*]	0.550
Root radius factor	[rhofP*]	0.160 (rhofPmax*=0.810)
Addendum coefficient	[haP*]	0.450
Tip radius factor	[rhoaP*]	0.000
Protuberance height coefficient	[hprP*]	0.000
Protuberance angle	[alfprP]	0.000
Tip form height coefficient	[hFaP*]	0.000
Ramp angle	[alfKP]	0.000
	not topping	

Gear reference profile 2 :

Reference profile	DIN 5480:2006 0.55 / 0.16 / 0.45 Broaching	
Dedendum coefficient	[hfP*]	0.550
Root radius factor	[rhofP*]	0.160 (rhofPmax*=0.810)
Addendum coefficient	[haP*]	0.450
Tip radius factor	[rhoaP*]	0.000
Protuberance height coefficient	[hprP*]	0.000
Protuberance angle	[alfprP]	0.000
Tip form height coefficient	[hFaP*]	0.000
Ramp angle	[alfKP]	0.000
	not topping	

Summary of reference profile gears:

Dedendum reference profile	[hfP*]	0.550	0.550
Tooth root radius Refer. profile	[rofP*]	0.160	0.160
Addendum Reference profile	[haP*]	0.450	0.450
Protuberance height coefficient	[hprP*]	0.000	0.000
Protuberance angle (°)	[alfprP]	0.000	0.000
Tip form height coefficient	[hFaP*]	0.000	0.000
Ramp angle (°)	[alfKP]	0.000	0.000

Transverse module (mm)	[mt]	1.500
Pressure angle at pitch circle (°)	[alft]	30.000
Base helix angle (°)	[betab]	0.000
Sum of profile shift coefficients	[Summexi]	0.0000

		------- SHAFT ---------	HUB --------
Profile shift coefficient	[x]	0.4500	-0.4500
Profile shift (x*m) (mm)	[x*m]	0.6750	-0.6750
Reference diameter (mm)	[d]	72.000	72.000
Base diameter (mm)	[db]	62.354	62.354
Tip diameter (mm)	[da]	74.700	72.000
Effective tip diameter (mm)	[da.e/i]	74.700 / 74.400	72.000 / 72.300
Tip diameter allowances (mm)	[Ada.e/i]	0.000 / -0.300	-0.000 / 0.300
Root diameter (mm)	[df]	71.700	75.000
Effective root diameter (mm)	[df.e/i]	71.550 / 71.250	75.100 / 75.400
Root diameter allowances (mm)	[Adf.e/i]	-0.150 / -0.450	0.100 / 0.400
Generating Profile shift coefficient	[xE.e/i]	0.3830 / 0.3311	-0.4789 / -0.5308
Root form diameter (mm)	[dFf.e/i]	71.791 / 71.495	74.849 / 74.981
(dFf2 calculated with virtual pinion type cutter (circa): z=	31 x=	0.000 rhoaP0*=0.1)	
Tooth height (mm)	[h]	1.500	1.500
Theoretical tip clearance (mm)	[c]	0.150	0.150
Effective tip clearance (mm)	[c.e/i]	0.500 / 0.200	0.525 / 0.225
Normal tooth thickness at tip circle (mm)	[san]	1.551	1.577
(mm)	[san.e/i]	1.621 / 1.337	1.708 / 1.437
Normal space width at root circle (mm)	[efn]	1.399	1.358

(mm)	[efn.e/i]	1.426 / 1.343	1.345 / 1.241
Pitch on reference circle (mm)	[pt]	4.712	
Base pitch (mm)	[pbt]	4.081	
Transverse pitch on contact-path (mm)	[pet]	4.081	

2. MEASUREMENTS FOR TOOTH THICKNESS

		------- SHAFT ---------	HUB --------
Accuracy grade		11	11
Tooth thickness deviation		DIN 5480 c	DIN 5480 H
Number of teeth spanned	[k]	9.0000	9.0000
Base tangent length (no backlash) (mm)	[Wk]	38.7155	38.7155
Diameter of contact point (mm)	[dMWk.m]	73.3539	73.4069
Theoretical diameter of ball/pin (mm)	[dm]	2.9096	2.7442
Effective diameter of ball/pin (mm)	[DMeff]	3.0000	2.7500
Theor. dimension over two balls (mm)	[MRe/Mri-ball]	78.0858	69.1809
Diametral measurement over pins without clearance (mm)	[MRe/Mri-pin]	78.0858	69.1809

Data for Actual Dimensions (DIN 5480:2006)

Tooth thickness / Spacewidth (mm)	[Smax/Smin, Emax/Emin]	3.0196 / 2.9296	3.2756 / 3.1856
Tooth thickness tolerance, normal section (mm)	[Tol.Smax/min]	-0.1160 / -0.2060	
Tooth space tolerance, normal section (mm)	[Tol.Emax/min]		0.1400 / 0.0500
Base tangent length (mm)	[Wk.Smax/Smin]	38.6151 / 38.5371	38.8368 / 38.7588
Diametral two ball measure (mm)	[MRe/Mri-ball]	77.9050 / 77.7641	69.4229 / 69.2676
Diametral measurement over pins (mm)	[MRe/Mri-pin]	77.9050 / 77.7641	69.4229 / 69.2676

Data for Effective Dimensions (DIN 5480:2006)

Tooth thickness / Spacewidth (mm)	[Svmax/min, Evmax/min]	3.0696 / 3.0196	3.1856 / 3.1356
Tooth thickness tolerance, normal section (mm)	[Tol.Svmax/min]	-0.0660 / -0.1160	
Tooth space tolerance, normal section (mm)	[Tol.Evmax/min]		0.0500 / 0.0000
Base tangent length (mm)	[Wk.Svmax/min]	(38.6584 / 38.6151)	(38.7588 / 38.7155)
Diametral two ball measure (mm)	[MRe/Mri-ball]	(77.9831 / 77.9050)	(69.2676 / 69.1809)
Diametral measurement over pins (mm)	[MRe/Mri-pin]	(77.9831 / 77.9050)	(69.2676 / 69.1809)
Tolerance data DIN 5480-1 (mm)	[TG]	0.1400	0.1400
(mm)	[Tact]	0.0900	0.0900
(mm)	[Teff]	0.0500	0.0500

Circumferential backlash (transverse section):

-Theoretical (without form errors) (mm)	[jt.th]	0.3460 / 0.1660
-Effective (with form errors) (mm)	[jt.eff]	0.1660 / 0.0660
Normal backlash theoretical (mm)	[jn.th]	0.2996 / 0.1438
Normal backlash (mm)	[jn.eff]	0.1438 / 0.0572
Theoretical radial clearance (mm)	[jr.th]	0.2919 / 0.1385
Radial clearance (mm)	[jr.eff]	0.1360 / 0.0519

Notice: When controlling splines with individual measurements (base tangent length/pin diameter) respect the values in 'Actual dimensions'.

3. GEAR ACCURACY

		------- SHAFT ---------	HUB --------
According to DIN 5480:2006:			
Accuracy grade	[Q-DIN5480]	11	11

Total profile deviation (µm)	[Fa]	41.0	41.0
Total helix deviation (µm)	[Fb]	18.0	18.0
Single pitch deviation (µm)	[fp]	38.0	38.0
Total cumulative pitch deviation (µm)	[Fp]	90.0	90.0
Runout (µm)	[Fr]	50.0	50.0

4. STRENGTH CALCULATION

Calculation method: G.Niemann, Machine Elements I, 4th edition.

Centering: flank centered		
Supporting length (mm)	[ltr]	0.80
Maximal circumferential force (N)	[Ft]	3517.38
Maximal circumferential force per tooth (N)	[Ft/z]	73.28
Force application diameter (mm)	[dm]	73.35
Tooth height (mm)	[h]	1.05
Distance a0 (mm)	[a0]	0.45
Length factor	[kl]	1.04
Participation factor (equivalent)	[kφßq]	4.00
Participation factor (maximum load)	[kφßmax]	3.00

The share factors kφß according to Niemann are determined according to the accuracy grade specified in DIN 5480..

[Q] 11

Nominal torque (Nm)	[Tnenn]	45.00
Application factor	[KA]	1.00
Service torque (Nm)	[Teq]	45.00
Maximum torque (Nm)	[Tmax]	129.00
Torque curve With alternating torque		
Number of load peaks	[NL]	3000000
Number of change of load direction	[NW]	1
Load direction changing coefficient	[fw]	1.00
Tolerance field according to DIN 5480		"H11"

SHAFT

Width on shaft (mm)	[l_W]	20.00
Supporting surface (mm²)	[Flw=ltr*h*z]	40.32
Tip form diameter (mm)	[dFa1.i]	74.40
Pressure stress (equivalent load) (N/mm²)	[peq]	126.31
Pressure stress (maximum load) (N/mm²)	[pmax]	271.57
Support factor	[fs]	1.20
Load peak coefficient	[fL]	1.15
Hardness influence coefficient	[fH]	1.15
Permissible pressure (N/mm²)	[pzuleq]	1104.00
Permissible pressure (N/mm²)	[pzulmax]	1272.13
fw * pzul / peq		8.74
fL * pzul / pmax		4.68
Required safety	[Smin]	1.00
Minimal safety	[S]	4.68

HUB

Width on hub (mm)	[l_N]	0.80
Supporting surface (mm²)	[Fln=ltr*h*z]	40.32
Tip form diameter (mm)	[dFa2.i]	-72.30

Small external diameter (mm)	[D1]	92.00
Big external diameter (mm)	[D2]	92.00
Width of hub-part with D2 (mm)	[c]	0.80
Equivalent diameter hub (mm)	[D]	92.00
Pressure stress (equivalent load) (N/mm²)	[peq]	126.31
Pressure stress (maximum load) (N/mm²)	[pmax]	271.57
Support factor	[fs]	1.50
Load peak coefficient	[fL]	1.15
Hardness influence coefficient	[fH]	1.00
Permissible pressure (N/mm²)	[pzuleq]	675.00
Permissible pressure (N/mm²)	[pzulmax]	777.79
fw * pzul / peq		5.34
fL * pzul / pmax		2.86
Required safety	[Smin]	1.00
Minimal safety	[S]	2.86

5. ADDITIONAL DATA

Moment of inertia (System referenced to wheel 1):
calculation without consideration of the exact tooth shape

single gears	((da+df)/2...di) (kg*m²)	[TraeghMom]	0.0002368	2.591e-005
System	((da+df)/2...di) (kg*m²)	[TraeghMom]	0.0002627	

Remark regarding mounting with clamping using small helix angle on shaft
(Clamping at the earliest at 0.33*b, spätestens bei 0.66*b)
Helix angle difference (°) [beta.min/max] 7.1250... 32.1612

6. MODIFICATIONS AND TOOTH FORM DEFINITION

Data for the tooth form calculation :

Calculation of Gear 1
Tooth form, Shaft, Step 1: Automatic (final machining)
haP*= 0.453, hfP*= 0.597, rofP*= 0.160

Calculation of Gear 2
Tooth form, Hub, Step 1: Automatic (final machining)
mn= 1.500 mm, alfn=30.000°, da= -72.150 mm, df= -75.250 mm, xE=-0.464, rf= 0.240 mm

REMARKS:

- Specifications with [.e/i] imply: Maximum [e] and Minimal value [i] with consideration of all tolerances
  Specifications with [.m] imply: Mean value within tolerance
- Concerning the calculation method:

h = (dFa1.i-ABS(dFa2.i)) / 2.0
dm = (dFa1.i + ABS(dFa2.i)) / 2.0;
Ft = Mmax * 2000 / dm
Pressure load: p(eq,max) = kphib(eq,max)*k1*M*2000/(dm*l*h*z); pmax >= peq
Coefficient for load direction changes according to DIN 6892:1998/ fig. 6
pzuleq = fs*fH*fw*(Rm,Rp)
pzulmax = fs*fH*fL*(Rm,Rp)

(Rm:for brittle material; Rp:for ductile material)

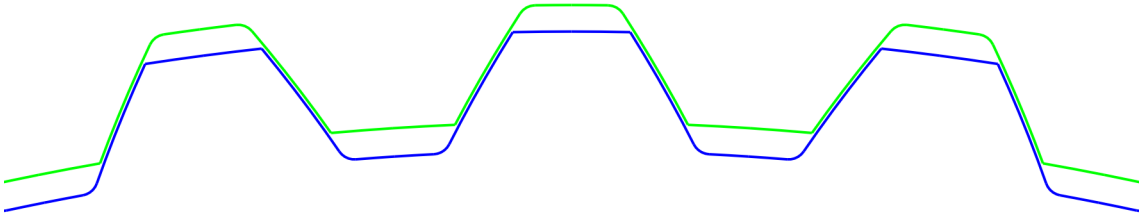

da1 = 74.5500 mm, df1 = 71.4000 mm, As1 = -0.0910 mm
da2 = -72.1500 mm, df2 = -75.2500 mm, As2 = -0.0250 mm

Figure: Meshing Shaft - Hub

End of Report lines: 281

KISSsoft Release 03/2017 B

BorgWarner TTS, SE-Landskrona

File

Name : Friction_disc_outer_spline
Changed by: skalkan on: 09.06.2019 at: 15:43:31

SPLINED JOINTS DIN 5480:2006

Shaft DIN5480 - W 100.00*3.00*32*8h
Hub DIN5480 - N 100.00*3.00*32*9H

Drawing or article number:
Shaft: 0.000.0
Hub: 0.000.0

1. TOOTH GEOMETRY AND MATERIAL

Normal module (mm)	[mn]	3.0000	
Nominal diameter DIN (mm)	[dB]	100.00	
Pressure angle at normal section (°)	[alfn]	30.000	
		------- SHAFT ---------	HUB --------
Number of teeth	[z]	32	-32
Helix angle at reference circle (°)	[beta]	0.0000	
Facewidth (mm)	[b]	0.90	20.00
Hand of gear	Spur gear		

Material
Gear 1: C60, Through hardened steel, unalloyed, through hardened
ISO 6336-5 Figure 5/6 (MQ)
Gear 2: 34 CrNiMo 6 (3), Through hardened steel, nitrided
ISO 6336-5 Figure 13b/14b (MQ)

		------- SHAFT ---------	HUB ----
Surface hardness		HBW 220	HV 650
Reference diameter material (mm)	[dB]	99	112
Tensile strength (N/mm²)	[σB]	750.00	1000.00
Yield point (N/mm²)	[σS]	450.00	800.00
Young's modulus (N/mm²)	[E]	206000	206000
Poisson's ratio	[v]	0.300	0.300
Roughness average value DS, flank (µm)	[RAH]	0.00	0.00
Roughness average value DS, root (µm)	[RAF]	0.00	0.00
Mean roughness height, Rz, flank (µm)	[RZH]	8.00	20.00
Mean roughness height, Rz, root (µm)	[RZF]	20.00	20.00

Gear reference profile 1 :
Reference profile DIN 5480:2006 0.55 / 0.16 / 0.45 Broaching

Dedendum coefficient	[hfP*]	0.550
Root radius factor	[rhofP*]	0.160 (rhofPmax*=0.810)
Addendum coefficient	[haP*]	0.450
Tip radius factor	[rhoaP*]	0.000
Protuberance height coefficient	[hprP*]	0.000
Protuberance angle	[alfprP]	0.000
Tip form height coefficient	[hFaP*]	0.000

Ramp angle	[alfKP]	0.000
		not topping

Gear reference profile	2 :	
Reference profile	DIN 5480:2006 0.55 / 0.16 / 0.45 Broaching	
Dedendum coefficient	[hfP*]	0.550
Root radius factor	[rhofP*]	0.160 (rhofPmax*=0.810)
Addendum coefficient	[haP*]	0.450
Tip radius factor	[rhoaP*]	0.000
Protuberance height coefficient	[hprP*]	0.000
Protuberance angle	[alfprP]	0.000
Tip form height coefficient	[hFaP*]	0.000
Ramp angle	[alfKP]	0.000
		not topping

Summary of reference profile gears:

Dedendum reference profile	[hfP*]	0.550	0.550
Tooth root radius Refer. profile	[rofP*]	0.160	0.160
Addendum Reference profile	[haP*]	0.450	0.450
Protuberance height coefficient	[hprP*]	0.000	0.000
Protuberance angle (°)	[alfprP]	0.000	0.000
Tip form height coefficient	[hFaP*]	0.000	0.000
Ramp angle (°)	[alfKP]	0.000	0.000

Transverse module (mm)	[mt]	3.000
Pressure angle at pitch circle (°)	[alft]	30.000
Base helix angle (°)	[betab]	0.000
Sum of profile shift coefficients	[Summexi]	0.0000

		------- SHAFT ---------	HUB --------
Profile shift coefficient	[x]	0.1167	-0.1167
Profile shift (x*m) (mm)	[x*m]	0.3501	-0.3501
Reference diameter (mm)	[d]	96.000	96.000
Base diameter (mm)	[db]	83.138	83.138
Tip diameter (mm)	[da]	99.400	94.000
Effective tip diameter (mm)	[da.e/i]	99.400 / 99.180	94.000 / 94.220
Tip diameter allowances (mm)	[Ada.e/i]	0.000 / -0.220	-0.000 / 0.220
Root diameter (mm)	[df]	93.400	100.000
Effective root diameter (mm)	[df.e/i]	93.366 / 93.303	100.052 / 100.139
Root diameter allowances (mm)	[Adf.e/i]	-0.035 / -0.097	0.052 / 0.139
Generating Profile shift coefficient	[xE.e/i]	0.1109 / 0.1005	-0.1254 / -0.1398
Root form diameter (mm)	[dFf.e/i]	93.920 / 93.862	99.609 / 99.693
(dFf2 calculated with virtual pinion type cutter (circa): z=	21 x=	0.000 rhoaP0*=0.1)	
Tooth height (mm)	[h]	3.000	3.000
Theoretical tip clearance (mm)	[c]	0.300	0.300
Effective tip clearance (mm)	[c.e/i]	0.479 / 0.326	0.458 / 0.317
Normal tooth thickness at tip circle (mm)	[san]	3.164	3.125
(mm)	[san.e/i]	3.280 / 3.106	3.219 / 3.046
Normal space width at root circle (mm)	[efn]	2.794	2.785
(mm)	[efn.e/i]	2.795 / 2.796	2.783 / 2.779
Pitch on reference circle (mm)	[pt]	9.425	
Base pitch (mm)	[pbt]	8.162	
Transverse pitch on contact-path (mm)	[pet]	8.162	

2. MEASUREMENTS FOR TOOTH THICKNESS

		------- SHAFT --------	HUB --------
Accuracy grade		8	9
Tooth thickness deviation		DIN 5480 h	DIN 5480 H
Number of teeth spanned	[k]	6.0000	6.0000
Base tangent length (no backlash) (mm)	[Wk]	49.7104	49.7104
Diameter of contact point (mm)	[dMWk.m]	96.8621	96.8732
Theoretical diameter of ball/pin (mm)	[dm]	5.6970	5.3640
Effective diameter of ball/pin (mm)	[DMeff]	6.0000	5.5000
Theor. dimension over two balls (mm)	[MRe/Mri-ball]	106.2753	88.2816
Diametral measurement over pins without clearance (mm)	[MRe/Mri-pin]	106.2753	88.2816

Data for Actual Dimensions (DIN 5480:2006)

Tooth thickness / Spacewidth (mm)	[Smax/Smin, Emax/Emin]	5.0966 / 5.0606	5.1966 / 5.1466
Tooth thickness tolerance, normal section (mm)	[Tol.Smax/min]	-0.0200 / -0.0560	
Tooth space tolerance, normal section (mm)	[Tol.Emax/min]		0.0800 / 0.0300
Base tangent length (mm)	[Wk.Smax/Smin]	49.6931 / 49.6620	49.7797 / 49.7364
Diametral two ball measure (mm)	[MRe/Mri-ball]	106.2443 / 106.1884	88.4309 / 88.3377
Diametral measurement over pins (mm)	[MRe/Mri-pin]	106.2443 / 106.1884	88.4309 / 88.3377

Data for Effective Dimensions (DIN 5480:2006)

Tooth thickness / Spacewidth (mm)	[Svmax/min, Evmax/min]	5.1166 / 5.0966	5.1466 / 5.1166
Tooth thickness tolerance, normal section (mm)	[Tol.Svmax/min]	0.0000 / -0.0200	
Tooth space tolerance, normal section (mm)	[Tol.Evmax/min]		0.0300 / 0.0000
Base tangent length (mm)	[Wk.Svmax/min]	(49.7104 / 49.6931)	(49.7364 / 49.7104)
Diametral two ball measure (mm)	[MRe/Mri-ball]	(106.2753 / 106.2443)	(88.3377 / 88.2816)
Diametral measurement over pins (mm)	[MRe/Mri-pin]	(106.2753 / 106.2443)	(88.3377 / 88.2816)
Tolerance data DIN 5480-1 (mm)	[TG]	0.0560	0.0800
(mm)	[Tact]	0.0360	0.0500
(mm)	[Teff]	0.0200	0.0300

Circumferential backlash (transverse section):

-Theoretical (without form errors) (mm)	[jt.th]	0.1360 / 0.0500
-Effective (with form errors) (mm)	[jt.eff]	0.0500 / 0.0000
Normal backlash theoretical (mm)	[jn.th]	0.1178 / 0.0433
Normal backlash (mm)	[jn.eff]	0.0433 / 0.0000

Notice: When controlling splines with individual measurements (base tangent length/pin diameter) respect the values in 'Actual dimensions'.

3. GEAR ACCURACY

		------- SHAFT --------	HUB --------
According to DIN 5480:2006:			
Accuracy grade	[Q-DIN5480]	8	9
Total profile deviation (µm)	[Fa]	19.0	25.0
Total helix deviation (µm)	[Fb]	10.0	13.0
Single pitch deviation (µm)	[fp]	15.0	21.0
Total cumulative pitch deviation (µm)	[Fp]	36.0	50.0
Runout (µm)	[Fr]	50.0	50.0

4. STRENGTH CALCULATION

Calculation method: G.Niemann, Machine Elements I, 4th edition.
Centering: flank centered

Supporting length (mm)	[ltr]	0.90
Maximal circumferential force (N)	[Ft]	2668.04
Maximal circumferential force per tooth (N)	[Ft/z]	83.38
Force application diameter (mm)	[dm]	96.70
Tooth height (mm)	[h]	2.48
Distance a0 (mm)	[a0]	0.45
Length factor	[kl]	1.03
Participation factor (equivalent)	[kφßq]	2.00
Participation factor (maximum load)	[kφßmax]	1.70

The share factors kφß according to Niemann are determined according to the accuracy grade specified in DIN 5480..

[Q] 9

Nominal torque (Nm)	[Tnenn]	0.00
Application factor	[KA]	1.00
Service torque (Nm)	[Teq]	0.00
Maximum torque (Nm)	[Tmax]	129.00
Torque - curve: No alternating torque		
Number of load peaks	[NL]	3000000
Number of change of load direction	[NW]	1
Load direction changing coefficient	[fw]	1.00
Tolerance field according to DIN 5480		"H9"

SHAFT

Width on shaft (mm)	[l_W]	0.90
Supporting surface (mm²)	[Flw=ltr*h*z]	71.42
Tip form diameter (mm)	[dFa1.i]	99.18
Pressure stress (equivalent load) (N/mm²)	[peq]	0.00
Pressure stress (maximum load) (N/mm²)	[pmax]	65.50
Support factor	[fs]	1.20
Load peak coefficient	[fL]	1.15
Hardness influence coefficient	[fH]	1.00
Permissible pressure (N/mm²)	[pzuleq]	540.00
Permissible pressure (N/mm²)	[pzulmax]	622.24
fw * pzul / peq		1.#J
fL * pzul / pmax		9.50
Required safety	[Smin]	1.00
Minimal safety	[S]	9.50

HUB

Width on hub (mm)	[l_N]	20.00
Supporting surface (mm²)	[Fln=ltr*h*z]	71.42
Tip form diameter (mm)	[dFa2.i]	-94.22
Small external diameter (mm)	[D1]	112.00
Big external diameter (mm)	[D2]	112.00
Width of hub-part with D2 (mm)	[c]	0.90
Equivalent diameter hub (mm)	[D]	112.00
Pressure stress (equivalent load) (N/mm²)	[peq]	0.00
Pressure stress (maximum load) (N/mm²)	[pmax]	65.50
Support factor	[fs]	1.50
Load peak coefficient	[fL]	1.15
Hardness influence coefficient	[fH]	1.15

Permissible pressure (N/mm²)	[pzuleq]	1380.00
Permissible pressure (N/mm²)	[pzulmax]	1590.16
fw * pzul / peq		1.#J
fL * pzul / pmax		24.28
Required safety	[Smin]	1.00
Minimal safety	[S]	24.28

5. ADDITIONAL DATA

Moment of inertia (System referenced to wheel 1):
calculation without consideration of the exact tooth shape

single gears	((da+df)/2...di) (kg*m²)	[TraeghMom]	3.764e-005	0.001052
System	((da+df)/2...di) (kg*m²)	[TraeghMom]	0.00109	

6. MODIFICATIONS AND TOOTH FORM DEFINITION

Data for the tooth form calculation :

Calculation of Gear 1
Tooth form, Shaft, Step 1: Automatic (final machining)
haP*= 0.435, hfP*= 0.558, rofP*= 0.160

Calculation of Gear 2
Tooth form, Hub, Step 1: Automatic (final machining)
mn= 3.000 mm, alfn=30.000°, da= -94.110 mm, df= -100.095 mm, xE=-0.121, rf= 0.480 mm

REMARKS:

- Specifications with [.e/i] imply: Maximum [e] and Minimal value [i] with consideration of all tolerances
  Specifications with [.m] imply: Mean value within tolerance
- Concerning the calculation method:

h = (dFa1.i-ABS(dFa2.i)) / 2.0
dm = (dFa1.i + ABS(dFa2.i)) / 2.0;
Ft = Mmax * 2000 / dm
Pressure load: p(eq,max) = kphib(eq,max)*k1*M*2000/(dm*l*h*z); pmax >= peq
Coefficient for load direction changes according to DIN 6892:1998/ fig. 6
pzuleq = fs*fH*fw*(Rm,Rp)
pzulmax = fs*fH*fL*(Rm,Rp)
(Rm:for brittle material; Rp:for ductile material)

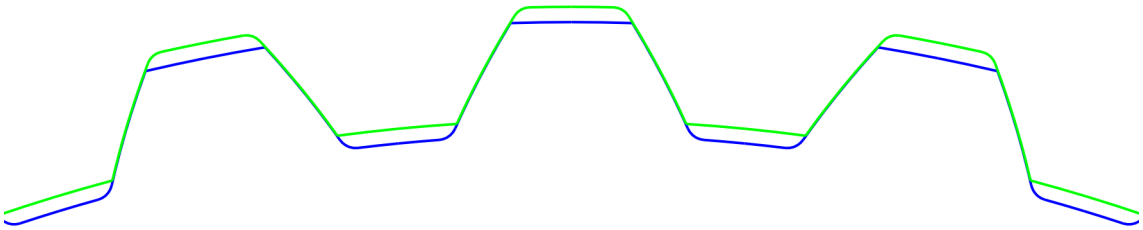

da1 = 99.2902 mm, df1 = 93.3344 mm, As1 = -0.0100 mm
da2 = -94.1102 mm, df2 = -100.0955 mm, As2 = -0.0150 mm

Figure: Meshing Shaft - Hub

End of Report lines: 275

File

Name : Sprocket_carrier_spline
Changed by: skalkan on: 09.06.2019 at: 15:38:19

SPLINED JOINTS DIN 5480:2006

Shaft DIN5480 - W 45.00*1.25*34*8h
Hub DIN5480 - N 45.00*1.25*34*9H

Drawing or article number:
Shaft: 0.000.0
Hub: 0.000.0

1. TOOTH GEOMETRY AND MATERIAL

Normal module (mm)	[mn]	1.2500	
Nominal diameter DIN (mm)	[dB]	45.00	
Pressure angle at normal section (°)	[alfn]	30.000	
		------- SHAFT --------	HUB --------
Number of teeth	[z]	34	-34
Helix angle at reference circle (°)	[beta]	0.0000	
Facewidth (mm)	[b]	13.60	17.00
Hand of gear	Spur gear		

Material
Gear 1: 34 CrNiMo 6 (1), Through hardened steel, alloyed, through hardened
ISO 6336-5 Figure 5/6 (MQ)
Gear 2: 34 CrNiMo 6 (3), Through hardened steel, nitrided
ISO 6336-5 Figure 13b/14b (MQ)

		------- SHAFT --------	HUB ----
Surface hardness		HBW 240	HV 650
Reference diameter material (mm)	[dB]	45	52
Tensile strength (N/mm²)	[σB]	1000.00	1000.00
Yield point (N/mm²)	[σS]	800.00	800.00
Young's modulus (N/mm²)	[E]	206000	206000
Poisson's ratio	[v]	0.300	0.300
Roughness average value DS, flank (µm)	[RAH]	0.00	1.05
Roughness average value DS, root (µm)	[RAF]	0.00	3.00
Mean roughness height, Rz, flank (µm)	[RZH]	8.00	8.00
Mean roughness height, Rz, root (µm)	[RZF]	20.00	20.00

Gear reference profile 1 :
Reference profile DIN 5480:2006 0.55 / 0.16 / 0.45 Broaching

Dedendum coefficient	[hfP*]	0.550
Root radius factor	[rhofP*]	0.160 (rhofPmax*=0.810)
Addendum coefficient	[haP*]	0.450
Tip radius factor	[rhoaP*]	0.000
Protuberance height coefficient	[hprP*]	0.000
Protuberance angle	[alfprP]	0.000
Tip form height coefficient	[hFaP*]	0.000

Ramp angle	[alfKP]	0.000
		not topping

Gear reference profile	2 :	
Reference profile	DIN 5480:2006 0.55 / 0.16 / 0.45 Broaching	
Dedendum coefficient	[hfP*]	0.550
Root radius factor	[rhofP*]	0.160 (rhofPmax*=0.810)
Addendum coefficient	[haP*]	0.450
Tip radius factor	[rhoaP*]	0.000
Protuberance height coefficient	[hprP*]	0.000
Protuberance angle	[alfprP]	0.000
Tip form height coefficient	[hFaP*]	0.000
Ramp angle	[alfKP]	0.000
		not topping

Summary of reference profile gears:

Dedendum reference profile	[hfP*]	0.550	0.550
Tooth root radius Refer. profile	[rofP*]	0.160	0.160
Addendum Reference profile	[haP*]	0.450	0.450
Protuberance height coefficient	[hprP*]	0.000	0.000
Protuberance angle (°)	[alfprP]	0.000	0.000
Tip form height coefficient	[hFaP*]	0.000	0.000
Ramp angle (°)	[alfKP]	0.000	0.000

Transverse module (mm)	[mt]	1.250
Pressure angle at pitch circle (°)	[alft]	30.000
Base helix angle (°)	[betab]	0.000
Sum of profile shift coefficients	[Summexi]	0.0000

		------- SHAFT ---------	HUB --------
Profile shift coefficient	[x]	0.4500	-0.4500
Profile shift (x*m) (mm)	[x*m]	0.5625	-0.5625
Reference diameter (mm)	[d]	42.500	42.500
Base diameter (mm)	[db]	36.806	36.806
Tip diameter (mm)	[da]	44.750	42.500
Effective tip diameter (mm)	[da.e/i]	44.750 / 44.590	42.500 / 42.660
Tip diameter allowances (mm)	[Ada.e/i]	0.000 / -0.160	-0.000 / 0.160
Root diameter (mm)	[df]	42.250	45.000
Effective root diameter (mm)	[df.e/i]	42.221 / 42.172	45.040 / 45.109
Root diameter allowances (mm)	[Adf.e/i]	-0.029 / -0.078	0.040 / 0.109
Generating Profile shift coefficient	[xE.e/i]	0.4382 / 0.4188	-0.4659 / -0.4936
Root form diameter (mm)	[dFf.e/i]	42.421 / 42.373	44.851 / 44.908
(dFf2 calculated with virtual pinion type cutter (circa): z=	22 x=	0.000 rhoaP0*=0.1)	
Tooth height (mm)	[h]	1.250	1.250
Theoretical tip clearance (mm)	[c]	0.125	0.125
Effective tip clearance (mm)	[c.e/i]	0.260 / 0.145	0.244 / 0.140
Normal tooth thickness at tip circle (mm)	[san]	1.285	1.314
(mm)	[san.e/i]	1.372 / 1.238	1.389 / 1.251
Normal space width at root circle (mm)	[efn]	1.164	1.117
(mm)	[efn.e/i]	1.164 / 1.163	1.115 / 1.110
Pitch on reference circle (mm)	[pt]	3.927	
Base pitch (mm)	[pbt]	3.401	
Transverse pitch on contact-path (mm)	[pet]	3.401	

2. MEASUREMENTS FOR TOOTH THICKNESS

		------- SHAFT --------	HUB --------
Accuracy grade		8	9
Tooth thickness deviation		DIN 5480 h	DIN 5480 H
Number of teeth spanned	[k]	7.0000	7.0000
Base tangent length (no backlash) (mm)	[Wk]	24.6466	24.6466
Diameter of contact point (mm)	[dMWk.m]	44.2920	44.3016
Theoretical diameter of ball/pin (mm)	[dm]	2.4948	2.2940
Effective diameter of ball/pin (mm)	[DMeff]	2.5000	2.5000
Theor. dimension over two balls (mm)	[MRe/Mri-ball]	47.5226	39.5175
Diametral measurement over pins without clearance (mm)	[MRe/Mri-pin]	47.5226	39.5175

Data for Actual Dimensions (DIN 5480:2006)

Tooth thickness / Spacewidth (mm)	[Smax/Smin, Emax/Emin]	2.5960 / 2.5680	2.6760 / 2.6360
Tooth thickness tolerance, normal section (mm)	[Tol.Smax/min]	-0.0170 / -0.0450	
Tooth space tolerance, normal section (mm)	[Tol.Emax/min]		0.0630 / 0.0230
Base tangent length (mm)	[Wk.Smax/Smin]	24.6318 / 24.6076	24.7011 / 24.6665
Diametral two ball measure (mm)	[MRe/Mri-ball]	47.4970 / 47.4548	39.6301 / 39.5587
Diametral measurement over pins (mm)	[MRe/Mri-pin]	47.4970 / 47.4548	39.6301 / 39.5587

Data for Effective Dimensions (DIN 5480:2006)

Tooth thickness / Spacewidth (mm)	[Svmax/min, Evmax/min]	2.6130 / 2.5960	2.6360 / 2.6130
Tooth thickness tolerance, normal section (mm)	[Tol.Svmax/min]	0.0000 / -0.0170	
Tooth space tolerance, normal section (mm)	[Tol.Evmax/min]		0.0230 / 0.0000
Base tangent length (mm)	[Wk.Svmax/min]	(24.6466 / 24.6318)	(24.6665 / 24.6466)
Diametral two ball measure (mm)	[MRe/Mri-ball]	(47.5226 / 47.4970)	(39.5587 / 39.5175)
Diametral measurement over pins (mm)	[MRe/Mri-pin]	(47.5226 / 47.4970)	(39.5587 / 39.5175)

Tolerance data DIN 5480-1 (mm)	[TG]	0.0450	0.0630
(mm)	[Tact]	0.0280	0.0400
(mm)	[Teff]	0.0170	0.0230

Circumferential backlash (transverse section):		
-Theoretical (without form errors) (mm)	[jt.th]	0.1080 / 0.0400
-Effective (with form errors) (mm)	[jt.eff]	0.0400 / 0.0000
Normal backlash theoretical (mm)	[jn.th]	0.0935 / 0.0346
Normal backlash (mm)	[jn.eff]	0.0346 / 0.0000

Notice: When controlling splines with individual measurements (base tangent length/pin diameter) respect the values in 'Actual dimensions'.

3. GEAR ACCURACY

		------- SHAFT --------	HUB --------
According to DIN 5480:2006:			
Accuracy grade	[Q-DIN5480]	8	9
Total profile deviation (µm)	[Fa]	15.0	21.0
Total helix deviation (µm)	[Fb]	9.0	11.0
Single pitch deviation (µm)	[fp]	12.0	17.0
Total cumulative pitch deviation (µm)	[Fp]	28.0	40.0
Runout (µm)	[Fr]	40.0	40.0

4. STRENGTH CALCULATION

Calculation method: G.Niemann, Machine Elements I, 4th edition.
Centering: flank centered

Supporting length (mm)	[ltr]	13.60
Maximal circumferential force (N)	[Ft]	69363.90
Maximal circumferential force per tooth (N)	[Ft/z]	2040.11
Force application diameter (mm)	[dm]	43.63
Tooth height (mm)	[h]	0.97
Distance a0 (mm)	[a0]	6.00
Length factor	[kl]	1.04
Participation factor (equivalent)	[kφßq]	2.00
Participation factor (maximum load)	[kφßmax]	1.70

The share factors kφß according to Niemann are determined according to the accuracy grade specified in DIN 5480..

[Q] 9

Nominal torque (Nm)	[Tnenn]	0.00
Application factor	[KA]	1.00
Service torque (Nm)	[Teq]	0.00
Maximum torque (Nm)	[Tmax]	1513.00
Torque - curve: No alternating torque		
Number of load peaks	[NL]	3000000
Number of change of load direction	[NW]	1
Load direction changing coefficient	[fw]	1.00
Tolerance field according to DIN 5480		"H9"

SHAFT

Width on shaft (mm)	[l_W]	13.60
Supporting surface (mm²)	[Flw=ltr*h*z]	446.22
Tip form diameter (mm)	[dFa1.i]	44.59
Pressure stress (equivalent load) (N/mm²)	[peq]	0.00
Pressure stress (maximum load) (N/mm²)	[pmax]	275.32
Support factor	[fs]	1.20
Load peak coefficient	[fL]	1.15
Hardness influence coefficient	[fH]	1.00
Permissible pressure (N/mm²)	[pzuleq]	960.00
Permissible pressure (N/mm²)	[pzulmax]	1106.20
fw * pzul / peq		1.#J
fL * pzul / pmax		4.02
Required safety	[Smin]	1.00
Minimal safety	[S]	4.02

HUB

Width on hub (mm)	[l_N]	17.00
Supporting surface (mm²)	[Fln=ltr*h*z]	446.22
Tip form diameter (mm)	[dFa2.i]	-42.66
Small external diameter (mm)	[D1]	52.00
Big external diameter (mm)	[D2]	52.00
Width of hub-part with D2 (mm)	[c]	13.60
Equivalent diameter hub (mm)	[D]	52.00
Pressure stress (equivalent load) (N/mm²)	[peq]	0.00
Pressure stress (maximum load) (N/mm²)	[pmax]	275.32
Support factor	[fs]	1.50
Load peak coefficient	[fL]	1.15
Hardness influence coefficient	[fH]	1.15

Permissible pressure (N/mm²)	[pzuleq]	1380.00
Permissible pressure (N/mm²)	[pzulmax]	1590.16
fw * pzul / peq		1.#J
fL * pzul / pmax		5.78
Required safety	[Smin]	1.00
Minimal safety	[S]	5.78

5. ADDITIONAL DATA

Moment of inertia (System referenced to wheel 1):
calculation without consideration of the exact tooth shape

single gears	((da+df)/2...di) (kg*m²)	[TraeghMom]	1.54e-005	4.733e-005
System	((da+df)/2...di) (kg*m²)	[TraeghMom]	6.274e-005	

6. MODIFICATIONS AND TOOTH FORM DEFINITION

Data for the tooth form calculation :
Data not available.

REMARKS:

- Specifications with [.e/i] imply: Maximum [e] and Minimal value [i] with consideration of all tolerances
  Specifications with [.m] imply: Mean value within tolerance
- Concerning the calculation method:

h = (dFa1.i-ABS(dFa2.i)) / 2.0
dm = (dFa1.i + ABS(dFa2.i)) / 2.0;
Ft = Mmax * 2000 / dm
Pressure load: p(eq,max) = kphib(eq,max)*k1*M*2000/(dm*l*h*z); pmax >= peq
Coefficient for load direction changes according to DIN 6892:1998/ fig. 6
pzuleq = fs*fH*fw*(Rm,Rp)
pzulmax = fs*fH*fL*(Rm,Rp)
(Rm:for brittle material; Rp:for ductile material)

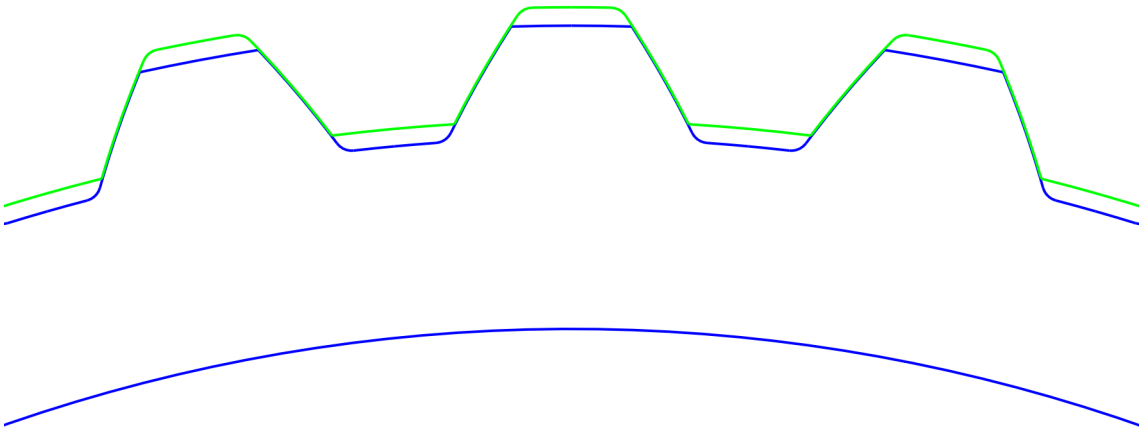

da1 = 44.6700 mm, df1 = 42.1963 mm, As1 = -0.0085 mm
da2 = -42.5800 mm, df2 = -45.0745 mm, As2 = -0.0115 mm

Figure: Meshing Shaft - Hub

End of Report lines: 266

BorgWarner TTS, SE-Landskrona

File

Name : Tripod_hub_spline_23mm
Changed by: skalkan on: 09.06.2019 at: 15:41:14

SPLINED JOINTS DIN 5480:2006

Shaft DIN5480 - W 23.00*0.80*27*8h
Hub DIN5480 - N 23.00*0.80*27*9H

Drawing or article number:
Shaft: 0.000.0
Hub: 0.000.0

1. TOOTH GEOMETRY AND MATERIAL

Normal module (mm)	[mn]	0.8000	
Nominal diameter DIN (mm)	[dB]	23.00	
Pressure angle at normal section (°)	[alfn]	30.000	
		------- SHAFT ---------	HUB --------
Number of teeth	[z]	27	-27
Helix angle at reference circle (°)	[beta]	0.0000	
Facewidth (mm)	[b]	15.00	36.00
Hand of gear	Spur gear		

Material
Gear 1: 34 CrNiMo 6 (1), Through hardened steel, alloyed, through hardened
ISO 6336-5 Figure 5/6 (MQ)
Gear 2: 34 CrNiMo 6 (3), Through hardened steel, nitrided
ISO 6336-5 Figure 13b/14b (MQ)

		------- SHAFT ---------	HUB ----
Surface hardness		HBW 240	HV 650
Reference diameter material (mm)	[dB]	23	28
Tensile strength (N/mm²)	[σB]	1100.00	1100.00
Yield point (N/mm²)	[σS]	900.00	900.00
Young's modulus (N/mm²)	[E]	206000	206000
Poisson's ratio	[v]	0.300	0.300
Roughness average value DS, flank (µm)	[RAH]	0.00	0.00
Roughness average value DS, root (µm)	[RAF]	0.00	0.00
Mean roughness height, Rz, flank (µm)	[RZH]	8.00	20.00
Mean roughness height, Rz, root (µm)	[RZF]	20.00	20.00

Gear reference profile 1 :
Reference profile DIN 5480:2006 0.55 / 0.16 / 0.45 Broaching

Dedendum coefficient	[hfP*]	0.550
Root radius factor	[rhofP*]	0.160 (rhofPmax*=0.810)
Addendum coefficient	[haP*]	0.450
Tip radius factor	[rhoaP*]	0.000
Protuberance height coefficient	[hprP*]	0.000
Protuberance angle	[alfprP]	0.000
Tip form height coefficient	[hFaP*]	0.000

Ramp angle	[alfKP]	0.000
		not topping

Gear reference profile	2 :	
Reference profile	DIN 5480:2006 0.55 / 0.16 / 0.45 Broaching	
Dedendum coefficient	[hfP*]	0.550
Root radius factor	[rhofP*]	0.160 (rhofPmax*=0.810)
Addendum coefficient	[haP*]	0.450
Tip radius factor	[rhoaP*]	0.000
Protuberance height coefficient	[hprP*]	0.000
Protuberance angle	[alfprP]	0.000
Tip form height coefficient	[hFaP*]	0.000
Ramp angle	[alfKP]	0.000
		not topping

Summary of reference profile gears:

Dedendum reference profile	[hfP*]	0.550	0.550
Tooth root radius Refer. profile	[rofP*]	0.160	0.160
Addendum Reference profile	[haP*]	0.450	0.450
Protuberance height coefficient	[hprP*]	0.000	0.000
Protuberance angle (°)	[alfprP]	0.000	0.000
Tip form height coefficient	[hFaP*]	0.000	0.000
Ramp angle (°)	[alfKP]	0.000	0.000

Transverse module (mm)	[mt]	0.800
Pressure angle at pitch circle (°)	[alft]	30.000
Base helix angle (°)	[betab]	0.000
Sum of profile shift coefficients	[Summexi]	0.0000

		------- SHAFT ---------	HUB --------
Profile shift coefficient	[x]	0.3250	-0.3250
Profile shift (x*m) (mm)	[x*m]	0.2600	-0.2600
Reference diameter (mm)	[d]	21.600	21.600
Base diameter (mm)	[db]	18.706	18.706
Tip diameter (mm)	[da]	22.840	21.400
Effective tip diameter (mm)	[da.e/i]	22.840 / 22.710	21.400 / 21.530
Tip diameter allowances (mm)	[Ada.e/i]	0.000 / -0.130	-0.000 / 0.130
Root diameter (mm)	[df]	21.240	23.000
Effective root diameter (mm)	[df.e/i]	21.214 / 21.171	23.035 / 23.097
Root diameter allowances (mm)	[Adf.e/i]	-0.026 / -0.069	0.035 / 0.097
Generating Profile shift coefficient	[xE.e/i]	0.3088 / 0.2817	-0.3467 / -0.3856
Root form diameter (mm)	[dFf.e/i]	21.347 / 21.305	22.921 / 22.978
(dFf2 calculated with virtual pinion type cutter (circa): z=	17 x=	0.100 rhoaP0*=0.1)	
Tooth height (mm)	[h]	0.800	0.800
Theoretical tip clearance (mm)	[c]	0.080	0.080
Effective tip clearance (mm)	[c.e/i]	0.193 / 0.097	0.180 / 0.093
Normal tooth thickness at tip circle (mm)	[san]	0.831	0.835
(mm)	[san.e/i]	0.900 / 0.788	0.893 / 0.779
Normal space width at root circle (mm)	[efn]	0.741	0.723
(mm)	[efn.e/i]	0.741 / 0.741	0.720 / 0.716
Pitch on reference circle (mm)	[pt]	2.513	
Base pitch (mm)	[pbt]	2.177	
Transverse pitch on contact-path (mm)	[pet]	2.177	

2. MEASUREMENTS FOR TOOTH THICKNESS

		------- SHAFT ---------	HUB --------
Accuracy grade		8	9
Tooth thickness deviation		DIN 5480 h	DIN 5480 H
Number of teeth spanned	[k]	5.0000	5.0000
Base tangent length (no backlash) (mm)	[Wk]	11.0600	11.0600
Diameter of contact point (mm)	[dMWk.m]	21.7279	21.7356
Theoretical diameter of ball/pin (mm)	[dm]	1.5952	1.4577
Effective diameter of ball/pin (mm)	[DMeff]	1.7500	1.5000
Theor. dimension over two balls (mm)	[MRe/Mri-ball]	24.9846	19.7537
Diametral measurement over pins without clearance (mm)	[MRe/Mri-pin]	24.9846	19.7537

Data for Actual Dimensions (DIN 5480:2006)

Tooth thickness / Spacewidth (mm)	[Smax/Smin, Emax/Emin]	1.5419 / 1.5169	1.6129 / 1.5769
Tooth thickness tolerance, normal section (mm)	[Tol.Smax/min]	-0.0150 / -0.0400	
Tooth space tolerance, normal section (mm)	[Tol.Emax/min]		0.0560 / 0.0200
Base tangent length (mm)	[Wk.Smax/Smin]	11.0470 / 11.0254	11.1085 / 11.0773
Diametral two ball measure (mm)	[MRe/Mri-ball]	24.9627 / 24.9263	19.8543 / 19.7898
Diametral measurement over pins (mm)	[MRe/Mri-pin]	24.9627 / 24.9263	19.8543 / 19.7898

Data for Effective Dimensions (DIN 5480:2006)

Tooth thickness / Spacewidth (mm)	[Svmax/min, Evmax/min]	1.5569 / 1.5419	1.5769 / 1.5569
Tooth thickness tolerance, normal section (mm)	[Tol.Svmax/min]	0.0000 / -0.0150	
Tooth space tolerance, normal section (mm)	[Tol.Evmax/min]		0.0200 / 0.0000
Base tangent length (mm)	[Wk.Svmax/min]	(11.0600 / 11.0470)	(11.0773 / 11.0600)
Diametral two ball measure (mm)	[MRe/Mri-ball]	(24.9846 / 24.9627)	(19.7898 / 19.7537)
Diametral measurement over pins (mm)	[MRe/Mri-pin]	(24.9846 / 24.9627)	(19.7898 / 19.7537)

Tolerance data DIN 5480-1 (mm)	[TG]	0.0400	0.0560
(mm)	[Tact]	0.0250	0.0360
(mm)	[Teff]	0.0150	0.0200

Circumferential backlash (transverse section):

-Theoretical (without form errors) (mm)	[jt.th]	0.0960 / 0.0350
-Effective (with form errors) (mm)	[jt.eff]	0.0350 / 0.0000
Normal backlash theoretical (mm)	[jn.th]	0.0831 / 0.0303
Normal backlash (mm)	[jn.eff]	0.0303 / 0.0000

Notice: When controlling splines with individual measurements (base tangent length/pin diameter) respect the values in 'Actual dimensions'.

3. GEAR ACCURACY

		------- SHAFT ---------	HUB --------
According to DIN 5480:2006:			
Accuracy grade	[Q-DIN5480]	8	9
Total profile deviation (µm)	[Fa]	13.0	19.0
Total helix deviation (µm)	[Fb]	9.0	10.0
Single pitch deviation (µm)	[fp]	11.0	15.0
Total cumulative pitch deviation (µm)	[Fp]	25.0	36.0
Runout (µm)	[Fr]	30.0	30.0

4. STRENGTH CALCULATION

Calculation method: G.Niemann, Machine Elements I, 4th edition.
Centering: flank centered

Supporting length (mm)	[ltr]	15.00
Maximal circumferential force (N)	[Ft]	81464.74
Maximal circumferential force per tooth (N)	[Ft/z]	3017.21
Force application diameter (mm)	[dm]	22.12
Tooth height (mm)	[h]	0.59
Distance a0 (mm)	[a0]	7.50
Length factor	[kl]	1.07
Participation factor (equivalent)	[kφßq]	2.00
Participation factor (maximum load)	[kφßmax]	1.70

The share factors kφß according to Niemann are determined according to the accuracy grade specified in DIN 5480..

[Q] 9

Nominal torque (Nm)	[Tnenn]	0.00
Application factor	[KA]	1.00
Service torque (Nm)	[Teq]	0.00
Maximum torque (Nm)	[Tmax]	901.00

Torque - curve: No alternating torque

Number of load peaks	[NL]	3000000
Number of change of load direction	[NW]	1
Load direction changing coefficient	[fw]	1.00
Tolerance field according to DIN 5480		"H9"

SHAFT

Width on shaft (mm)	[l_W]	15.00
Supporting surface (mm²)	[Flw=ltr*h*z]	238.95
Tip form diameter (mm)	[dFa1.i]	22.71
Pressure stress (equivalent load) (N/mm²)	[peq]	0.00
Pressure stress (maximum load) (N/mm²)	[pmax]	618.97
Support factor	[fs]	1.20
Load peak coefficient	[fL]	1.15
Hardness influence coefficient	[fH]	1.00
Permissible pressure (N/mm²)	[pzuleq]	1080.00
Permissible pressure (N/mm²)	[pzulmax]	1244.47
fw * pzul / peq		1.#J
fL * pzul / pmax		2.01
Required safety	[Smin]	1.00
Minimal safety	[S]	2.01

HUB

Width on hub (mm)	[l_N]	36.00
Supporting surface (mm²)	[Fln=ltr*h*z]	238.95
Tip form diameter (mm)	[dFa2.i]	-21.53
Small external diameter (mm)	[D1]	28.00
Big external diameter (mm)	[D2]	28.00
Width of hub-part with D2 (mm)	[c]	15.00
Equivalent diameter hub (mm)	[D]	28.00
Pressure stress (equivalent load) (N/mm²)	[peq]	0.00
Pressure stress (maximum load) (N/mm²)	[pmax]	618.97
Support factor	[fs]	1.50
Load peak coefficient	[fL]	1.15
Hardness influence coefficient	[fH]	1.15

Permissible pressure (N/mm²)	[pzuleq]	1552.50
Permissible pressure (N/mm²)	[pzulmax]	1788.93
fw * pzul / peq		1.#J
fL * pzul / pmax		2.89
Required safety	[Smin]	1.00
Minimal safety	[S]	2.89

5. ADDITIONAL DATA

Moment of inertia (System referenced to wheel 1):
calculation without consideration of the exact tooth shape

single gears	((da+df)/2...di) (kg*m²)	[TraeghMom]	2.364e-006	1.021e-005
System	((da+df)/2...di) (kg*m²)	[TraeghMom]	1.257e-005	

6. MODIFICATIONS AND TOOTH FORM DEFINITION

Data for the tooth form calculation :

Calculation of Gear 1
Tooth form, Shaft, Step 1: Automatic (final machining)
haP*= 0.417, hfP*= 0.572, rofP*= 0.160

Calculation of Gear 2
Tooth form, Hub, Step 1: Automatic (final machining)
mn= 0.800 mm, alfn=30.000°, da= -21.465 mm, df= -23.066 mm, xE=-0.336, rf= 0.128 mm

REMARKS:

- Specifications with [.e/i] imply: Maximum [e] and Minimal value [i] with consideration of all tolerances
  Specifications with [.m] imply: Mean value within tolerance
- Concerning the calculation method:

h = (dFa1.i-ABS(dFa2.i)) / 2.0
dm = (dFa1.i + ABS(dFa2.i)) / 2.0;
Ft = Mmax * 2000 / dm
Pressure load: p(eq,max) = kphib(eq,max)*k1*M*2000/(dm*l*h*z); pmax >= peq
Coefficient for load direction changes according to DIN 6892:1998/ fig. 6
pzuleq = fs*fH*fw*(Rm,Rp)
pzulmax = fs*fH*fL*(Rm,Rp)
(Rm:for brittle material; Rp:for ductile material)

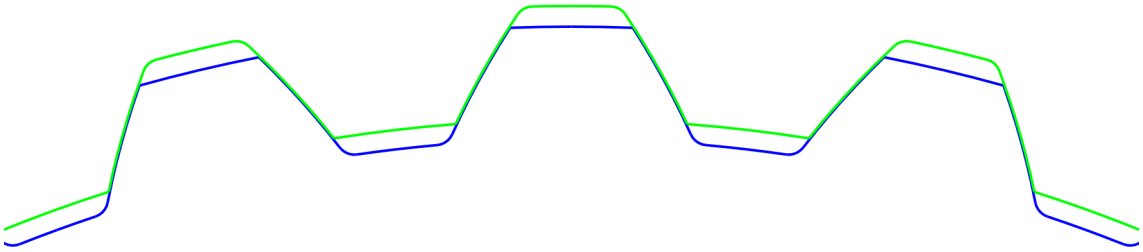

da1 = 22.7750 mm, df1 = 21.1924 mm, As1 = -0.0075 mm
da2 = -21.4650 mm, df2 = -23.0658 mm, As2 = -0.0100 mm

Figure: Meshing Shaft - Hub

End of Report lines: 275

13.4 Appendix D - DIN 2093 disc spring data

DISC SPRING

DS, DIN 2093

Disc springs for static and dynamic load

Disc springs are particularly suited for use in applications that require a high force but have limited space. By combining the springs in various ways, it is possible to obtain different forces and characteristics. See figures opposite.

The disc springs we stock are of the highest quality and have a special profile, which keeps the inner diameter unchanged when the spring is compressed. As a result, these springs produce very little friction, exhibit low working loss and have a considerably longer lifespan.

Disc springs are divided into three groups:

- Group 1: Springs with a thickness (t) < 1.25 mm have not been chamfered on inner or outer diameters.
- Group 2: Springs with a thickness (t) from 1.25 up to 6.0 mm are chamfered on inner and outer diameters.
- Group 3: Springs with a thickness (t) > 6.0 mm are chamfered on all sides. In addition, all contact surfaces are ground flat.

Disc springs for static load

We can manufacture disc springs of a simpler design in varying material qualities. These disc springs are intended for static loads, e.g. as tensioning washers in a threaded joint reinforcement.

Custom dimensions

Upon request, we also manufacture disc springs in custom sizes using both standard materials and special materials, e.g. stainless, acid-proof and heat-resistant materials, in a wide selection of qualities.

Packs

Disc springs are sold only in the pack sizes shown below. This does not apply to DS low force or DS-S (stainlees steel), they are sold individually.

≤ 28	x 14.2	x 1.5	= 200 pcs
≥ 31.5	x 16.3	x 1.25	= 100 pcs
≥ 40	x 14.3	x 1.25	= Individually

Stock

Disc springs up to De < 150 are kept in stock.

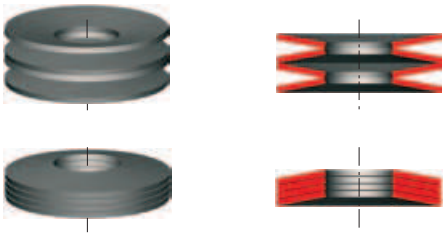

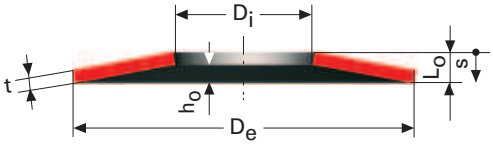

Group 1 and Group 2 springs

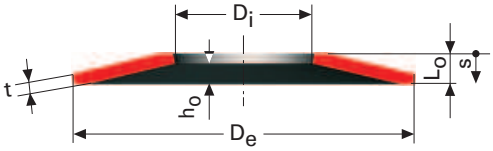

Group 3 springs

All dimensions are in mm

D_e = Outer diameter
D_i = Inner diameter
t = Material thickness
t_1 = Material thickness (Group 3)
L_o = Unloaded length
h_o = Cup height, max. deflection
s = Deflection
F = Spring force in Newtons

Material: Group 1: CK 67/51CrV4
Group 2: 51CrV4
Group 3: 51CrV4

Finish: Shot peened, phosphated, blackened and oiled

1 kp = 9.80665 Newtons, 1 Newton = 0.10197 kp

DISC SPRING

DS, DIN 2093

Spring location

D_i and D_e mm	Diametrical play mm
<16	0,2
>16–20	0,3
>20–26	0,4
>26–31,5	0,5
>31,5–50	0,6
>50–80	0,8
>80–140	1,0
>140–150	1,6
>250	2,0

Progressive characteristic

By combining springs of different thickness in varying sequences, it is possible to obtain different progressive spring characteristics.

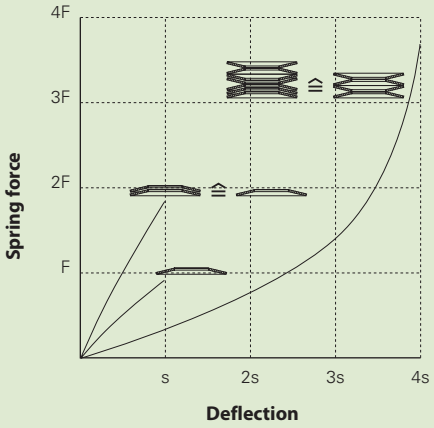

Characteristic for one spring

At dynamic load, cup height should only be used for 0.75 x h_O. The diagram shows how the spring characteristic is influenced by the ratio between cup height and material thickness (h_O/t). Information about this ratio can be found in the dimension tables. We can provide diagrams for each type and dimension on request.

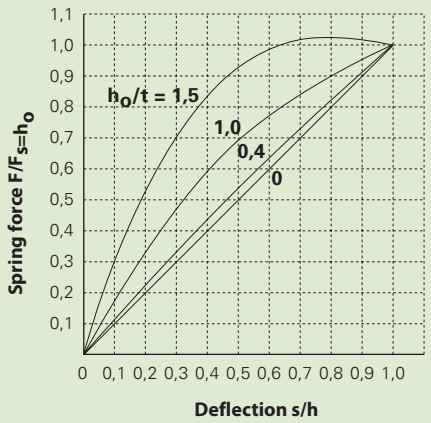

Characteristic for different combinations

A. 3 parallel stacked springs. The force according to the table x no. of parallel springs.

B. 2 parallel stack springs in series. Force according to the table x no. of parallel springs (in this case 2). Deflection h_O x no. of series (in this case 3).

C. Single stacked springs. Force as shown in the table. Deflection according to the table x no. of springs.

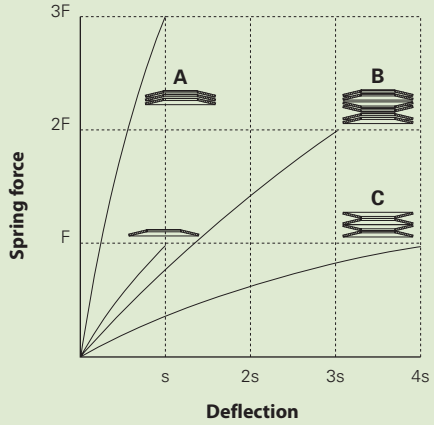

DISC SPRING

DS, DIN 2093

Diameter tolerances

Tolerance D_e and D_i mm	Tolerance D_e mm	D_i mm
>3–6	0 / -0,12	0 / +0,12
>6–10	0 / -0,15	0 / +0,15
>10–18	0 / -0,18	0 / +0,18
>18–30	0 / -0,21	0 / +0,21
>30–50	0 / -0,25	0 / +0,25
>50–80	0 / -0,30	0 / +0,30
>80–120	0 / -0,35	0 / +0,35
>120–180	0 / -0,40	0 / +0,40
>180–250	0 / -0,46	0 / +0,46
>250–315	0 / -0,52	0 / +0,52
>315–400	0 / -0,57	0 / +0,57
>400–500	0 / -0,63	0 / +0,63
>500–600	0 / -0,68	0 / +0,68

Concentricity tolerances

D_e mm	Tolerance mm
>3–6	0,15
>6–10	0,18
>10–18	0,22
>18–30	0,26
>30–50	0,32
>50–80	0,60
>80–120	0,70
>120–180	0,80
>180–250	0,92
>250–315	1,04
>315–400	1,14
>400–500	1,26
>500–600	1,36

Thickness and free height tolerances

Group	Tolerance Thickness (t / t_1) mm	Tolerance Thickness (t) mm	Free height (L_o) mm
1	0,2–0,6	+0,02 / -0,06	+0,10 / -0,05
1	>0,6–<1,25	+0,03 / -0,09	+0,10 / -0,05
2	1,25–2,0	+0,04 / -0,12	+0,15 / -0,08
2	>2,0–3,0	+0,04 / -0,12	+0,20 / -0,10
2	>3,0–3,8	+0,04 / -0,12	+0,30 / -0,15
2	>3,8–6,0	+0,04 / -0,12	+0,30 / -0,15
3	>6,0–15	±0,10	±0,30
3	>15–25	±0,12	±0,50*
3	>25–40	±0,15	±1,00*

* Applies to springs with D_e / t < 20

Spring force tolerances

Group	Thickness (t / t_1) mm	Tolerance at $s = 0.75\ h_o$ %
1	<1,25	+25 / -7,5
2	1,25–3,0	+15 / -7,5
2	>3,0–6,0	+10 / -5
3	>6,0–15	±5

Information about disc springs with reduced thickness (t_1)

Disc springs belonging to group 3 are produced with flat contact surfaces.

- This means that the effective lever is reduced, in order to compensate for the force increase which results these disc springs are manufactured with reduced thickness.
- This means that the deflection becomes greater, due to the reduced material section.
- The value used in the table for s = 0,25 h_0 / 0,5 h_0 / 0,75 h_0 is the the same as for disc springs with non reduced thickness.
- Correct h_0 dimension is table value + reduction of material (t - t_1).
- sc (max deflection) = h_0 = L_0 - t of disc springs without contact surfaces (Group 1 and group 2).
- sc (max deflection) = h_0 = L_0 - t_1 for disc springs with contact surfaces (Group 3).

Contact us if you need more information.

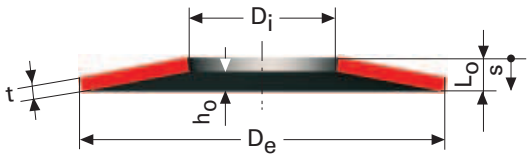

DISC SPRING

DS, DIN 2093

							s = 0.25 h_o		s = 0.5 h_o		s = 0.75 h_o		s = h_o | s = L_o - t_1		Cat.
D_e	D_i	t	t_1	L_o	h_o	h_o/t	s	F	s	F	s	F	s	F	No
60	20,5	2		4,2	2,2	1,1	0,55	2528	1,1	4097	1,65	5026	2,2	5636	4365
60	20,5	2,5		4,7	2,2	0,88	0,55	4151	1,1	7102	1,65	9255	2,2	11008	4366
60	20,5	3		5,2	2,2	0,733	0,55	6434	1,1	11429	1,65	15465	2,2	19022	4367
60	25,5	2,5		4,4	1,9	0,76	0,475	3447	0,95	6081	1,425	8175	1,9	9997	4368
60	25,5	3		4,65	1,65	0,55	0,412	4495	0,825	8352	1,237	11784	1,65	15002	4369
60	30,5	2,5		4,5	2	0,8	0,5	4059	1	7088	1,5	9432	2	11433	4370
60	30,5	2,75		4,75	2	0,727	0,5	5125	1	9117	1,5	12356	2	15217	4371
60	30,5	3		4,7	1,7	0,566	0,425	5083	0,85	9407	1,275	13226	1,7	16792	4372
60	30,5	3,5		5	1,5	0,428	0,375	6591	0,75	12574	1,125	18153	1,5	23528	4373
63	31	1,8		4,15	2,35	1,305	0,587	2364	1,175	3658	1,762	4238	2,35	4463	4374
63	31	2,5		4,25	1,75	0,7	0,437	2942	0,875	5270	1,312	7189	1,75	8904	4375
63	31	3		4,7	1,7	0,566	0,425	4524	0,85	8373	1,275	11772	1,7	14946	4376
63	31	3,5		4,9	1,4	0,4	0,35	5399	0,7	10359	1,05	15025	1,4	19545	4377
70	24,5	3		5,3	2,3	0,766	0,575	5080	1,15	8948	1,725	12007	2,3	14663	4378
70	24,5	3,5		6	2,5	0,714	0,625	8446	1,25	15076	1,875	20495	2,5	25309	4379
70	25,5	2		4,5	2,5	1,25	0,625	2408	1,25	3771	1,875	4437	2,5	4755	4380
70	30,5	2,5		4,9	2,4	0,96	0,6	3755	1,2	6297	1,8	8031	2,4	9360	4381
70	30,5	3		5,1	2,1	0,7	0,525	4676	1,05	8376	1,575	11426	2,1	14152	4382
70	35,5	3		5,1	2,1	0,7	0,525	5028	1,05	9007	1,575	12287	2,1	15218	4383
70	35,5	3,5		5,3	1,8	0,514	0,45	6077	0,9	11384	1,35	16177	1,8	20714	4384
70	35,5	4		5,8	1,8	0,45	0,45	8757	0,9	16634	1,35	23923	1,8	30919	4385
70	40,5	4		5,7	1,7	0,425	0,425	9025	0,85	17230	1,275	24889	1,7	32274	4386
70	40,5	5		6,4	1,4	0,28	0,35	13646	0,7	26719	1,05	39410	1,4	51911	4387
71	36	2		4,6	2,6	1,3	0,65	2861	1,3	4432	1,95	5144	2,6	5426	4388
71	36	2,5		4,5	2	0,8	0,5	2894	1	5054	1,5	6725	2	8152	4389
71	36	4		5,6	1,6	0,4	0,4	7379	0,8	14157	1,2	20535	1,6	26712	4390
80	30,5	2,5		5,3	2,8	1,12	0,7	3664	1,4	5911	2,1	7211	2,8	8039	4391
80	31	3		5,5	2,5	0,833	0,625	4531	1,25	7847	1,875	10352	2,5	12451	4392
80	31	4		6,1	2,1	0,525	0,525	7319	1,05	13677	1,575	19394	2,1	24791	4393
80	35,5	4		6,2	2,2	0,55	0,55	8118	1,1	15083	1,65	21280	2,2	27093	4394
80	36	3		5,7	2,7	0,9	0,675	5401	1,35	9196	2,025	11919	2,7	14106	4395
80	41	2,25		5,2	2,95	1,311	0,737	3698	1,475	5715	2,212	6613	2,95	6950	4396
80	41	3		5,3	2,3	0,766	0,575	4450	1,15	7838	1,725	10518	2,3	12844	4397
80	41	4		6,2	2,2	0,55	0,55	8726	1,1	16213	1,65	22874	2,2	29122	4398
80	41	5		6,7	1,7	0,34	0,425	11821	0,85	22928	1,275	33559	1,7	43952	4399
90	46	2,5		5,7	3,2	1,28	0,8	4232	1,6	6585	2,4	7684	3,2	8157	4400
90	46	3,5		6	2,5	0,714	0,625	5836	1,25	10416	1,875	14161	2,5	17487	4401
90	46	5		7	2	0,4	0,5	11267	1	21617	1,5	31354	2	40786	4402

DISC SPRING

DS, DIN 2093

							$s = 0.25\ h_o$		$s = 0.5\ h_o$		$s = 0.75\ h_o$		$s = h_o \mid s = L_o - t_1$		Cat.
D_e	D_i	t	t_1	L_o	h_o	h_o/t	s	F	s	F	s	F	s	F	No
100	41	4		7,2	3,2	0,8	0,8	8715	1,6	15219	2,4	20251	3,2	24547	4403
100	41	5		7,75	2,75	0,55	0,687	12345	1,375	22937	2,062	32361	2,75	41201	4404
100	51	2,7		6,2	3,5	1,296	0,875	4779	1,75	7410	2,625	8609	3,5	9091	4405
100	51	3,5		6,3	2,8	0,8	0,7	5624	1,4	9823	2,1	13070	2,8	15843	4406
100	51	4		7	3	0,75	0,75	8673	1,5	15341	2,25	20674	3	25338	4407
100	51	5		7,8	2,8	0,56	0,7	13924	1,4	25810	2,1	36339	2,8	46189	4408
100	51	6		8,2	2,2	0,366	0,55	17061	1,1	32937	1,65	48022	2,2	62711	4409
100	51	7	6,55	9,2	2,2	0,314	0,55	27374	1,1	52454	1,65	75840	2,65	115982	4410
112	57	3		6,9	3,9	1,3	0,975	5834	1,95	9038	2,925	10489	3,9	11064	4411
112	57	4		7,2	3,2	0,8	0,8	7639	1,6	13341	2,4	17752	3,2	21518	4412
112	57	6		8,5	2,5	0,416	0,625	15800	1,25	30215	1,875	43707	2,5	56737	4413
125	51	4		8,5	4,5	1,125	1,125	10096	2,25	16265	3,375	19817	4,5	22060	4414
125	51	5		8,9	3,9	0,78	0,975	13063	1,95	22931	2,925	30669	3,9	37342	4415
125	51	6		9,4	3,4	0,566	0,85	17027	1,7	31514	2,55	44307	3,4	56254	4416
125	61	5		9	4	0,8	1	14615	2	25526	3	33965	4	41170	4417
125	61	6		9,6	3,6	0,6	0,9	19789	1,8	36336	2,7	50722	3,6	64028	4418
125	61	8	7,5	10,9	2,9	0,362	0,725	34434	1,45	65305	2,175	93577	3,4	138144	4419
125	64	3,5		8	4,5	1,285	1,125	8514	2,25	13231	3,375	15416	4,5	16335	4420
125	64	5		8,5	3,5	0,7	0,875	12238	1,75	21924	2,625	29908	3,5	37041	4421
125	64	6		9,6	3,6	0,6	0,9	20348	1,8	37362	2,7	52155	3,6	65836	4422
125	64	7	6,55	10	3	0,428	0,75	25528	1,5	47615	2,25	67216	3,45	95795	4423
125	64	8	7,5	10,6	2,6	0,325	0,65	31118	1,3	59520	1,95	85926	3,1	129972	4861
125	71	6		9,3	3,3	0,55	0,825	19538	1,65	36302	2,475	51217	3,3	65207	4424
125	71	8	7,45	10,9	2,9	0,362	0,725	38416	1,45	72705	2,175	103964	3,45	154927	4425
125	71	10	9,3	11,8	1,8	0,18	0,45	42821	0,9	84082	1,35	124124	2,5	223282	4426
140	72	3,8		8,7	4,9	1,289	1,225	9514	2,45	14773	3,675	17195	4,9	18199	4862
140	72	5		9	4	0,8	1	12014	2	20982	3	27920	4	33843	4427
140	72	8	7,5	11,2	3,2	0,4	0,8	31903	1,6	59967	2,4	85251	3,7	123137	4428

13.5 Appendix E - Euler buckling cases

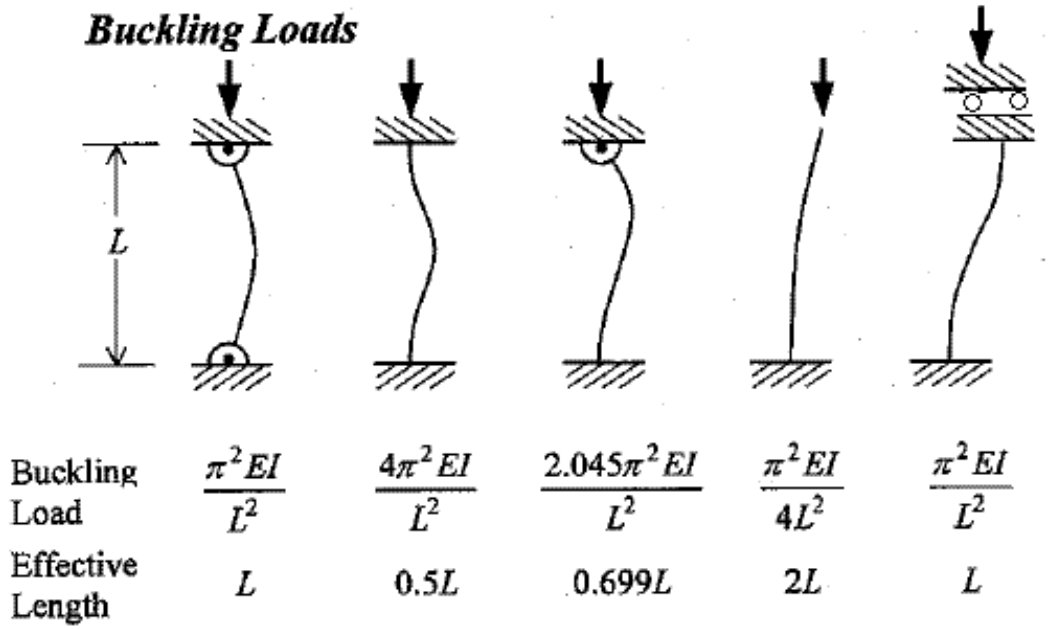

Figure 79: Euler buckling cases

14 References

References

[1] Bbs halmstad din 50150 hardness conversion. https://www.bbshalmstad.se/en/infocenter/hardness-conversion-table/. Accessed: 2019-05-20.

[2] Formula student germany magazine 2018. https://www.formulastudent.de/fileadmin/user_upload/all/2018/PR_Media/FSG2018_magazine_v20180725_LQ.pdf. Accessed: 2019-04-26.

[3] Formula student rules 2019. https://www.formulastudent.de/fileadmin/user_upload/all/2019/rules/FS-Rules_2019_V1.1.pdf. Accessed: 2019-03-14.

[4] Mechanical properties of round extruded aluminium bars, alumeco. https://www.alumeco.com/knowledge-technique/mechanical-properties/round-bars-extruded?s=0#. Accessed: 2019-06-03.

[5] Ovako steel navigator, 34crnimo6 steel. https://steelnavigator.ovako.com/steel-grades/34crnimo6/. Accessed: 2019-05-20.

[6] Radigan engineering excel belleville spring calculator. https://radiganengineering.com/2013/11/excel-belleville-spring-calculator/. Accessed: 2019-05-19.

[7] Stahlhärterei haupt, nitriding data. http://www.haerterei-haupt.de/wp-content/uploads/2017/12/Haupt_Downloads-2017_Gasnitriding.pdf. Accessed: 2019-05-20.

[8] Thermal conductivity of metals, metallic elements and alloys. https://www.engineeringtoolbox.com/thermal-conductivity-metals-d_858.html. Accessed: 2019-05-19.

[9] Optimum G. Differential behaviour. http://downloads.optimumg.com/Technical_Papers/DifferentialAnalysis_BertaReport.pdf. Accessed: 2019-03-14.

[10] N. Amati J. Ghosh, A. Tonoli. Improvement of lap-time of a rear wheel drive electric racing vehicle by a novel motor torque control strategy. *SAE Technical Paper 2017-01-0509*, 14(3):342–351, 2017.

[11] H. Cabral D. Herven V.P. Jones J. Maguire T.L. Perttola J.A Peterson L. Pritchard J.A Barlage, T. Brink. *All-Wheel Drive: A Practical Manual, second edition.* 2016.

[12] K. Inoue K. Sawase, Y. Ushiroda. Effect of the right-and-left torque vectoring system in various types of drivetrain. *SAE Technical Paper 2007-01-3645*, 2007.

[13] J. P. Caltagirone D. Reungoat G. Mermaz-Rollet L. Osmar, S. Vincent. Convective heat transfer of an impinging oil jet between a two phase flow and a hot surface. *Atomization and Sprays*, 22(3):185–205, 2012.

[14] R. Mäki. Wet clutch tribology - friction characteristics in all-wheel drive differentials. 2003.

[15] C. Saravanan P. Kaviyarasu. Experimental investigation of convective heat transfer through rough and smooth surfaced aluminium 6063 pin-fin apparatus. *International Research Journal of Advanced Engineering and Science*, 2(2):279–285, 2017.

[16] SKF. *Rullningslager, skolutgåva.* 2014.

[17] R. Poulson V. Siddapureddy, I. Dmitrieva. Experimental investigations of forced cooling for aluminum heat sinks of high power electronics. *SAE Technical Paper 2017-01-0509*, 1999.

[18] L. Vedmar. *Transmissioner.* 2014.

[19] Douglas L. Milliken William F. Milliken. *Race car vehicle dynamics*, volume 3. 1995.

[20] P. Wright. *Formula 1 technology.* 2000.